AD-A081 392 BRITISH COLUMBIA UNIV VANCOUVER INST OF OCEANOGRAPHY F/G 4/2
THE TURBULENT FLUXES OF MOMENTUM AND SENSIBLE HEAT OVER THE OPE--ETC(U)
AUG 79 W G LARGE N00014-76-C-0446
NL

UNCLASSIFIED

1 OF 3
AD
A081 392

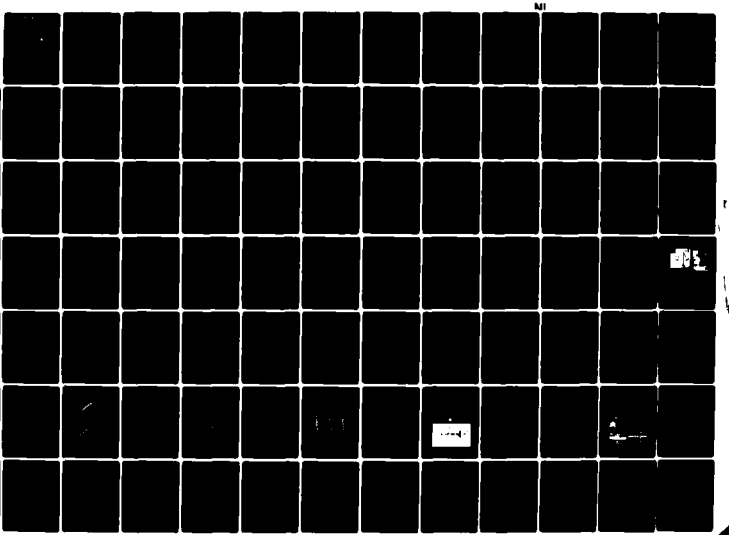

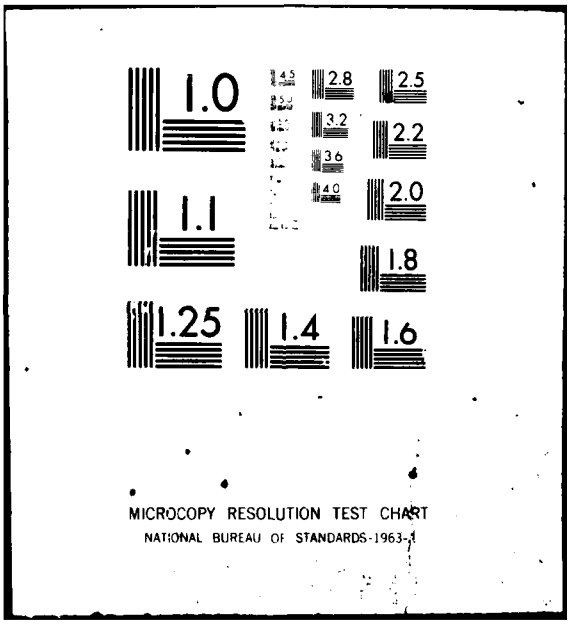
1.0
1.1
1.25
1.4
1.6
1.8
2.0
2.2
2.5
2.8
3.2
3.6
4.0
MICROCOPY RESOLUTION TEST CHART
NATIONAL BUREAU OF STANDARDS-1963-A

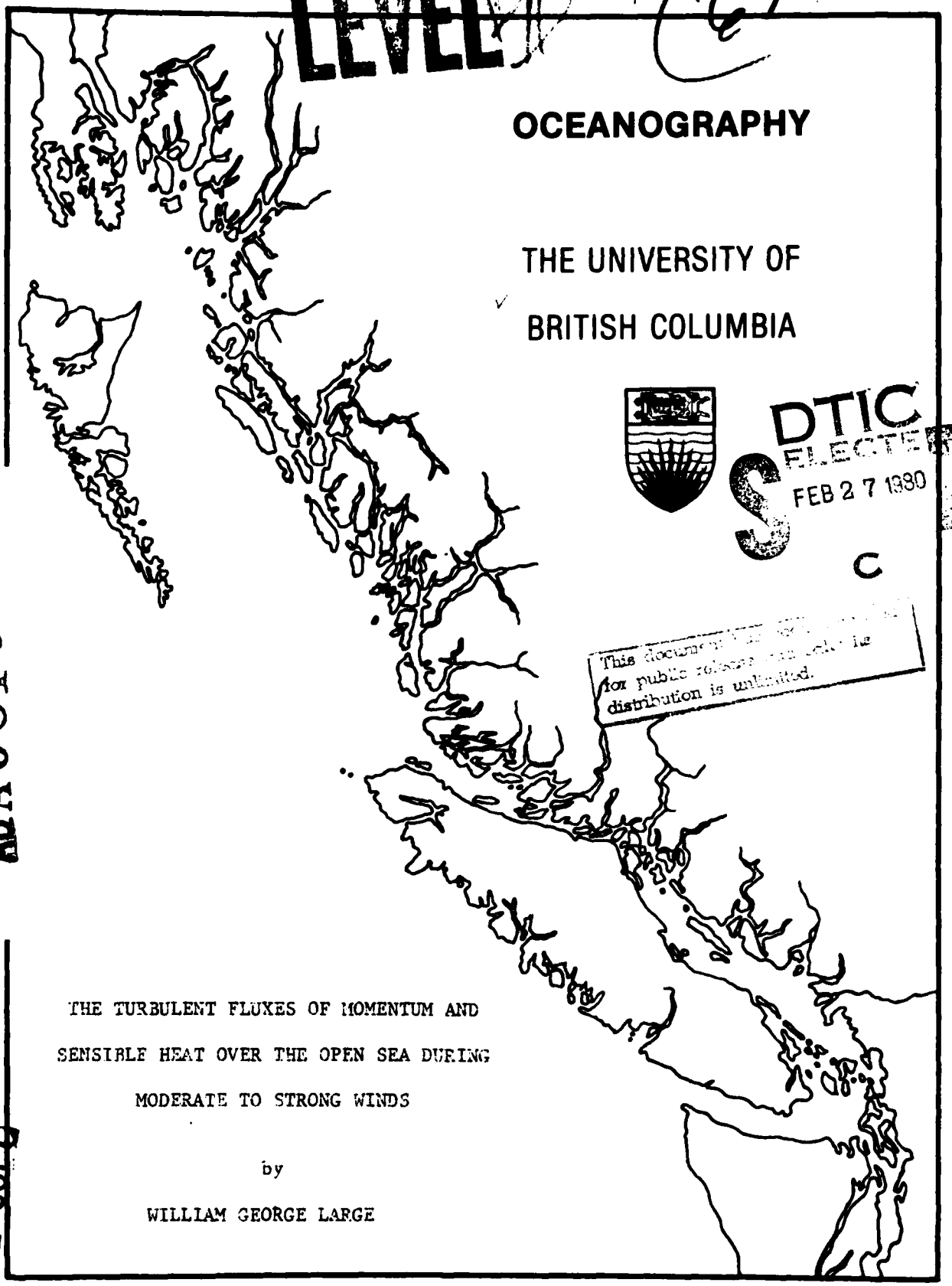

OCEANOGRAPHY

THE UNIVERSITY OF

BRITISH COLUMBIA

THE TURBULENT FLUXES OF MOMENTUM AND SENSIBLE HEAT OVER THE OPEN SEA DURING MODERATE TO STRONG WINDS

by

WILLIAM GEORGE LARGE

SECURITY CLASSIFICATION OF THIS PAGE (When Data Entered)

REPORT DOCUMENTATION PAGE		READ INSTRUCTIONS BEFORE COMPLETING FORM
1. REPORT NUMBER - -	2. GOVT ACCESSION NO.	3. RECIPIENT'S CATALOG NUMBER
4. TITLE (and Subtitle) THE TURBULENT FLUXES OF MOMENTUM AND SENSIBLE HEAT OVER THE OPEN SEA DURING MODERATE TO STRONG WINDS		5. TYPE OF REPORT & PERIOD COVERED Ph.D. Thesis 6. PERFORMING ORG. REPORT NUMBER - -
7. AUTHOR(s) William George Large		8. CONTRACT OR GRANT NUMBER(s) N00014-76-C-0446 NR 083-207
9. PERFORMING ORGANIZATION NAME AND ADDRESS Department of Oceanography, University of British Columbia, Vancouver, B.C., Canada. V6T 1W5		10. PROGRAM ELEMENT, PROJECT, TASK AREA & WORK UNIT NUMBERS - -
11. CONTROLLING OFFICE NAME AND ADDRESS Office of Naval Research, Code 481, NSTL STATION, Mississippi 39529.		12. REPORT DATE August, 1979 13. NUMBER OF PAGES 180
14. MONITORING AGENCY NAME & ADDRESS(if different from Controlling Office)		15. SECURITY CLASS. (of this report) Unclassified 15a. DECLASSIFICATION/DOWNGRADING SCHEDULE - -

16. DISTRIBUTION STATEMENT (of this Report)

Unlimited

17. DISTRIBUTION STATEMENT (of the abstract entered in Block 20, if different from Report)

18. SUPPLEMENTARY NOTES

- -

19. KEY WORDS (Continue on reverse side if necessary and identify by block number)

momentum and heat fluxes at high wind speeds,
drag coefficient: moderate to strong winds,
air-sea interaction.

20. ABSTRACT (Continue on reverse side if necessary and identify by block number)

Two systems for remote measurements of the air-sea fluxes of momentum, sensible heat and moisture during moderate to strong winds are described. One employs the dissipation method and the other the Reynolds flux or eddy correlation method. A modified Gill propeller-vane anemometer is the velocity sensor and a method of resolving the vertical velocity component, that accounts for the propeller's non-cosine behavior and avoids its non-linear operating region, is derived. The dynamic responses of the sensors are

DD FORM 1 JAN 73 1473 EDITION OF 1 NOV 65 IS OBSOLETE
S/N 0102-LF-014-6601

Unclassified
SECURITY CLASSIFICATION OF THIS PAGE (When Data Entered)

found from measurements in the actual turbulent conditions of the flux measurements.

The results of an experiment on the Bedford tower, a stable platform moored in 59m of water 10 km offshore, are presented. Spectra, cospectra, turbulence statistics and transfer coefficients are calculated from the Reynolds flux velocity and temperature data and found to be comparable to previously reported values. Simultaneous dissipation and Reynolds flux estimates of both the momentum and sensible heat fluxes in up to 20 m/s winds are shown to be in excellent agreement.

Also presented are the results of a second experiment where the systems were deployed on the weathership CCGS Quadra. A comparison of ship and tower drag coefficients from the dissipation system, demonstrates that the Bedford tower is essentially an open ocean site. The neutral drag coefficient, CDN, is found, on average, to be nearly constant at 1.14×10^{-3} for winds between 4 and 10 m/s and to increase almost linearly to about 2.18×10^{-3} at 26 m/s. No variation with either fetch (greater than 10 km) or stability is observed. Dissipation estimates of the sensible heat flux from a wide range of conditions are presented. The neutral transfer coefficient, CTN, is found, on average, to vary from about 0.69×10^{-3} in stable stratification to 1.08×10^{-3} in the unstable case. An increase in CTN with increasing wind speed is suggested by only some of the data.

Time series of the fluxes are used to investigate additional sources of variation in the transfer coefficients. Their statistical variability about a running mean is seen to be about 10%. Evidence is presented that indicates that persistent departures from average values are related to sea surface conditions. CDN is observed to be significantly smaller, on average, during rising winds than during falling winds or after a change in wind direction.

THE TURBULENT FLUXES OF MOMENTUM AND SENSIBLE HEAT OVER THE OPEN SEA DURING MODERATE TO STRONG WINDS.

by

WILLIAM GEORGE LARGE

B.A.Sc., University of British Columbia, 1972

N00014-76-C-0476,
N00014-66-C-0477

A THESIS SUBMITTED IN PARTIAL FULFILMENT OF

THE REQUIREMENTS FOR THE DEGREE OF

DOCTOR OF PHILOSOPHY

in

THE FACULTY OF GRADUATE STUDIES

DEPARTMENT OF PHYSICS

INSTITUTE OF OCEANOGRAPHY

We accept this thesis as conforming

to the required standard

Stephen Pond

T.R. Oke

R.W. Burling

THE UNIVERSITY OF BRITISH COLUMBIA

Aug[redacted]79

ABSTRACT

Two systems for remote measurements of the air-sea fluxes of momentum, sensible heat and moisture during moderate to strong winds are described. One employs the dissipation method and the other the Reynolds flux or eddy correlation method. A modified Gill propeller-vane anemometer is the velocity sensor and a method of resolving the vertical velocity component, that accounts for the propeller's non-cosine behavior and avoids its non-linear operating region, is derived. The dynamic responses of the sensors are found from measurements in the actual turbulent conditions of the flux measurements.

The results of an experiment on the Bedford tower, a stable platform moored in 59m of water 10 km offshore, are presented. Spectra, cospectra, turbulence statistics and transfer coefficients are calculated from the Reynolds flux velocity and temperature data and found to be comparable to previously reported values. Simultaneous dissipation and Reynolds flux estimates of both the momentum and sensible heat fluxes in up to 20 m/s winds are shown to be in excellent agreement.

Also presented are the results of a second experiment where the systems were deployed on the weathership CCGS Quadra. A comparison of ship and tower drag coefficients from the dissipation system, demonstrates that the Bedford tower is essentially an open ocean site. The neutral drag coefficient, CDN, is found, on average, to be nearly constant at 1.14×10^{-3} for winds between 4 and 10 m/s and to increase almost linearly to about 2.18×10^{-3} at 26 m/s. No variation with either fetch

(greater than 10 km) or stability is observed. Dissipation estimates of the sensible heat flux from a wide range of conditions are presented. The neutral transfer coefficient, CTN, is found, on average, to vary from about 0.69×10^{-3} in stable stratification to 1.08×10^{-3} in the unstable case. An increase in CTN with increasing wind speed is suggested by only some of the data.

Time series of the fluxes are used to investigate additional sources of variation in the transfer coefficients. Their statistical variability about a running mean is seen to be about 10%. Evidence is presented that indicates that persistent departures from average values are related to sea surface conditions. CDN is observed to be significantly smaller, on average, during rising winds than during falling winds or after a change in wind direction.

Stephen Pond

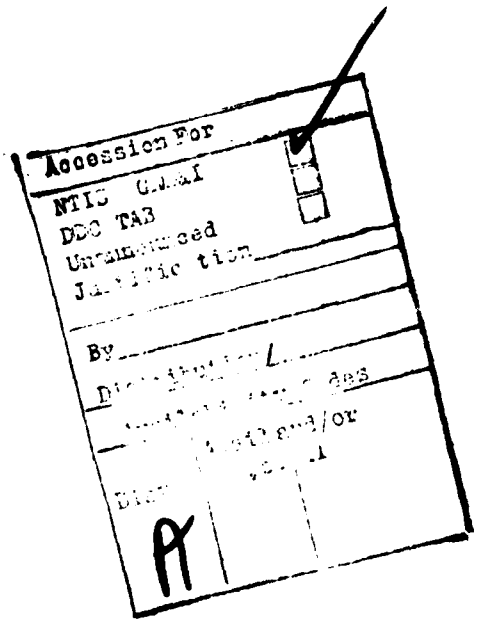

TABLE OF CONTENTS

LIST OF TABLES

LIST OF FIGURES

ACKNOWLEDGEMENT

I should like to express my thanks to the many persons who have contributed to the success of this work. The project was initiated by Dr. S. Pond, who, as research supervisor, continually provided his efforts, guidance and enthusiasm. A great deal is owed to E. Meyer (Meyer Systems Inc.), who designed the electronics and made them work. B. Walker developed much of the mini-computer software. I applaud the efforts of D. English, P. Merchant, H. Heckl and others of the IOUBC staff in building and deploying the instruments.

Throughout the Bedford tower experiment Dr. S. D. Smith and his air-sea interaction group and others at the Bedford Institute provided both logistic and moral support. R. Anderson and D. Hendsbee often serviced the instrumentation in my absence. The co-operation of Captain Dykes, the officers and the crew of CCGS Quadra was essential to the weathership operations. Some servicing was possible at PAPA, thanks to aid from Dr. M. Miyake and his staff (IOS Patricia Bay) and from T. Neuhaus (Seakem Oceanography).

The project was generously supported by the United States Office of Naval Research (Contracts N 00014-66-C-0047 and N 00014-76-C-0446 under Project 083-207) and by the National Research Council of Canada (Grant A8301). I personally received post graduate scholarships from NRC and a fellowship from UBC.

CHAPTER 1 INTRODUCTION

This thesis describes an experimental program designed to measure the turbulent exchanges between the open ocean and the atmosphere in moderate to strong (5-50 m/s) winds. Measurements of the most important exchanges have been the subject of recent reviews, in which they are parameterized by non-dimensional transfer coefficients. Recent determinations of the drag coefficient, which is used to express the momentum flux in terms of the square of the mean wind speed, have been reviewed by Garratt, 1977. The sensible heat and moisture fluxes are parameterized by Friehe and Schmitt, 1976, in terms of the surface - air temperature and humidity differences, respectively and the mean wind speed. There are several obstacles that make open ocean measurements in high winds difficult and that have, therefore, restricted the majority to low winds and to near or onshore platforms. The most common methods of obtaining the fluxes, the Reynolds flux (or eddy correlation) and profile, work best on stable platforms with minimal flow distortion, but these conditions are not easy to satisfy during storms at sea. Adverse conditions accompanying high winds, cause towers to collapse and many sensors either to fail completely or to lose their calibration.

The air-sea energy exchanges are involved in a number of important processes, including the large scale circulations of the ocean and atmosphere and, at smaller scales, thermocline development and wave generation. By extending the existing data set to the open ocean and to higher wind speeds, this

experimental program should be relevant to the study of these processes.

Modelling and predicting large scale features require the fluxes, which are too difficult and costly to measure directly on this scale, to be calculated from easily measured quantities through parameterizations based on relatively few direct observations. For this purpose, extension of the measured transfer coefficients to 20 m/s ought to suffice, because higher winds rarely contribute very much to the fluxes averaged over a month or more (Fissel et al., 1977). A further extension to about 25 m/s should clearly reveal any wind speed dependencies of the coefficients. At present there is an opinion that, in view of the scatter, a constant drag coefficient up to about a 14 m/s wind speed is appropriate (Stewart, 1974), while Smith and Banke, 1975, and others find a significant increase with wind speed. The average stress computed from either type of drag coefficient formulation should be nearly the same, because the trend is, at most, small, but the curl of the wind stress could be affected to a greater degree. The large amount of scatter, typical of turbulence measurements, suggests, that in order to arrive at a representative picture of the open sea, a great deal of data from all possible conditions are required. With a large data set it would be possible to examine the effects of stability, the wave field and other sources of variability in the transfer coefficients apart from the real statistical scatter and systematic instrumentation errors.

Continuous records over a long period of time should include a variety of local and short-lived phenomena, such as frontal passages, for which a large scale parameterization may not be applicable. In some cases it may be possible to find appropriate transfer coefficients and in others direct stress estimates may be the simpler approach. The capability to operate in winds above 40 m/s should allow the entire time histories (winds, temperatures and fluxes) of most storms to be followed. Such time series should be useful for the investigation of many small scale processes.

A modified Gill propeller-vane anemometer proved to be a very suitable velocity sensor for this study. The momentum flux and drag coefficient were successfully measured in 26 m/s winds. Temperature and humidity sensors were housed in protective enclosures. The microbead thermistors were often broken by spray and contaminated by salt, however they did survive some high winds and heat transfer coefficients corresponding to large fluxes were obtained. No useful humidity data were ever recorded, because of the failure of several types of sensors. For open sea work a ship is the most convenient platform and its motion and flow distortion can be tolerated by the dissipation method of measuring fluxes (Pond and Large, 1978). This method was first tested on a stable offshore platform where its results compared favourably to the Reynolds flux method. It was then employed on a ship, allowing open sea data to be collected. In order to gather as much data as possible, the instrumentation was designed to record continuously for a month or more, while operating remotely.

CHAPTER 2 EXISTING THEORY AND EXPERIMENTAL RESULTS

2.1 Air-Sea Interaction

Exchanges between the atmosphere and ocean are most easily measured in the atmospheric surface layer where the transfer processes are dominated by turbulence. Viscous and diffusive molecular transfers are negligible in this layer, which begins a few centimeters above the surface and extends up to a level where the earth's rotation and the geostrophic pressure gradient become important. Detailed treatments of the turbulent flow in the layer may be found in Lumley and Panofsky, 1964, Monin and Yaglom, 1965 and 1967, and Kraus, 1972. This chapter and Busch, 1977, are specifically concerned with the theory related to turbulent flux measurements and their interpretation. Here the sensible heat flux and the momentum flux are treated explicitly and the theory is also extended to any passive atmospheric scalar quantity, R. Following Reynolds' convention, the turbulent properties are partitioned into a mean (< > denotes a time average) and a fluctuation (lower case symbols). The components of the instantaneous wind vector, $\vec{V} = U\vec{i}+V\vec{j}+W\vec{k}$, where $\vec{i}$, $\vec{j}$, and $\vec{k}$ are unit vectors of an x-y-z coordinate system, become $U=\langle U\rangle+u$, $V=\langle V\rangle+v$ and $W=\langle W\rangle+w$. The usual orientation of the axes puts $\vec{k}$ vertically up and $\vec{i}$ along the mean horizontal wind vector such that the mean cross-stream and vertical components, $\langle V\rangle$ and $\langle W\rangle$, are both zero (Burling and Stewart, 1967). Similarly any scalar field R becomes $\langle R\rangle+r$ (and the air temperature $T=\langle T\rangle+t$ and the air pressure $P=\langle P\rangle+p$). By definition $\langle u\rangle$, $\langle v\rangle$, $\langle w\rangle$, $\langle t\rangle$ and $\langle r\rangle$ are all zero.

It is the fluctuating vertical velocity which bodily transports fluid properties up and down, giving rise to the Reynolds fluxes defined by:

$$\begin{aligned} &\text{Momentum flux} && \tau = -\rho \langle uw \rangle \\ &\text{Sensible heat flux} && Hs = \rho\, Cp \langle wt \rangle \\ &\text{any scalar flux} && Hr = \langle wr \rangle , \end{aligned} \qquad (2.1)$$

where ρ is the mean air density and Cp is the specific heat at constant pressure. Since, $\langle W \rangle = \langle w \rangle = 0$, the fluctuating quantities in 2.1 can be replaced by their instantaneous values U, T and R. In this coordinate system $\langle vw \rangle$ should tend to zero with a long enough averaging period, so τ represents the total momentum flux. Since it gives rise to a force in the direction of the mean wind on a unit area of underlying surface, τ is also referred to as the Reynolds stress. Hs is a turbulent heat transfer (positive up). The moisture flux, also an important air-sea exchange, is expressed by simply substituting absolute humidity for R. Similarly gas fluxes such as carbon dioxide may also be considered. Often the terms momentum flux and sensible heat flux refer to the kinematic fluxes $\langle uw \rangle$ and $\langle wt \rangle$.

The Reynolds fluxes arise in the equation of motion and in scalar conservation equations where their surface values become important boundary conditions for both the atmosphere and ocean. In the equation for $\langle U \rangle$ in the boundary layer, the Coriolis force due to the cross-stream component, V, is, on average, zero. The equations for the mean flow and mean temperature in the surface layer, assuming horizontally homogenous turbulence

(Busch, pp 74 and 75), but retaining terms with the largest mean horizontal gradients, are:

$$\rho \frac{\partial \langle U \rangle}{\partial t} = \frac{\partial \tau}{\partial z} - \frac{\partial \langle P \rangle}{\partial x}$$

$$\frac{\partial \langle T \rangle}{\partial t} + \langle U \rangle \frac{\partial \langle T \rangle}{\partial x} + \frac{\partial}{\partial z}\left(\frac{Hs + RT}{\rho\, Cp}\right) = 0 , \qquad (2.2)$$

where RT is the vertical heat transfer due to radiation. With negligible horizontal pressure, horizontal temperature and vertical radiative flux gradients and a steady mean state, the turbulent fluxes are constant throughout the layer. It is then possible to measure the surface fluxes above wave influences at a convenient height, Z. However, away from the surface, rotation and the large scale horizontal gradients eventually become influential.

In steady flow, the measured stress, $\tau(Z)$, is less than the surface stress, τ_o. If the difference at a height, hc, is 10% (Lumley and Panofsky, 1964, arbitrarily use 20%), then the flow below can be regarded as being a "constant flux" or "constant stress" layer. Effectively, hc is taken to be the upper limit of the atmospheric surface layer. In mid-latitudes winds above the surface layer are governed by the geostrophic balance,

$$f\ Ug = 1/\rho\ \partial \langle P \rangle / \partial n ,$$

where f is the Coriolis parameter (about $1 \times 10^{-4}\ s^{-1}$), Ug is the geostrophic wind and n is a horizontal coordinate perpendicular to the Ug direction. Observations have shown Ug to be about

1.3 $\langle U \rangle$ and about 16° to the right of the $\vec{i}$ direction (Deacon, 1973). Substituting, $\partial \langle P \rangle / \partial x \cong \sin 16° \; \partial \langle P \rangle / \partial n$, into the first of 2.2 yields,

$$\frac{\partial \langle U \rangle}{\partial t} \cong \frac{1}{\rho} \frac{\partial \tau}{\partial z} + 1.3 \; f \langle U \rangle \sin 16° \; .$$

In steady flow a 10% reduction is found when

$$0.1 = \frac{\tau_o - \tau(z)}{\tau_o} \cong \frac{1.3 \; f \langle U \rangle}{\tau_o / \rho} \sin 16° \; z \; ,$$

$$\text{so} \quad hc \cong \frac{0.1 \langle uw \rangle}{1.3 \; f \langle U \rangle \sin 16°} \cong 2790 \text{ seconds } \frac{\langle uw \rangle}{\langle U \rangle}. \qquad (2.3)$$

Measurements over the sea at 10m have almost always shown $\langle uw \rangle / \langle U \rangle$ to average more than 10^{-3} $\langle U \rangle$ (drag coefficient > 1×10^{-3}, Garratt, 1977), setting 14m as a lower limit of hc, when $\langle U \rangle$=5 m/s. In unsteady flow, $\partial \langle U \rangle / \partial t$ can easily be the same order of magnitude as (1.3 f $\langle U \rangle$ sin 16°) ≅ 0.13 $\langle U \rangle$ /hour. On the rising wind the acceleration is down the pressure gradient and hc rises, because a smaller stress gradient is sufficient to balance 2.2. On the falling wind the loss of flux with height is enhanced by the deceleration and in this situtaion hc may be considerably lower. These arguments are possibly good to a factor of 2 despite the neglect of horizontal advection terms, relative to $\partial \langle P \rangle / \partial x$. They serve to point out that, with the same surface stress, the measured 10m stress may be greater on the rising wind than during falling winds, when it could be less than the surface stress by 5 to 10%.

The height to which the sensible heat flux remains within 10% of its surface value is not obvious and it may sometimes be below usual measurement heights. Since $\partial\langle T\rangle/\partial x$ is not simply related to the large scale pressure gradient, it is not possible to scale the vertical divergence of Hs to a Coriolis term as was done for the Reynolds stress. Neglecting radiation, a 10% change in Hs is found at a height hc given by

$$hc = 0.1 \langle wt \rangle (\delta T/\delta t)^{-1} ,$$

where δT is the change in temperature due to the vertical heat flux divergence, during a time interval δt. Measurements over the sea show that $\langle wt \rangle$ is of order $10^{-3} \langle U \rangle \Delta T$ (Friehe and Schmitt, 1976), where ΔT is the temperature difference between the sea surface and atmosphere. To keep hc above 10m, with $\langle U \rangle \Delta T$ as low as 10 °Cm/s requires

$$\delta T/\delta t < 0.36 \text{ °C/hour},$$

which may not necessarily be satisfied. When $\partial\langle T\rangle/\partial t$ over the sea is large, presumably horizontal advection is the major contributor with $\delta T/\delta t$ hopefully remaining small. When the temperature is steady $\langle U \rangle \partial\langle T\rangle/\partial x$ must balance $\partial Hs/\partial z$ in 2.2, giving

$$hc = 10^{-4} \Delta T (\partial\langle T\rangle/\partial x)^{-1}$$

and implying that hc is only above 10m when the horizontal

temperature gradient is rather small, less than 0.01 °C/km for a ΔT of 1°C. A further complication arises during low winds when infrared absorption by water vapour may produce a radiative flux divergence that tends to cause Hs to increase with height (Busch, 1977). This effect enhances the positive flux gradient when ΔT is negative, but reduces the loss of sensible heat flux with height when ΔT is positive. It will be assumed that Hs anywhere in the "constant stress" layer over a temperate sea is equivalent to the surface flux to within the accuracy of the measurement. Hopefully, this assumption is true on average, but verification would require a direct measurement of Hs at two levels.

2.2 Monin-Obukhov Similarity Theory

The understanding of the turbulent atmospheric surface layer is largely due to Monin-Obukhov similarity theory (Monin and Yaglom, p 425 ff). The theory assumes that turbulent characteristics depend only on a few physical parameters, which facilitates the application of dimensional analysis. Above the direct influence of the bottom boundary the important parameters are the height (the only spatial variable left in the assumed horizontally homogenous turbulence), the air density, the turbulent transports and the stability of the air column. The supposed height independence of the fluxes naturally leads to the following scales which incorporate the transports through the layer and the density:

$$\begin{aligned} \text{friction velocity} \quad u^* &= (\tau_o/\rho)^{1/2} = |-\langle uw\rangle|^{1/2} \\ \text{temperature scale} \quad t^* &= -\langle wt\rangle / Ku^* \\ \text{scalar scale} \quad r^* &= -\langle wr\rangle / Ku^* , \end{aligned} \tag{2.4}$$

where von Karman's constant, K, is included to simplify later equations, but other scales

$$T^* = -\langle wt\rangle / u^*$$

and

$$R^* = -\langle wr\rangle / u^*$$

are sometimes used. An appropriate stability parameter, Z/L, is obtained from the ratio of the convective or buoyant turbulent kinetic energy, B, produced in a non-neutral air column, to the purely mechanical production in the equivalent neutral case, Po. It will be seen in section 2.5, that

$$B = g\langle w\, Tv\rangle / To \quad \text{and} \quad Po = u^{*3}/KZ , \tag{2.5}$$

where Tv, the virtual temperature in degrees Kelvin, accounts for the fluctuating temperature and moisture contributions to the fluctuating density, g is gravitational acceleration and To is the local average virtual temperature. The important scale is the Monin-Obukhov length, L, whose magnitude gives the height at which $Po = |B|$, thus

$$\frac{-Z}{L} = \frac{B}{Po} \quad \text{and} \quad L = \frac{-u^{*3}\, To}{K\, g\, \langle w\, Tv\rangle} . \tag{2.6}$$

In neutral stratification $\langle w\, Tv\rangle$ and Z/L go to zero while L

approaches infinity and the sign is chosen to make L and Z/L positive in stable conditions. Dimensional analysis predicts that all turbulent functions non-dimensionalized by Z, u*, r* and L should be functions of the only possible dimensionless group, Z/L. Note that each additional scalar adds both a scale and a dimension to the problem. Use of spectra introduces a frequency, f, making a further dimensionless group, fZ/u*, possible, but because of the difficulty in obtaining u* the dimensionless natural frequency n = fZ/<U> is usually substituted. Normalized spectra and cospectra can be regarded as non-dimensional turbulent functions and therefore should be functions of both n and Z/L, whereas their integrals such as $(\sigma u)^2 = \langle u^2 \rangle$ and $(\sigma t)^2 = \langle t^2 \rangle$ should depend only on Z/L. With the important parameters common to all surface layer flows, the structure of the turbulence, according to this theory, must always be "similar", with any dependencies on Z/L and n being universally applicable.

An important consequence of similarity theory is the logarithmic profile of the mean wind and mean scalars. Dimensional considerations lead directly to the forms:

$$\frac{Kz}{u^*}\frac{\partial \langle U \rangle}{\partial z} = \phi_m(Z/L)$$

$$\text{and} \quad \frac{z}{r^*}\frac{\partial \langle R \rangle}{\partial z} = \phi_r(Z/L) \ , \qquad (2.7)$$

where von Karman's constant sets $\phi_m=1$ at neutral stability and has already been included in the definition of r* so that $\phi_r(0)=1$. Measured values of K vary between about 0.35 and 0.42

(Busch, 1977), so at least a 5% error in its customary value of 0.40 must be allowed. In a review of flux-profile relationships, Dyer, 1974, suggests that the best forms of the universal functions are

$$0 < Z/L < 0.2: \qquad \phi_m = \phi_r = 1 + 5\, Z/L$$

$$-1.0 < Z/L < 0: \qquad \phi_m = (1 - 16\, Z/L)^{-1/4}$$

$$\phi_r = (1 - 16\, Z/L)^{-1/2} ,$$

where the unstable case is the Businger-Dyer representation provided by Dyer and Hicks, 1970. The mean values at a height Z, UZ and RZ, are found by integrating 2.7, (Paulson, 1970),

$$UZ = (u^*/K) \cdot [\ln(Z/Zo) - \Psi_m(Z/L)\ ]$$

$$RZ = RSFC + r^* [\ln(Z/Zor) - \Psi_r(Z/L)\ ], \qquad (2.8)$$

where $\Psi(Z/L) = \int_0^{Z/L} [1 - \phi(\xi)]/\xi \; d\xi$

stable: $\Psi_m(Z/L) = \Psi_r(Z/L) = -5\, Z/L$

unstable: $\Psi_m(Z/L) = 2 \ln[(1+X)/2] + \ln[(1+X^2)/2] - 2 \tan^{-1}X + \pi/2$

$$\Psi_r(Z/L) = 2 \ln[(1+X^2)/2]$$

with $X = (1 - 16\, Z/L)^{1/4}$.

At neutral stability the integral vanishes, leaving $\Psi(0)=0$. The constants of integration Zo and Zor, assumed to be much

smaller than Z, are the roughness lengths, which fully describe the surface as "seen" by the turbulence, but they are not simply related to sea surface parameters such as wave height and temperature. They need to be included in the dimensional analysis only near the surface where they set the magnitude, but not the structure, of the turbulence throughout the layer.

2.3 Bulk Aerodynamic Parameterizations

The fluxes are parameterized in terms of the mean wind, the sea surface-air temperature difference and surface-air mean scalar difference, ΔR, with the bulk aerodynamic formulae:

$$\begin{aligned} \tau/\rho &= u^{*2} = -\langle uw \rangle = CD \langle U \rangle^2 \\ Hs/\rho Cp &= -K u^* t^* = \langle wt \rangle = CT \langle U \rangle \Delta T \\ Hr &= -K u^* r^* = \langle wr \rangle = CR \langle U \rangle \Delta R, \end{aligned} \qquad (2.9)$$

with $\Delta T = TSCF - TZ$ and $\Delta R = RSFC - RZ$, where TSFC and RSFC are the mean surface temperature and scalar values, respectively. The non-dimensional transfer coefficients CD and CT are the drag coefficient and Stanton number while the corresponding coefficient of moisture transport, CE, is the Dalton number. Their dependence on stability, roughness and height is evident from 2.8, but Zo over the sea has a complicated functional form (Burling and Stewart, 1967). However, they can also be determined experimentally from 2.9 using measured fluxes and bulk quantities and such calculated coefficients provide a

convenient means of comparing flux measurements. To eliminate the variation with height they are commonly evaluated at 10m as:

$$\begin{aligned} C10 &= -\langle uw \rangle / (U10)^2 \\ CT10 &= \langle wt \rangle / [U10\ (TSFC-T10)] \\ CR10 &= \langle wr \rangle / [U10\ (RSFC-R10)]\ . \end{aligned} \qquad (2.10)$$

Equation 2.8 shows the wind speed, temperature and scalar means at 10m (U10, T10 and R10) to be:

$$\begin{aligned} U10 &= UZ - (u^*/K)[\ln(Z/10m) - \Psi_m(Z/L) + \Psi_m(10m/L)] \\ T10 &= TZ - t^*[\ln(Z/10m) - \Psi_t(Z/L) + \Psi_t(10m/L)] \\ R10 &= RZ - r^*[\ln(Z/10m) - \Psi_r(Z/L) + \Psi_r(10m/L)]\ . \end{aligned} \qquad (2.11)$$

For comparative purposes it is convenient to eliminate the stability dependence by evaluating the roughness lengths from 2.8 and using them to find the coefficients in the equivalent neutral case at 10m from:

$$\begin{aligned} CDN &= K^2 / [\ln(10m/Zo)]^2 \\ CTN &= K^2 / [\ln(10m/Zot) \cdot \ln(10m/Zo)] \\ CRN &= K^2 / [\ln(10m/Zor) \cdot \ln(10m/Zo)]\ . \end{aligned} \qquad (2.12)$$

The neutral coefficients should be constants over homogeneous terrain where the roughness lengths can be regarded as constant. This prediction has been verified over land where Zo, for example, is exclusively determined by topography and vegetation. It is not unreasonable to expect this concept to

work even better over the sea where there is only one type of surface. However, direct measurements, reviewed by Garratt (1977) are very scattered and indicate that the neutral drag coefficient varies with wind speed and is much smaller than that found over land. This result implies that there are additional important parameters determining the roughness of the sea surface. An obvious difference between a land and sea boundary is surface gravity waves, so it seems appropriate to add the acceleration due to gravity, g, to the problem. This leads to the Charnock (1955) dimensionless group for flow near the waves,

$$Zo \quad g \; / \; u^{*2} \; = \; \alpha \qquad (2.13)$$

where $\alpha = 0.0144$ is suggested by Garratt (1977). Stewart, 1974, notes that for winds below 10 m/s the Charnock representation with α constant predicts a more rapid increase in CDN with wind speed than is indicated by the results of Brocks and Krüggermeyer (1970) and this feature is also present in Garratt's review. It appears, therefore, that more surface parameters may be important to this aspect of turbulent flow. Stewart discusses the possible roles of surface tension (capillary waves), the length and phase speed of the longest excited waves, the wave slope and the total wind generation force which is proportional to (wind speed - wave speed). Kitaigorodskii and Zaslavskii, 1974, consider the phase speed of the dominant wave and a purely viscous momentum flux. Burling and Stewart, 1967, examine the implications of dependency on various moments of the wave spectrum. With the roughness

lengths possibly depending on many parameters it appears that a rather detailed knowledge of the sea surface would be required before the turbulent fluxes over the sea could be found from Zo and Zor.

The parameterizations can also be regarded as empirical formulae. An experimental formulation of the neutral coefficients at 10m, 2.12, for example, would allow the fluxes to be estimated from mean or bulk quantities, UZ, TZ and TSFC (ΔT = TSFC-TZ), with Z/L, if known, providing a stability correction.

The momentum flux can be found from 2.9 by finding the drag coefficient at the measurement height, Z, the wind speed, UZ, and the stability, Z/L, from CDN. Elimination of Zo from 2.12 and 2.8 and substitution into 2.9 leaves,

$$CD = CDN \{1+ CDN^{1/2} K^{-1} (\ln(Z/10m) - \Psi_m(Z/L))\}^{-2}, \quad (2.14)$$

where $\ln(Z/10m)$ and $\Psi_m(Z/L)$ describe the variation of the drag coefficient with height and stability, respectively. If CDN is given as a function of the 10m wind, then UZ must first be shifted to 10m before a drag coefficient can be determined. Substituting $u^*/UZ = CD^{1/2} = C10^{1/2}\ U10/UZ$, into 2.11 and solving for UZ/U10 leaves,

$$UZ/U10 = 1+ C10^{1/2}\ K^{-1} [\ln(Z/10m) - \Psi_m(Z/L) + \Psi_m(10m/L)].$$

The term in square brackets, K(Z,Z/L), is usually dominated by

$\ln(Z/10m)$, which, with $C10^{1/2}/K \cong 0.1$, makes U10 about 10% larger or smaller than UZ for a Z of 3.7m and 27m, respectively. Throughout this height range neglect of the stability portion of $K(Z,Z/L)$ introduces an error in U10 of less than 2% for $-1.0 < Z/L < 0.08$, however at Z=27m it decreases U10 by about an additional 6% with Z/L=0.2 and 3% at Z/L=0.1, so it is not ignored. C10 is equivalent to CD at Z=10m, so 2.14 gives

$$C10^{1/2} = CDN^{1/2} \{1 - K^{-1} CDN^{1/2} \Psi_m(10m/L)\}^{-1} .$$

Since $\Psi_m(10m/L)$ ranges from about 1 at Z/L= -1 to about -1 at Z/L=0.2, taking the term in curly brackets to be 1.0 introduces an error of only 1% in U10, which is within usual measurement error, when it is calculated from UZ, CDN and Z/L using

$$U10 \cong UZ \; [1 + CDN^{1/2} \; K^{-1} \; K(Z,Z/L)]^{-1}. \qquad (2.15)$$

Should CDN itself depend on U10, 2.15 may have to be solved with an iterative technique.

If the stability is in the range $-1.0 < Z/L < 0.2$, but is unknown and assumed to be neutral, errors arise from an inaccurate U10, in finding CDN from U10 and through 2.14, because CDN is not shifted to the proper stability. The total error in U10's found from 2.15 should be less than 10%. Smith and Banke, 1975, report a drag coefficient equal to 0.00061 + 0.000075 U10, so a 10% error in U10 at 20 m/s, reduces to 7% in CDN and the momentum flux, which is less than the error associated with direct measurements. With $\Psi_m(Z/L)$ ranging from

1.0 to -1.0, taking it to be zero could lead to a 20% error in the momentum flux. Only in the range $-0.25 < Z/L < 0.1$ does the total error in assuming neutral stability remain less than 10%.

If CD and CDN are available, the analogous procedure can be followed to find the sensible heat flux from TZ, TSFC, and UZ, using 2.9. The Stanton number, CT, is expressed as a function of CTN, CDN, CD, and Z/L, by eliminating Zo and Zot from 2.12 and 2.8, then substituting into 2.9:

$$CT = \frac{CTN \quad (CD/CDN)^{1/2}}{[\,1+CTN\ K^{-1}\ CDN^{-1/2}\ (\ln(Z/10m)-\psi_t(Z/L))\,]} \quad (2.16)$$

The major error comes from the uncertainty in CTN. The errors in CDN and CD due to U10 cancel in (CD/CDN) and a 10% error in CDN and CTN introduces a 2% error in the denominator. Since $\psi_t(Z/L)$ is not very different from $\psi_m(Z/L)$, assuming neutral stability causes about the same error in CT as in CD. However, this assumption is never needed, because a means of estimating Z/L from UZ and ΔT, which are required in 2.9, is developed in section 2.6. The uncertainty of this estimate (section 4.2) should result in about a 5% error in CT and CD.

The sensible heat flux is sometimes parameterized as

$$\langle wt \rangle = a\ U10\ (TSFC-T10) + b\ ,$$

where a and b are experimentally determined functions of stability and wind speed. The air temperature at 10m, T10, can be found as follows; from 2.11

$$TZ - T10 = t^* [\ln(Z/10m) - \psi_t(Z/L) + \psi_t(10m/L)],$$

where the term in square brackets, to be denoted as $Kt(Z,Z/L)$, behaves as $K(Z,Z/L)$ and the stability contribution can again be ignored in near neutral conditions. Substituting for t^* using 2.9 gives

$$T10 = TZ + (CT/CD^{1/2})\, K^{-1}\, (TSFC-TZ)\, Kt(Z,Z/L). \qquad (2.17)$$

2.4 The Reynolds Flux Method

The Reynolds flux or eddy correlation method is the most direct measurement of the fluxes and has been employed over the sea by Pond *et al.*, 1971, Hicks, 1972, Smith and Banke, 1975, and others. It involves integrating the cospectra of w and either u or r to obtain the covariances and hence fluxes. The spectral forms of the covariances are:

$$\begin{aligned} \langle uw \rangle &= \int \phi_{uw}(f)\, df \\ \langle wt \rangle &= \int \phi_{wt}(f)\, df \\ \langle wr \rangle &= \int \phi_{wr}(f)\, df. \end{aligned} \qquad (2.18)$$

In practice the cospectra are determined by digital fast Fourier transform techniques, which give discrete values of $\phi(f)$ at intervals of f such that $\phi(f)\,\Delta f$ gives the covariance in a band centered at f of width Δf. The highest frequency computed, the Nyquist frequency, fny, is set by the digitization period Δt:

($f_{ny}=1/2\Delta t$). Contributions from higher frequencies can be allowed to alias back below f_{ny} so that the effective upper limit of the integration is increased (to about 2 f_{ny} in the system described in section 3.3). The contributions to the covariances from natural frequencies, $n=fZ/\langle U\rangle$, greater than 1 are only a few per cent of the total. With 20 m/s winds, measurements at 10 m will therefore include most of the high frequency contributions if Δt is no longer than $Z/\langle U\rangle$, about 0.5 seconds. The lowest calculated frequency, f_1, is the reciprocal of the duration of the measurement and $\phi(f_1)$ includes the covariance down to $f_1/2$. Some cospectra are still non-zero at $n=0.001$, so in order to be able to measure fluxes in 5 m/s winds at 10 m the samples must be taken for about $Z/(0.002\langle U\rangle) \cong 1000$ seconds or about 15 minutes. However $\phi(f_1)$ is not a statistically well determined quantity and in practice at least 3 sequential determinations need to be averaged, requiring the duration of a flux run to be at least 45 minutes.

Unfortunately, measurements cannot be extended to more than about 1 hour because stationarity begins to be lost as a new flow situation develops. The low frequency contributions to the fluxes are often not well established by the Reynolds flux method. It is also clear that another disadvantage to this method is the large amount of data required. For example, a single $\langle uw\rangle$ estimate from a 45 minute run with $\Delta t=0.5$ seconds requires about five thousand digitizations of each variable. Of course the spectra of the measured quantities may also be found from the same data and are often a great advantage in checking sensor performance. The sensitivity of the Reynolds flux method

to instrument orientation is a great handicap on ships and buoys, whose motion and mean tilt effect the measured covariances. A one degree error in the mean tilt of an anemometer may induce errors in <uw> in the order of 10% (Pond, 1968). It is possible to measure the instantaneous platform motion and to correct the velocities point by point (Mitsuta and Fujitani, 1974), but this greatly increases the recording requirements and is not a very practical means of obtaining large amounts of open sea flux measurements.

The Reynolds flux method is not very applicable to remote open sea operation, but it has become the standard to which other methods are compared either directly or through the calculated transfer coefficients.

2.5 The Dissipation Method

Following Deacon's, 1959, suggestion the dissipation method has been employed in open sea conditions by Pond *et al.*, 1971, Wucknitz, 1976, Denman and Miyake, 1973, and others. It is a very attractive method because it does not invclve an explicit measurement of the vertical velocity, allowing moving platforms to be used and reducing measurement errors. In addition, flow distortions that would hinder covariance measurements, can be tolerated. Instead, the major sources of error arise in the uncertainty of various constants and in the necessary assumptions. In the cited studies its results have been

compared to direct Reynolds flux measurements up to moderate winds, but further comparison at high wind speeds is still necessary.

In the case of the momentum flux the method stems from a consideration of the balance of turbulent kinetic energy per unit mass, $e = (u^2 + v^2 + w^2)/2$, in horizontally homogeneous flow (Busch, 1977),

$$\frac{\partial \langle e \rangle}{\partial t} = u^{*2} \frac{\partial \langle U \rangle}{\partial z} + g \frac{\langle w\, Tv \rangle}{To} - \epsilon - \frac{\partial}{\partial z} \left[\langle we \rangle + \frac{1}{\rho} \langle wp \rangle \right]$$

$$= \quad P \quad + \quad B \quad - \epsilon - \quad D \,, \qquad (2.19)$$

where Tv is the virtual temperature in degrees Kelvin and To its local average and p is the fluctuating pressure. Turbulent fluctuations are chiefly produced by mechanical interactions of the Reynolds stress with the mean flow represented by the first term, $P = u^{*2}\, \partial \langle U \rangle / \partial Z$ and lost at small scales to molecular dissipation, ϵ. From Lumley and Panofsky, 1964 p95, B is recognizable as the loss or gain due to buoyancy referred to in section 2.2. D is the sum of two vertical divergences: the first, of the turbulent kinetic energy flux $\langle we \rangle$ and the second, of the work done per unit area by the fluctuating pressure, $\langle wp \rangle / \rho$. These are referred to as the turbulent and pressure transports of kinetic energy, respectively. The complete divergence term has been investigated by McBean and Elliot, 1975. In this work $\langle we \rangle$ and $\langle wp \rangle$ were measured over land at one height for a range of Z/L values. A fit between $-0.31 < Z/L < 0.12$ gave

$$\langle wp \rangle / (\rho u^{*3}) = 2.3\, z/L - 0.20 .$$

Their <we> results were plotted with those of Garratt, 1972, and Banke and Smith, 1973. In view of the scatter it is not unreasonable to assume a relation

$$\langle we \rangle / u^{*3} \cong -2.3\, z/L + \text{constant}.$$

Extensive measurements over land of the turbulent transport term have been made by Wyngaard and Coté, 1971, over a wider range of stabilities. In unstable conditions their results can be expressed as

$$\langle we \rangle / u^{*3} = -2.5\, z/L + \text{constant}.$$

The combined experimental evidence in the range $-1 < z/L < 0.1$ suggests that to a very good approximation

$$\langle we \rangle + \langle wp \rangle/\rho \cong \text{a constant}$$

Differentiation by z implies that on average, the kinetic energy gained through pressure transport nearly balances that lost by turbulent transport, that is, D=0. Wyngaard and Coté also conclude that the effects of horizontal inhomogeneities and non-stationarity are negligible by more than two orders of magnitude, that is, $\partial \langle e \rangle / \partial t \cong 0$.

Combining 2.6 and the profile equations, 2.7, with the remaining terms in 2.19 results in the simple set of equations:

$$P = (u^{*3} / KZ)\ \phi_m(Z/L) = Po\ \phi_m(Z/L)$$

$$B = -(u^{*3} / KZ)\ Z/L = -Po\ Z/L$$

$$\epsilon = Po\ [\phi_m(Z/L) - Z/L]$$

where Po, introduced in section 2.2, is the mechanical production in the equivalent neutral case. Thus u* can be simply expressed as a function of ϵ and Z/L:

$$u^{*3} = K\ Z\ \epsilon\ /\ [\phi_m(Z/L) - Z/L]\ . \qquad (2.20)$$

In a similar fashion the problem of evaluating r* and the scalar fluxes can be simplified to finding u* and the dissipation rate of scalar fluctuations, Nr. The analogue of 2.19 is the simpler scalar variance budget, (Busch, 1977),

$$\frac{1}{2}\frac{\partial \langle r^2 \rangle}{\partial t} = -\langle wr \rangle \frac{\partial \langle R \rangle}{\partial z} - Nr - \frac{1}{2}\frac{\partial \langle wr^2 \rangle}{\partial z}\ . \qquad (2.21)$$

The study of Wyngaard and Coté (1971) investigates this equation thoroughly for temperature. The vertical divergence term turns out to be an order of magnitude smaller than the production term and the time rate of change and inhomogeneities are again negligible. Substituting for $\partial \langle R \rangle / \partial z$ from 2.7 gives the straightforward relationship

$$r^{*2} = Nr \; Z \; / \; [K \; u^* \; \phi r(Z/L)] \; . \qquad (2.22)$$

Direct measurements of ϵ and Nr are difficult because they involve centimeter scales (frequencies well beyond 100 Hz). However, they can be inferred from the spectra of the scalars, $\phi r(f)$, and downstream velocity, $\phi u(f)$, at frequencies, f, in the -5/3 region where the Kolmogoroff hypothesis predicts

$$\phi u(f) = K' \epsilon^{2/3} \; (2\pi/\langle U \rangle)^{-2/3} \; f^{-5/3}$$
$$\phi r(f) = Br' \; Nr \; \epsilon^{-1/3} \; (2\pi/\langle U \rangle)^{-2/3} \; f^{-5/3} \; , \qquad (2.23)$$

where Taylor's hypothesis is used to replace the downstream radian wavenumber with $(2\pi f/\langle U \rangle)$. The form of these equations is also based on dimensional analysis so the 1-dimensional Kolmogoroff constants K' and Br' may be functions of stability, but they are not, as yet, well enough established for any dependency to be observable. Reasonable values are K' = 0.55 and Br' = 0.80 for both temperature and moisture (Paquin and Pond, 1971 and Busch, 1977), with a possible 10% error. In terms of the natural frequency, $n=fZ/\langle U \rangle$, the -5/3 region has been found to be well developed by n=1 so that dissipation estimates may be obtained from relatively low frequencies (about 2 Hz, for 20 m/s winds at 10m height).

Several methods of calculating the momentum flux from measurements of ϵ and Z/L are feasible. The simplest, method 1, used by Denman and Miyake, 1973, is to employ the neutral form of 2.20

$$\langle uw\rangle_{DISS1} = (K Z \epsilon)^{2/3} . \qquad (2.24)$$

This equation is also valid in non-neutral conditions providing there is an overall balance between the vertical divergences, the buoyant production and the stability modification of the mechanical production. The experimental evidence over land suggests that the complete form of 2.20 should be tested over the sea. Method 2, therefore, assumes only that the vertical divergences balance and uses

$$\langle uw\rangle_{DISS2} = (K Z \epsilon)^{2/3} \cdot (\phi_m(Z/L) - Z/L)^{-2/3} \qquad (2.25)$$

This is the method used by Khalsa and Businger, 1978, and by Wucknitz, 1976, but the latter uses a Richardson number formulation and the former assume a balance, following Wyngaard and Coté, of buoyancy and turbulent transport with a pressure transport of order -Z/L to arrive at 2.25. It has often been assumed that local production, P, balances dissipation (Smith and Banke, 1975), implying an overall balance between the two divergences and buoyancy. This is the assumption of method 3, which states

$$\langle uw\rangle_{DISS3} = (K Z \epsilon)^{2/3} \cdot [\phi_m(Z/L)]^{-2/3} . \qquad (2.26)$$

Pond *et al.*, 1971, found that in unstable conditions the momentum flux from the dissipation and Reynolds flux methods were in the best agreement if they assumed that the reduction in mechanical production due to stability modification of the

profile was compensated by the net gain in turbulent energy from vertical divergences, that is, $\epsilon = Po + B$. This fourth method is expressed by

$$\langle uw \rangle DISS4 = (K Z \epsilon)^{2/3} \cdot (1 - Z/L)^{-2/3}. \qquad (2.27)$$

The general expression of the four dissipation methods is

$$\begin{aligned} \langle uw \rangle DISS &= (K Z \epsilon)^{2/3} \cdot FX \\ \text{Method 1} \quad F1 &= 1 \\ \text{Method 2} \quad F2 &= [\phi_m(Z/L) - Z/L]^{-2/3} \\ \text{Method 3} \quad F3 &= [\phi_m(Z/L)]^{-2/3} \\ \text{Method 4} \quad F4 &= [1 - Z/L]^{-2/3}. \end{aligned} \qquad (2.28)$$

The functions, FX, are plotted in figure 1 over the range of stabilities likely to be encountered over the sea at mid-latitudes. It is apparent that a reasonable measure of stability is important to all but method 1. Any one of the methods may be valid over an individual run, but over any stability range there should be one dissipation method that is the most appropriate, on average.

Equations 2.23 and 2.28 indicate that $\langle uw \rangle$ from all the dissipation methods is proportional to

$$[K Z]^{2/3} K^{1-1} (\phi_u(f) \langle U \rangle^{-2/3}). \qquad (2.29)$$

Even with no error in the measurement of $\phi_u(f)$ and $\langle U \rangle$, the uncertainties in K, 5%, in the measurement height Z, say 0.5m in

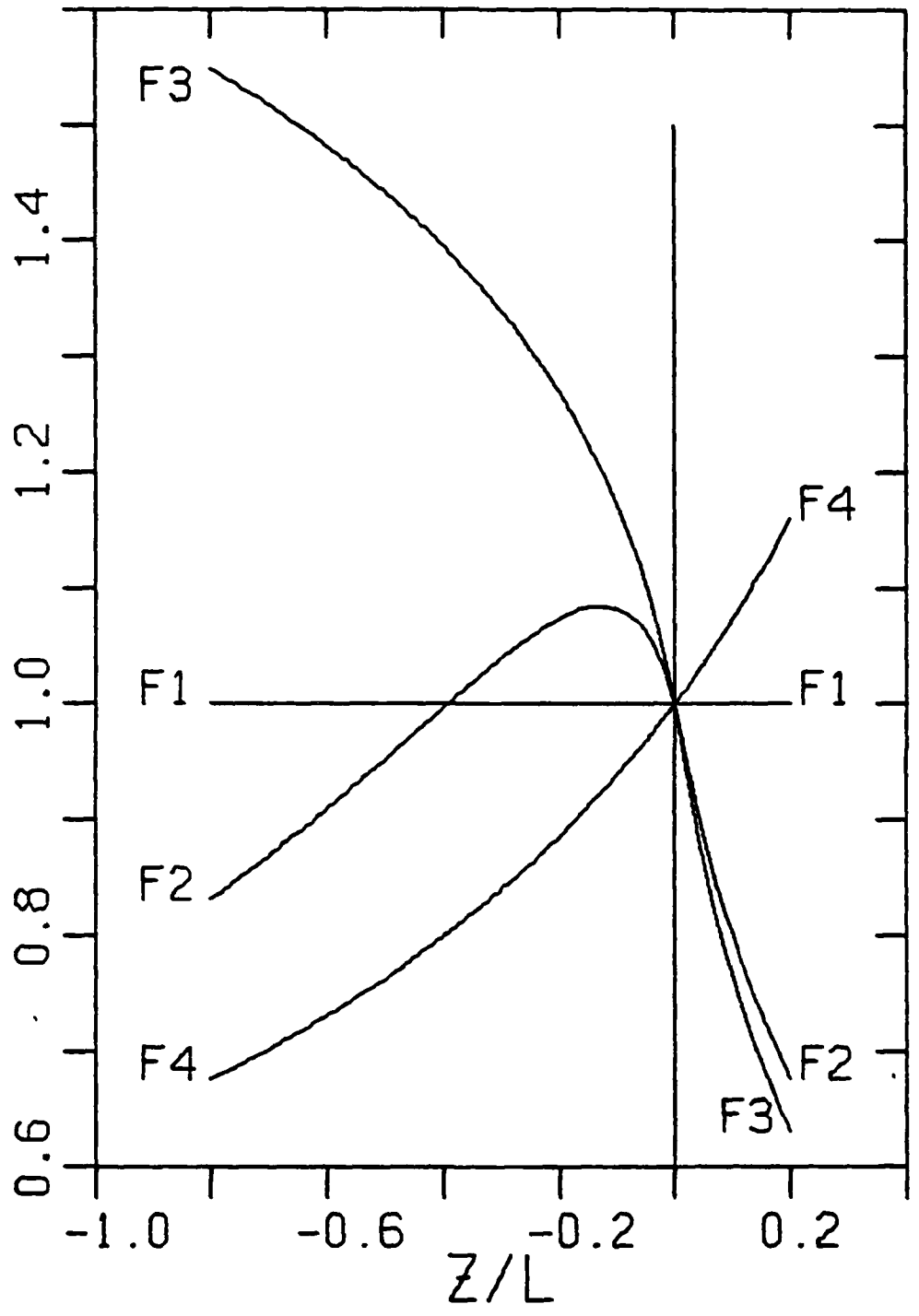

FIGURE 1 Stability adjustments to the four dissipation methods of estimating the momentum flux.

10m and in K', 10%, could combine to produce a 15% error in <uw>. These errors and assumption errors are likely to be somewhat systematic, but fortunately they are not the same in the Reynolds flux method. Intercomparisons with Reynolds flux measurements are therefore essential, in order to establish the "best" dissipation method and to ensure that there are no major systematic errors.

There are fewer ways of "juggling" the terms of 2.21 to arrive at Nt, and only two methods of calculating the sensible heat flux are practical. At neutral stability and when the vertical divergence term is balanced by stability modification of the temperature profile, method 1, gives

$$\langle wt \rangle_{DISS1} = [\, K\, u^*\, N_t\, Z \,]^{1/2} . \qquad (2.30)$$

Again the experimental evidence over land suggests using 2.22 from which method 2 assumes

$$\langle wt \rangle_{DISS2} = [\, K\, u^*\, N_t\, Z \,]^{1/2} \cdot [\, \phi_t (Z/L) \,]^{-1/2} . \qquad (2.31)$$

The general form of calculating the sensible heat flux is simply

$$\langle wt \rangle_{DISS} = [\, K\, u^*\, N_t\, Z \,]^{1/2} \cdot FX$$

$$\text{Method 1} \quad F1 = 1.0 \qquad (2.32)$$

$$\text{Method 2} \quad F2 = [\, \phi_t (Z/L) \,]^{-1/2} .$$

F1 and F2 are shown in figure 2. The methods differ considerably even near neutral stability, therefore, the "best"

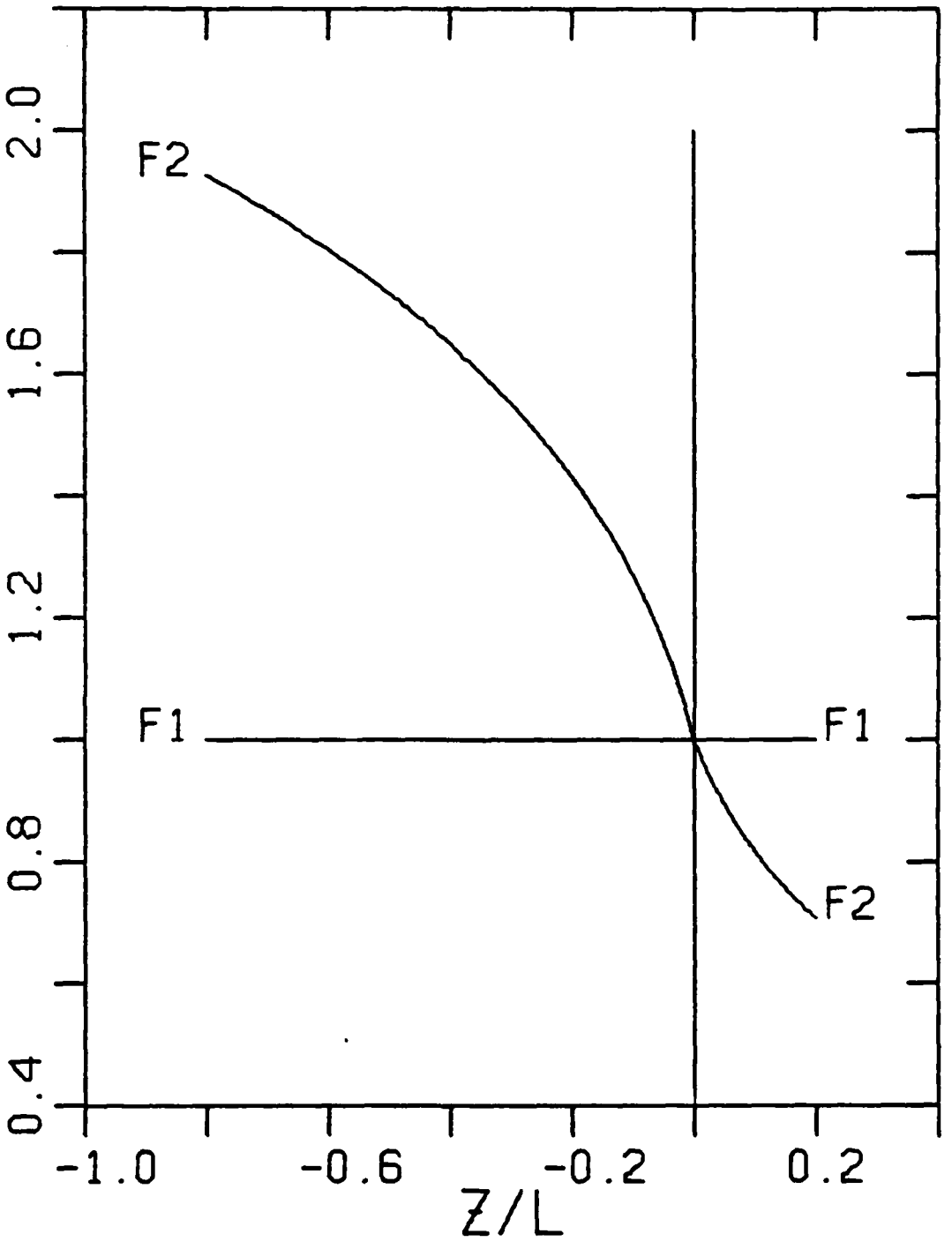

FIGURE 2 Stability adjustments of the two dissipation methods of estimating the sensible heat flux.

method should be easy to establish, depending on the accuracy of the stability measurements, since method 2 is sensitive to errors in Z/L.

Equations 2.32, 2.23 and 2.20 indicate that <wt> from both dissipation methods is proportional to

$$\frac{(K\,Z)^{2/3}}{[Bt'\,K']^{1/2}} \quad [\phi t\ \phi u]^{1/2} \quad \langle U\rangle^{-2/3} \ . \qquad (2.33)$$

Again uncertainty in K, Z and the Kolmogoroff constants together could produce a 15% error in <wt>DISS. However, it should be possible to substantially reduce systematic errors through Reynolds flux intercomparisons.

2.6 Estimating The Stability Parameter Z/L

In section 2.2, the stability of the air column is characterized by a stability parameter, Z/L, which plays a fundamental role in the theory and measurement of turbulence. Unfortunately, it is difficult to obtain with 2.6, so three means of estimating it from incomplete data will now be investigated. The complete expression from 2.6 is,

$$\frac{Z}{L} = -\frac{K\,Z}{u^{*3}}\,g \quad \frac{\langle w\ Tv\rangle}{To} \ .$$

Tv and To, the instantaneous and local average virtual temperatures, are defined as the temperatures required to give

dry air the same density as actual moist air at the same pressure. Lumley and Panofsky, 1964, show that;

$$Tv \cong T\,(1 + 0.61\,m),$$

where Tv and the air temperature, T, are in degrees Kelvin and m is specific humidity. Lumley and Panofsky (p 96) also approximate the virtual temperature flux by

$$\langle w\,Tv\rangle \cong \langle wt\rangle + 0.61\,TZ\,\langle wm\rangle,$$

where TZ is the mean air temperature at the height Z. The conversion to absolute humidity, Q, in g/m^3, is accomplished with (Phelps, 1971),

$$Q \cong 1298\ (273^{\circ}K\ /\ To)\ m$$

$$\text{so}\quad Tv \cong T\ [1 + To\ Q\ 1.72 \times 10^{-6}].$$

Over temperate seas at Z more than about 10m there is not a large temperature gradient and the virtual and air temperatures differ by less than 2%, making

$$To = \langle Tv\rangle \cong TZ + TZ^2\ QZ\ 1.72 \times 10^{-6}$$

$$\frac{Z}{L} \cong -\frac{K\,Z}{u^{*3}}\,g\,\frac{\langle wt\rangle}{To} \cdot \left[1 + To^2\ 1.72\times10^{-6}\,\frac{\langle wQ\rangle}{\langle wt\rangle}\right] \qquad (2.34)$$

reasonable approximations.

Over temperate seas the moisture content of the atmosphere and the atmospheric pressure, affect the air density by about 1% and 5% respectively. For dynamic flux calculations, it is enough to only include the atmospheric pressure, PA in kPa, by calculating the density from

$$\rho = 1.29 \quad (273/TZ) \quad (PA/101) \; . \qquad (2.35)$$

Very often the absolute humidity and moisture flux, <wQ>, are unknown and Z/L must be approximated from measurements of u*, <wt> and the mean air and surface temperatures. The ratio of sensible heat flux to latent heat flux, the Bowen ratio, G, can be used to give

$$\frac{\langle wQ \rangle}{\langle wt \rangle} = \rho_L C_p \; G \approx \frac{0.534}{G} \quad (273/TZ)$$

in g/m³/°C, where the pressure and moisture effects on the density have been neglected. Phelps and Pond, 1971, report a value of 0.24 for G from their San Diego results. Substituting into 2.34 gives

$$\frac{Z}{L} \approx - \frac{K \; Z}{u^{*3}} \; g \quad \frac{\langle wt \rangle}{To} \cdot [1 + 0.001 \quad To],$$

which shows that the moisture flux may contribute about one-third as much to the stability as does the sensible heat flux.

An *in situ* Bowen ratio can be estimated from the bulk aerodynamic parameterizations, section 2.3, viz:

$$G = \frac{\rho C_p}{L} \frac{\langle wt \rangle}{\langle wQ \rangle} \cong \frac{\rho C_p}{L} \frac{\langle U \rangle C_T}{\langle U \rangle C_E} \frac{\Delta T}{\Delta Q} .$$

The Stanton number, CT, and Dalton number, CE, have sometimes been found to be nearly equivalent (Pond *et al.*, 1971), but Francey and Garratt, 1978, find CT to be 30% lower than CE. Because the humidity is not the major contributor to Z/L and because of the large error in ΔQ, CE and CT will be assumed equal. The saturation humidity as a function of temperature, is given by Hertzman *et al.*, 1974, as

$$QSAT(T) = C1 \exp(C2/T)$$

with $C1 = 6.4038 \times 10^6$ and $C2 = -5107.4$. This expression is a fit to a table of saturation humidities over pure water at various temperatures so that the surface humidity over salt water, QSFC, is 0.98 QSAT(TSFC). In order to reduce systematic errors, a relative humidity of 75% will be assumed, which is in the middle of the humidity range expected over temperate seas. Since humidity contributes only about 30% to Z/L, this assumption should introduce a random error in Z/L of about 20% at worst and usually of less than 10%. The sea-air humidity difference, ΔQ, and hence a Bowen ratio, can now be found from TSFC and TZ using

$$G(\Delta T) \cong (\rho\ Cp/L)\ \Delta T\ [0.98\ QSAT(TSFC) - 0.75\ QSAT(TZ)]^{-1}.$$

Substituting into 2.34 estimates Z/L from u*, <wt>, TZ and TSFC:

$$\frac{Z}{L}(u^*,\langle wt\rangle) \cong -\frac{K\,Z}{u^{*3}}\,g\,\frac{\langle wt\rangle}{To}\cdot\left[1+\frac{To\;2.5\times10^{-4}}{G(\Delta T)}\right] \qquad (2.36)$$

In cases where <wt> is also unknown, bulk parameterization replaces it with CT UZ ΔT. The review by Priehe and Schmitt, 1978, indicates that CT is about 1×10^{-3} in unstable stratification and about 0.86×10^{-3} in stable. Therefore, a simpler estimate of Z/L is given by

$$Z/L(u^*,\Delta T) \cong -\frac{K\,Z}{u^{*3}}\,g\,CT\,\frac{UZ\;\Delta T}{To}\left[1+\frac{To\;2.5\times10^{-4}}{G(\Delta T)}\right]. \qquad (2.37)$$

Following Deardorff, 1968, the bulk formula, 2.9, replaces u^{*3} with $CD^{3/2}\,UZ^3$ so that a stability parameter $Z/L(\Delta T)$ can be determined soley from the bulk parameters, UZ, TZ, and TSFC. A portion of the Z/L expression is identified as a bulk Richardson number

$$Ri(\Delta T) = -g\,\frac{Z}{UZ^2}\,\frac{\Delta T}{To}\left(1+To\,\frac{2.5\times10^{-4}}{G(\Delta T)}\right],$$

$$\text{so}\quad Z/L(\Delta T) \cong K\,\frac{CT}{CD}\,\frac{}{CD^{1/2}}\,Ri(\Delta T)\ .$$

A reasonable average CD is 1.25×10^{-3} (Garratt, 1977), so

$$Z/L(\Delta T) \cong 11\ Ri(\Delta T)\ (CT/\ CD) \qquad (2.38)$$

$$\text{with}\quad CT/CD = 0.70 \quad \text{for} \quad \Delta T < 0$$
$$= 0.80 \qquad\qquad \Delta T > 0$$

is a very practical estimate of the stability parameter. This differs from Deardorff's final form of $Z/L = 12\ Ri\ (\Delta T)$ for unstable conditions, as it reflects more recent determinations of the bulk coefficients. However, it ought to be compared to the more exact expression, 2.36, whenever <wt> and u* are both available.

CHAPTER 3 THE INSTRUMENTATION AND EXPERIMENTAL PROGRAM

3.1 Introduction

In order to collect the desired amount of high wind speed data a Reynolds flux system and a dissipation system have been designed for unattended operation. Additional aspects of both systems including error analysis, design criteria, and sensor response requirements are given in Pond and Large, 1978, and the detailed analysis of the velocity measurement is also in Pond et al., 1979. The essential considerations are low power consumption and a large recording capability to keep the servicing period long and sensors able to function in the hoped for 30-40 m/s winds and accompanying spray. When operating in a hostile environment for long periods of time, sensors and electronics are likely to fail periodically, so whenever possible the important measurements are either duplicated or their sensors are calibrated in situ.

The results from two field operations are to be presented in this study. The first was conducted on the Bedford tower near Halifax Nova Scotia, which provided a stable enough platform to allow meaningful Reynolds flux measurements to be used to "calibrate" the dissipation system. Intercomparisons are also possible with the air-sea interaction system from the Bedford Institute of Oceanography, BIO, which was also installed on the tower. In a preliminary experiment on Sable Island all systems were found to be compatible when operating on the same platform. The results of that intercomparison and of a previous

BIO experiment on the island are reported in Smith et al., 1976, and Smith and Banke, 1975, respectively. The dissipation measurements were extended to higher wind speeds and more open sea conditions in a second experiment conducted from the CCGS Quadra during its patrols at ocean weather station "PAPA".

3.2 The Sensors

The velocity measurements are based on the Gill propeller-vane anemometer (R.M. Young Co.), whose propellers are carefully constructed helicoids that turn a precise number of revolutions for each meter of passing air (Baynton, 1970). This number was checked in a wind tunnel and found to be within 2% of the factory calibration. This accuracy is maintained from propeller to propeller and is not affected by considerable ablation of the leading edge. A problem does arise when the axial wind falls below about 1 m/s, because the inertia and friction begin to produce a non-linear output. Another problem is that when the wind vector makes an angle θ (angle of attack) greater than about 20°, to the propeller axis the apparent axial velocity component is less than the expected $\cos(\theta)$ times the magnitude of the wind, by a factor $\beta(\theta)$. For angles of attack between 35 and 75 degrees, this non-cosine behavior is approximated by $\beta(\theta) \cong 1.103 - 0.27\,\theta$, for θ in radians (Pond and Large, 1978). Although these problems pose no serious difficulties in determining the horizontal velocity components, they complicate the measurement of the vertical velocity. W is

derived from a propeller, Gill-w, whose axis is tilted at an angle, $\alpha \cong 60°$, to the axis of a standard, Gill-u, propeller, which is generally tilted at a small angle δ from the horizontal (figure 3). At an average wind speed greater than about 4 m/s the axial component of the tilted propeller always contains enough of the horizontal wind to avoid its non-linear regime. The propeller axes and instantaneous wind vector are kept in essentially the same plane by the vane and in this way the geometry of figure 3B is always maintained and corrections for the non-cosine behavior are possible.

The twin propeller-vane anemometer of figure 3 is described fully in the references cited, so only an outline of how the velocity components are resolved follows. The defined angles of figure 3C and the following notation conform to these previous publications. The Gill-w (taking the non-cosine behavior at $\Theta = \alpha$ into its calibration) and Gill-u signals from the Reynolds flux system supply the velocities:

$$\text{Gill-u} = V1 = Q \cos\delta + w \sin\delta$$

$$\text{and} \quad \frac{\text{Gill-w}}{B(\alpha)} = V2 = \{Q\cos(\alpha+\delta) + w\sin(\alpha+\delta)\} \cdot \left[1 - \frac{0.27}{B(\alpha)}(\delta - \tan^{-1}(w/Q))\right]$$

$$\text{with} \quad \Theta = \alpha + \delta - \tan^{-1}(w/Q) , \qquad (3.1)$$

where Q and w are the horizontal and vertical velocity components, respectively. Because V2 contains a considerable contribution from the horizontal wind, the low frequency variations in the Gill-u and Gill-w signals track one another very closely, providing a check that everything is working

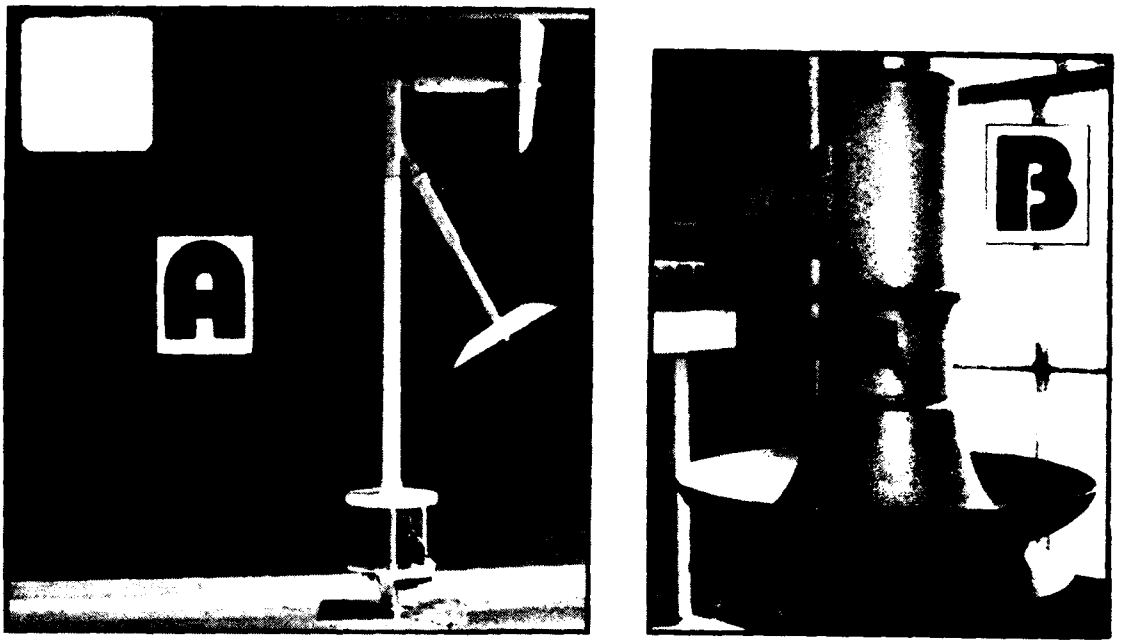

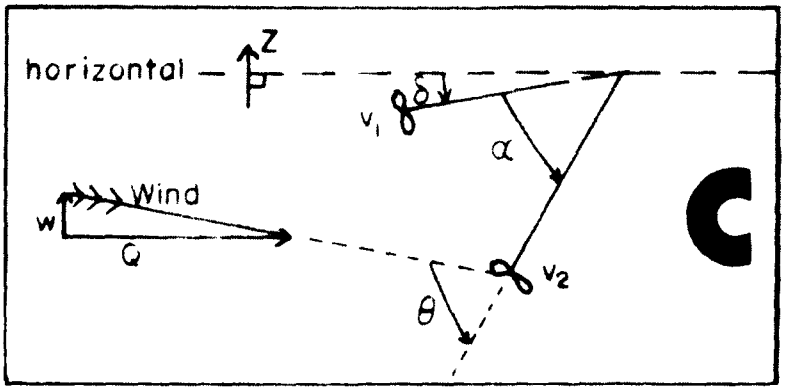

FIGURE 3 A: The Gill twin propeller-vane anemometer.
B: The HAT sensor housing.
C: Definition of angles used in resolving the velocity components and calculating the tilt angle δ.

properly. The tilt angle δ needs to be evaluated before Q can be removed from the Gill-w signal and w calculated. Since the average vertical velocity must eventually go to zero, a good estimate of δ is that angle of rotation needed to make the calculated $\langle W \rangle$ exactly 0, where $\langle\ \rangle$ denotes the averaging period. An average δ is measured over at least 15 minutes to give good averages of the ratio $Y = \langle V1 \rangle / \langle V2 \rangle$ from which it is derived. Assuming $\tan^{-1}(w/Q) \cong w/Q$ and $\langle w \rangle = 0$,

$$\langle V1 \rangle = \langle Q \rangle \cos \delta \quad \text{and}$$

$$\langle V2 \rangle = \langle Q \rangle \{\cos(\alpha+\delta) [1-0.27\,\delta/\beta(\alpha)] + \langle w^2 \rangle \langle Q \rangle^{-2} \sin(\alpha+\delta)\ 0.27/\beta(\alpha)\}$$

are correct to second order. The term in $\langle w^2 \rangle \langle Q \rangle^{-2}$ is only about 0.2% of the previous term, leaving

$$Y = \{1-0.27\,\delta/\beta(\alpha)\} [\cos\alpha - \sin\alpha \tan\delta],$$

which, assuming $\delta \cong \tan\delta$, gives a quadratic in δ. It is the negative square root of the quadratic formula that is needed, so δ is estimated from

$$\delta = b - \{ b^2 + (\beta(\alpha)/0.27)\ (Y-\cos\alpha)/\sin\alpha \}^{1/2}$$

$$b = 0.5\,[\cot\alpha + \beta(\alpha)/0.27]. \qquad (3.2)$$

This expression shows that offset errors, which enter Y, and errors in α and the β relation produce apparent tilts that can seriously affect Reynolds stress measurements. Now some

straight forward algebra yields:

$$V2 - Y\,V1 = B\,w + (A/V1)\,w^2$$
$$A = [0.27/\beta(\alpha)\,]\ \sin(\alpha+\delta)\ \cos\delta \qquad (3.3)$$
$$B = \cos(\alpha+\delta)\ 0.27/\beta(\alpha) + \{1-0.27\,\delta/\beta(\alpha)\}\ \sin\alpha/\cos\delta,$$

where Q has been replaced by $V1/\cos\delta$ and a term in $\langle w^2\rangle/\langle Q\rangle^2$ and terms of order $(w/Q)^3$ have been neglected. On a fixed platform the instantaneous tilt actually depends on the wind direction, but the use of the "average" δ introduces very little error (Pond and Large, 1978). The quadratic in w is solved using the positive square root of the quadratic formula, to give an estimate of w for each pair of recorded Gill-w and Gill-u values in the averaging period. The instantaneous horizontal velocity components are then found from:

$$Q = V1/\cos\delta - w\tan\delta$$
$$U = Q\cos(an) \qquad (3.4)$$
$$V = v = Q\sin(an)\ ,$$

where the instantaneous wind direction, AN, equals $\langle AN\rangle$+an and the mean direction, $\langle AN\rangle$, is chosen such that the average cross-stream velocity $\langle V\rangle = \langle Q\sin(an)\rangle = 0$. The possible errors associated with resolving U,v,w and Q in this manner are summarized in table I (reproduced from Pond and Large, 1978), together with their effects on the calculated momentum flux and drag coefficient. Some errors should tend to cancel, so hopefully there is no more than a ±10% error in the average CD.

SOURCE		|<uw>|	CD	COMMENTS
α error of ±1°		±5%	±5%	The α error is believed to be within ±.5° with 2-3% effects
Offset errors	at 5m/s	±2%	±3%	Offset errors partly cancel rather than add giving about 1/2 the effects
	at 10m/s	±1%	±2%	
±2% in calibration		±4%	±1%	
$\beta(\theta)$ relation		±3%	±3%	
δ fluctuations		Negligible	Negligible	
Non-cosine response of V1 propeller	δ=0	±1%	±1%	For $\|\delta\|$ < 2-3° error is similar to δ=0. For $\|\delta\|$ =5° it is likely within ±5%.
	δ=±10°	±10%	±10%	

TABLE I Summary of possible errors in the velocity measurement and their effects on the Reynolds flux method.

Only the dissipation method is practicable on a moving platform, because the δ derived from Y may be very different from the instantaneous tilt needed to find w. U is also not calculated from this type of data because it is not a simple matter to separate the wind effect from the platform motion in the vane's signal. The Gill-u signal from the dissipation system does give an average V1/cos δ (from which a ship's velocity is removed vectorally) and approximate average values of Q (and U, since $\langle Q \rangle \cong 1.005 \langle U \rangle$). In this method the velocity measurement is not the major source of error (section 2.5). A

+2% calibration error only leads to 2.7% and -1.3% errors in $|\langle uw \rangle|$ and CD respectively and at 5m/s they are affected by the offset error by only 0.3% and 1.3%. However, only frequencies above those contaminated by the platform motion may be utilized. The Gill-w signal functions as a check that the Gill-u propeller and electronics are working properly and, if necessary, as an input to the dissipation method.

The enclosure, HAT, of figure 3, serves as a radiation shield and offers protection against rain and spray for the temperature and humidity sensors that are mounted in it. Glass coated microbead thermistors (Victory Engineering Corp.) measure both the mean and fluctuating air temperature while glass rod thermistors potted in epoxy measure both the sea temperature and a mean air temperature. All these transducers form part of similar bridge circuits whose non-linearity balances that of the thermistors, making the output of an operational amplifier detector linear over about a 25°C range. All probes were initially calibrated in a water bath against a standard mercury thermometer but later the rod thermistor provides an *in situ* calibration check of the microbead. The two temperature measurements should not differ by more than 0.1°C, when both the rod and microbead are working properly.

Although no latent heat flux data are as yet available, a brief description of the attempted humidity measurements follows. On Sable Island the humidity fluctuations were taken with an aluminium-oxide sensor (Panametrics Corp.) and a Brady array (Thunder Scientific Corp.), but these failed because the

sensors deteriorated in the salt air environment. This occurred less rapidly in the case of the Brady so an attempt was made on the Bedford tower to provide an *in situ* calibration by replacing the aluminium-oxide probe with a second Brady covered with a 60 micron stainless steel sintered filter. The calibration drift was much reduced, but still serious, making both Brady arrays unsuitable for long unattended operation. For up to a week or two the drift of the filtered Brady was not too bad, but its calibration was complicated by what may have been hysteresis effects and temperature sensitivity. In addition, the response of an open Brady is marginal at best (Smith *et al.*, 1976). It therefore seemed best to abandon the Brady array and to regard all the data from it as unreliable.

For the ship operations where power requirements are not restrictive a Lyman-alpha humidiometer (Electromagnetic Research Corp.) has been employed to give the fluctuating humidity, while a Cambridge Systems (Model 2000) dewpoint system provided the *in situ* calibration and average . The latter worked properly for over a month before needing servicing and is promising. It also gives an aspirated mean air temperature for checking the microbead. The Lyman-alpha, however, required constant attention as its windows quickly became so dirty that its signal went off scale before providing any useful data.

3.3 The Reynolds Flux System

This system includes the sensors, an electronics package and 6 digital cassette tape recorders to sample, digitize, and record the data needed to determine the turbulent fluxes by the Reynolds flux method, section 2.4. It processes each of its 6 channels in the same manner as shown in figure 4, which illustrates the data flow and parameters considered in converting stored data back to the original physical quantities sensed by the transducers (V1,V2,AN,R, where R is any scalar). Although the data processing is, for convenience, shown for the spectra, it is actually performed on the Fourier coefficients from which the spectra and cospectra are derived. A Reynolds flux record consists of NG sequential groups, each formed by sampling first the prewhitener, Vp, at 3Hz, NF times, then the low-pass filter, VL, at 1/SSP, NS times. The slow sampling period, SSP, is made as long as possible to conserve power and tape. The high frequency variance and covariance lost because the low-pass filter prevents full aliasing is recovered by the fast subsamples. The 3 Hz rate is fixed because it is as fast as 6 channels can be recorded by a pair of parallel recorders, each receiving 3 channels. NF,NS,NG and SSP are programmed by means of thumbwheel switches and together they determine the record length, the subsampling scheme and the portions of frequency space covered by each sampling rate. An additional switch sets the time interval between the start of records. In order to prevent the cassettes filling with low wind speed data, a wind speed limit can be set by another switch so that a scheduled record is not taken if the average wind speed in the

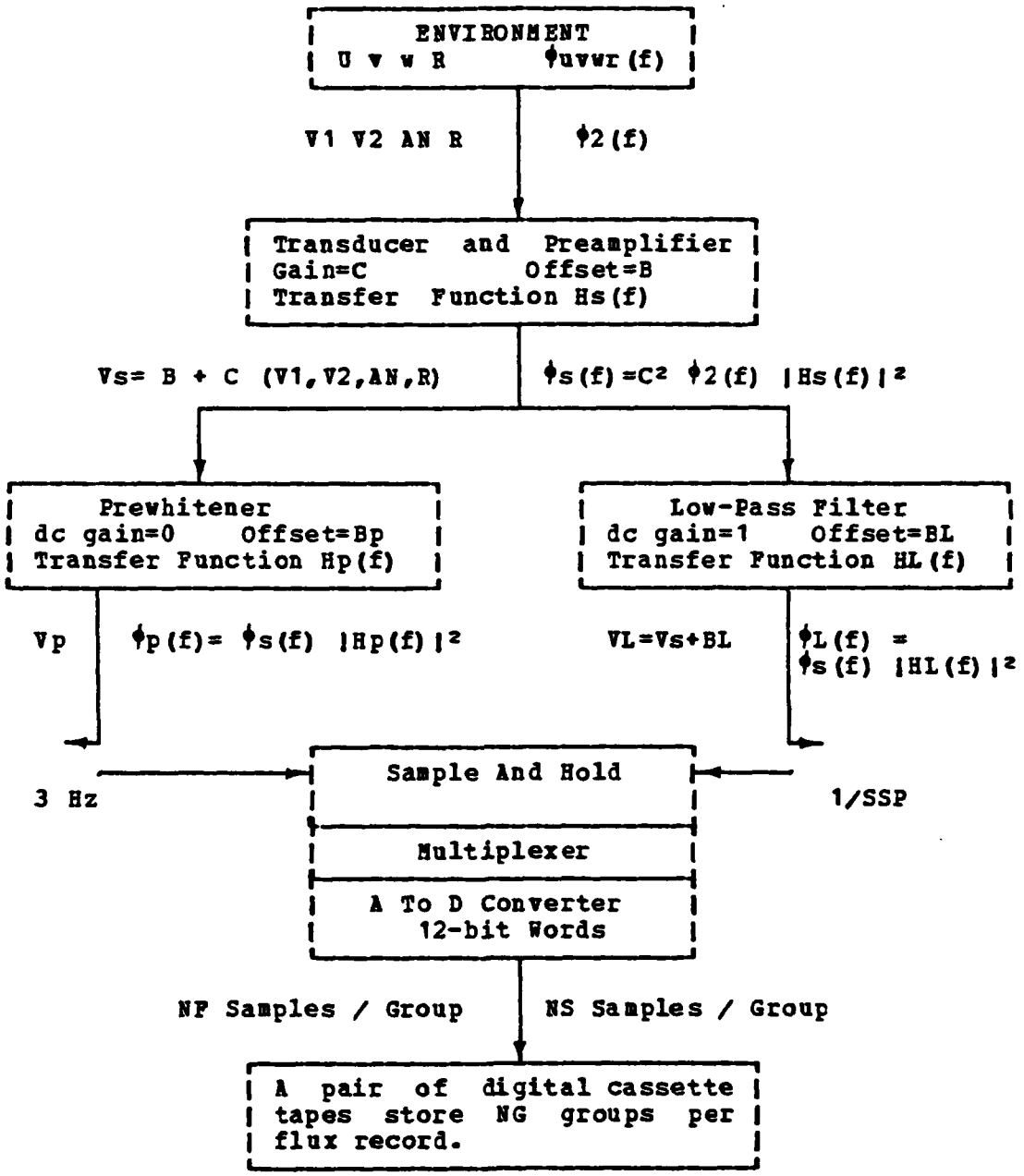

FIGURE 4: Signal processing in the Reynolds flux system, showing the sampling scheme and all parameters considered in the analysis.

previous six minutes is less than the set limit. The system continues to collect data until the three pairs of cassettes are full.

The low frequency u,v,w and r Fourier coefficients and spectra $\Phi_{uvwr}(f)$, are available from the slow samples. The low-pass filters have a 1 second time constant and transfer function, HL(f) (3db down at fL= 0.16 Hz). SSP has always been set to 3 seconds, giving a Nyquist frequency fsn, (1/6 Hz), almost equal to fL, so the filter loss and aliasing should nearly cancel one another. The sensor transfer function, Hs(f), is ignored because it is typically 3db down at more than 5 times fsn. A fast Fourier transform of the slow samples produces spectra, $\Phi_L(f)$, which must be nearly equivalent to $C^2\,\Phi_2(f)$ for f< fsn, where the gain, C, includes the dimensional conversion from physical units to voltage. Because of the non-linearity in the w calculation, the velocity data must first be converted to V1, V2 and AN = C^{-1} (VL-BL-B) and then to U, v and w with equations 3.3 and 3.4, before transforming and obtaining the $\Phi_{uvw}(f)$ spectra. NS has always been set to 256, so one group of slows lasts 12.8 minutes and its Fourier cofficients occur at frequencies from 0.0013 Hz to fns and contain the variance and covariance from 0.00065 Hz to 0.167 Hz.

Finding the high frequency cofficients from the fast samples is more complicated because the prewhitener, Hp(f), and sensor responses are explicitly involved. The prewhitener circuits behave as time differentiators at low frequencies to increase the signal levels and eliminate spectral distortion

from non-sampled frequencies, then roll off as R-C low-pass filters at the higher frequencies. By design their response is maximum and nearly flat at the fast sampling Nyquist frequency, 1.5 Hz, so that aliasing occurs without much loss of contributions below a few Hz. The Fourier coefficients of the fast samples (corresponding to $\phi p(f)$) are easily converted to

$$\phi 2(f) = \phi p(f) \left[C \, |Hs(f)| \, |Hp(f)| \right]^{-2} .$$

With the velocity channels, the $\phi 2(f)$ are inverse Fourier transformed and a dc level is added to make the last fast sample of V1, V2 and AN equal to the first slow sample of each group. U, v, and w are then calculated using the mean coordinates axes as determined by the slow samples, and it is the Fourier coefficients of these time series that are used to produce the desired high frequency $\phi uvw(f)$ spectra and cospectra. Without the non-linear w calculation only one transform need be performed and this possibility is discussed in the cited references. NF has always been set to 128 making the lowest fast frequency 0.0234 Hz, so all the variance and covariance of the lower 6 and part of the seventh frequency bands are already contained in the slow samples.

Flux estimates and statistical quantities are calculated from runs of NGRP sequential groups of a record. The total run time is used as the averaging period in the δ calculation and coordinate determination. The group spectra and cospectra are averaged together over the run. An attempt has been made to use the overlapping frequency bands to adjust the high frequency

portion, however, this has not been successful because the lower 6 estimates from the fast samples are not statistically very certain and often radically different from one another and from the other high frequency estimates. The 128 low frequency values span 0.00065 <f< 0.167 Hz, but the eighth high frequency band does not begin until f= 0.176 Hz so an intermediate value at f= 0.1715 Hz (bandwidth 0.009 Hz) is formed by interpolating between the seventh and eighth values.

The resulting 186 point spectra and cospectra are integrated in three different ways. The first, the I1 method, is to simply multiply each value by its bandwidth and sum, that is, to integrate from f= 0.00065 Hz. There are two disadvantages with this method: first, the lowest natural frequency, n= fZ/<U>, included in the integration decreases with <U> and this could give rise to apparent wind speed dependencies; second, the lowest frequencies are not as statistically certain as one would like and failure to converge over a flux run could create a great deal of variability in observations. A second integration method, I2, alleviates the first problem by including the variance and covariance of the individual group means about the overall mean of a run. This effectively adds a further NGRP samples at a 13.5 minute period, which contain the contributions from 0.00062/NGRP to 0.00062 Hz. However, the statistical uncertainty in this additional contribution is very high, enhancing the second I1 problem. Note that a small spectral gap from 0.00062 to 0.00065 Hz is present in the I2 integration, because the slow sampling is suspended during the fast sampling. The I3 method always begins

its integration at the same natural frequency, n= 0.004, where the spectral values are reasonably well established. The integral is then multiplied by a constant factor E to compensate for the excluded low frequency contributions. The value of E for each quantity is found from the normalized spectrum or cospectrum, $N\phi(n)$, which is determined in section 4.3 from averages over all available runs. The non-dimensional $N\phi(n)$, plotted against log(n) for convenience, should display a universal form, depending only on Z/L. In section 4.3, E is calculated from the normalized wt and uw cospectra and is found to be a function of stability. Although the implied low frequency contribution may not be exact, the results should give representative averages and be subject to minimal variability. The three methods are expressed by:

$$I1 = \int_{.00065}^{\infty} \phi(f)\, df$$

$$I2 = I1 + \int_{.00062/NGRP}^{.00062} \phi(f)\, df \qquad (3.5)$$

$$I3 = E \int_{f=.004<U>/Z}^{\infty} \phi(f)\, df$$

$$E = \int_{0}^{\infty} N\phi(n)\, d(\log n) \;/\; \int_{0.004}^{\infty} N\phi(n)\, d(\log n).$$

The I3 method is the most attractive and is compared with the others in section 4.5 to determine if it is universally applicable.

3.4 The Dissipation System

This system employs the same sensors and preamplifiers, but has its own electronics package and two digital cassette recorders. It provides the estimates of ϵ and Nr for the flux calculations (section 2.5) and the mean sea and air temperatures, humidity and wind for parameterization (section 2.3) and stability calculations (section 2.6). The architecture of the data flow is shown in figure 5. Between recording at intervals of Dt, each band-pass filter output is sampled at 20 Hz, digitized, squared and summed NI times. The sums are stored in internal memory units until they are written onto a cassette, at which time all the low-pass filter channels are also sampled and recorded. Switches program NI to be as large as possible while still allowing the summation to be completed before the start of a tape write. Dt is usually set to 4 or 5 minutes, making this recording system very economical of tape.

The low-pass filters are single pole R-C circuits with a 25 second time constant, followed by a unity gain operational amplifier, hence they are well suited for providing the mean velocity and scalar values over the averaging period used for the δ calculation and velocity computations of section 3.1. These averaged results may be combined to give the means over longer time intervals if desired.

The band-pass filters consist of double pole high and low pass stages centered nominally at fc= 0.4, 0.8 and 1.6 Hz. The prewhitener is a differentiator at low frequencies that rolls off as a single pole R-C filter above 10-15 Hz. The two filters

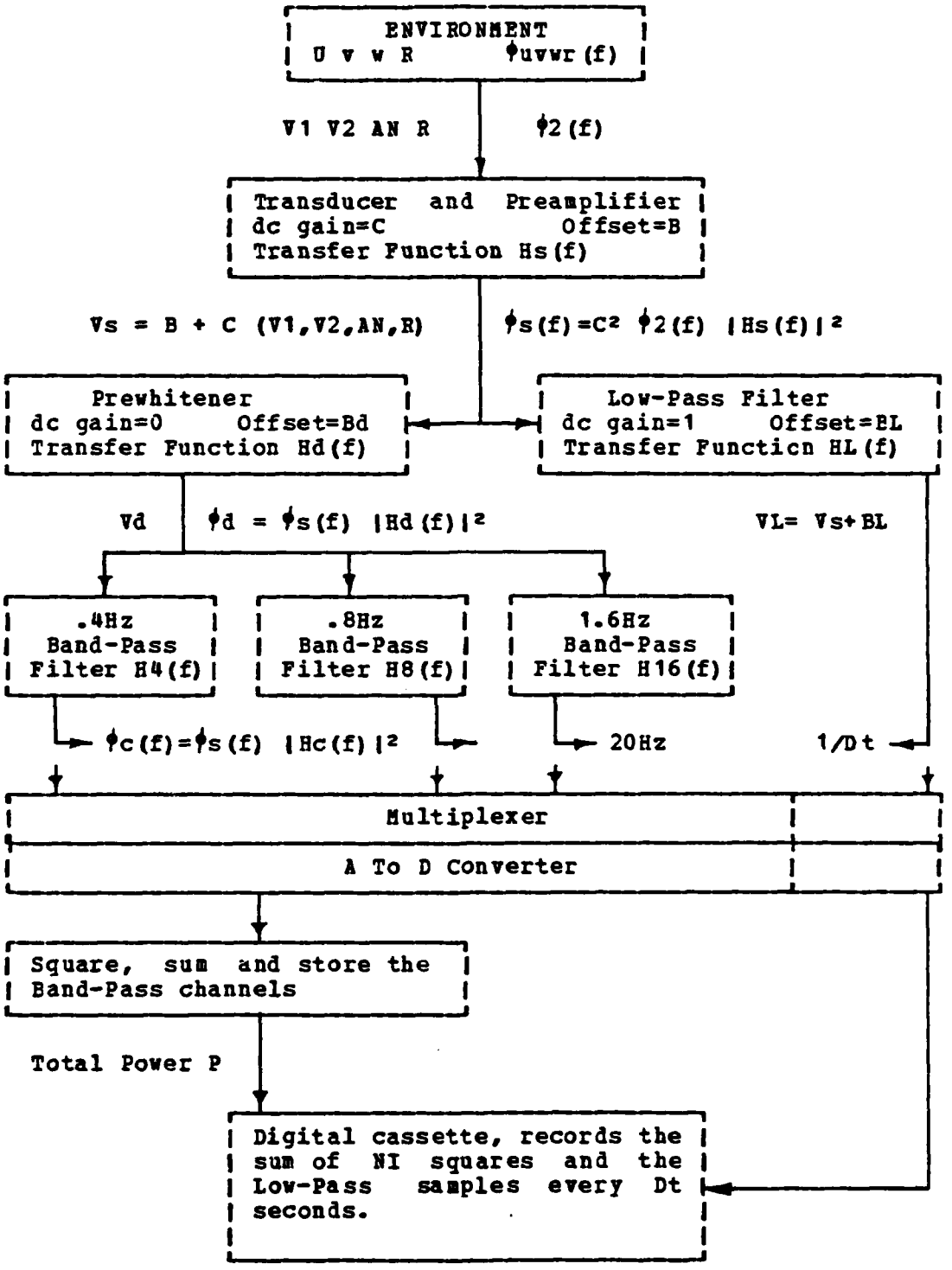

FIGURE 5: Signal processing in the dissipation system.

together form band-pass filters represented by combined transfer functions Hc(f) with center frequencies at about 0.55, 1.05 and 2.1 Hz. Since the input spectrum falls off rapidly ($f^{-5/3}$) the frequencies of greatest power output are near the fc values. The stored data words divided by NI give the average power, <P>, passing through each band-pass filter. A -5/3 spectrum across Hc is assumed in order to get a discrete spectral value at each fc for all selected channels from

$$\langle P \rangle = RHO \ \phi(fc)$$

$$\text{where} \quad RHO = C^2 \int (f/fc)^{-5/3} \ |Hs(f)|^2 \ |Hc(f)|^2 \ df$$

with the integral taken over the range of frequencies passed by the filters. Because RHO contains Hs(f), a function of U (section 3.5), the integral must be evaluated at each wind speed for each band-pass filter channel.

Equation 2.23 relates $\phi(fc)$ to the dissipation of scalar fluctuations, Nr, the molecular dissipation, ϵ, and the one-dimensional Kolmogoroff constants, Br' and K'. In the case of scalars $\phi r(f) = \phi 2(f)$ and

$$Nr = \frac{\langle P \rangle \ \epsilon^{1/3}}{RHO \ Br'} \ (2\pi/\langle U \rangle)^{2/3} \ fc^{5/3} \qquad (3.6)$$

is available from each scalar band-pass filter once ϵ has been determined. Calculating ϵ from the velocity signals is more complicated because V2 always contains some w and a non-zero tilt introduces some w into V1 as well. Some error is thus

introduced into RHO, because at the frequencies utilized only $\phi u(f)$, and not $\phi w(f)$, is expected to be proportional to $f^{-5/3}$ and hence neither V1 nor V2 should have exactly a -5/3 spectrum. Since the spectral values of the horizontal velocity component are nearly equal to those of the downstream component, $\phi u(f)$, (Pond and Large, 1978), 3.1 gives

$$\phi 2(f) = A \; \phi u(f) \; S(\delta, f)$$

for the V1 signal $A = \cos^2 \delta$

$$S(\delta, f) = [1 + \tan^2\delta \; \phi w(f)/\phi u(f) + 2\tan\delta \; \phi uw(f)/\phi u(f)].$$

$S(\delta, f)$ should really be placed inside the integral of the RHO expression and integrated over the band-passed frequencies, but because $\phi w(f)/\phi u(f)$ and $\phi uw(f)/\phi u(f)$ can only be approximated, they are taken to be constants over each filter and placed outside the integral to give an approximate $S'(\delta)$. In the inertial subrange $\phi w(f)/\phi u(f) = 4/3$, but this behavior is not observed near the fc's and instead it is taken to be 0.81, 1.11 and 1.29 at fc = 0.4, 0.8 and 1.6 Hz respectively. These are simply the averages of 14 sonic anemometer observations from Sable Island which also show $\phi uw(fc)/\phi u(fc)$ to average -0.11, -0.16 and -0.15. $S'(\delta)$ is only a small correction (about 1.03 at δ=-5° and 0.98 at δ=+5°), but not accounting for it introduces a systematic error, which on a leaning tower could turn out to be a function of wind direction and hence fetch. Therefore, $S'(\delta)$ is applied to reduce the error and make it more random. The correction is larger and the error more serious in

the V2 case where 3.1 gives

$$A = [\ \cos(\alpha+\delta)\ \ \beta(\theta)/\beta(\alpha)\ ]^2$$

$$S(\delta,f) = \{1+\tan^2(\alpha+\delta)\ \ \phi w(f)/\phi u(f) + 2\tan(\alpha+\delta)\ \ \phi uw(f)/\phi u(f)\}$$

An approximate $S'(\delta)$ can again be used, but $\theta \cong \delta+\alpha$ must be assumed since the data to calculate the instantaneous angle of attack at each digitization is not available. Therefore, whenever possible it is far more desirable to calculate the dissipation from the Gill-u rather than the Gill-w data. With these approximations and reservations each velocity band pass filter gives:

$$\epsilon^{2/3} = \frac{(2\pi/\langle U\rangle)^{2/3}\ \ \langle P\rangle\ \ fc^{5/3}}{A\ \ K'\ \ RHO\ \ S'(\delta)} \qquad (3.7)$$

3.5 Sensor Response

When calculating ϵ and Nr, sensor response corrections are essential and they are of some importance to the Reynolds flux measurements. Fortunately, the dissipation system provides a means of establishing Hs(f) under the actual turbulent conditions encountered. Assuming the sensors behave as an R-C filter (3db down at fo : $Hs(f) = (1+jf/fo)^{-1}$, $j=\sqrt{-1}$), either Nr or ϵ values from any two band-pass filters can be made equal by an appropriate choice of fo. Of course random departures of the input spectrum from its average -5/3 slope create scatter in these fo's, but on average nearly the same response is indicated

by all three pairs of filters (the 0.4 and 0.8 Hz, the 0.4 and 1.6 Hz and the 0.8 and 1.6 Hz). The success of this technique establishes that the assumption of an R-C response is appropriate and that there is a consistent average -5/3 region throughout the range of frequencies passed by the three filter combinations.

The response of mechanical sensors, such as the Gill propellers, is characterized by a distance constant, D = the wind passage required for a 63% recovery from a step change in velocity. The R-C filter analogue gives $2\pi fo = \langle U \rangle / D$. It is more important to establish fo during low winds where the response is poor. In figure 6, the hourly averaged wind speed is plotted against the $2\pi fo$ required to make the Gill-u calculations of ϵ from the 0.8 and 1.6 Hz filters equal. Now if D were truely a constant this plot would be a straight line through the origin of slope D. The data imply that below 12 m/s, D is about 0.65m, a significantly better response than the quoted value of 0.8m. At higher speeds the response appears to improve even more than expected (D decreases) and this is incorporated by using the solid line of figure 6a, D = 0.56m U/(U-1.0m/s). The line is a fit, for U> 4m/s, to comparisons of all three band-pass filter outputs over the entire time that this particular anemometer-propeller (19cm, 2-bladed) combination was in use. The response changes only slightly with a different anemometer, but depends strongly on the type and weight of the propeller. Heavier propellers of similar construction, used on Sable Island, give D = 1.0m U/(U-0.7m/s) and 19cm 4-bladed ones show D = 0.79m U/(U-1.8m/s).

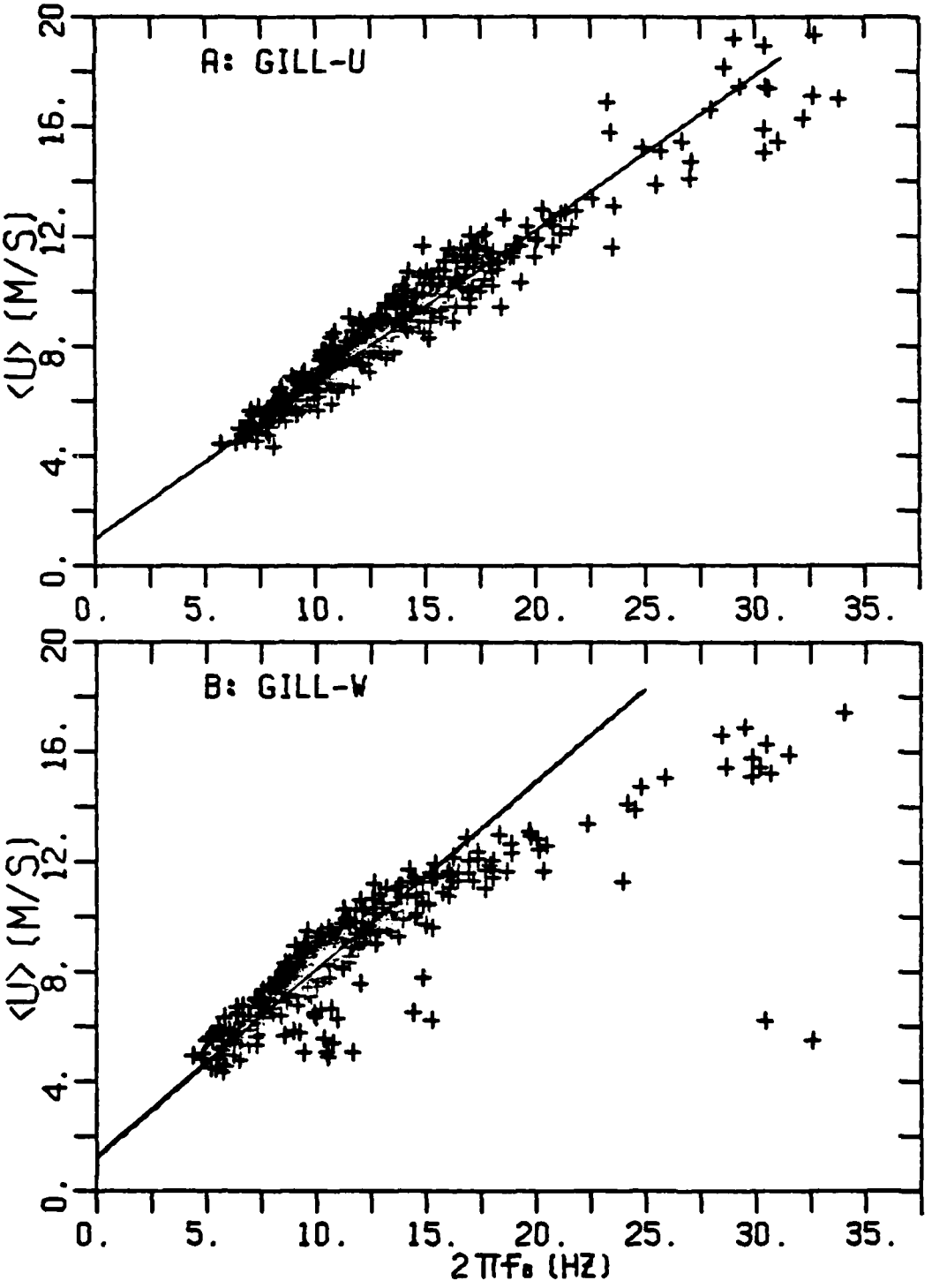

FIGURE 6: Determination of the distance constants from the 0.8 : 1.6 Hz band-pass filter ratios of
A: the Gill-u horizontal propeller,
B: the Gill-w tilted propeller, α = 59.5°.

The data of figures 6A and 6B come from the same time periods, but evidently more air must pass in the horizontal (longer distance constant, DT) before the tilted propeller responds. This may reflect the non-cosine behavior, because assuming $DT=D/\beta(\alpha)$ gives the solid line of figure 6B and $DT=1.22\ D$ for $\alpha=60°$, which is an acceptable fit for U<12 m/s. The technique fails at higher speeds because the w spectrum which forms a large part of the input signal, V2, is no longer -5/3 throughout the Gill-w 0.8 Hz band-pass filter. This means that useful Gill-w data are less plentiful as well as more uncertain than that of the Gill-u, so it seems preferable to take the distance constant of the tilted propeller as $D/\beta(\alpha)$. Such an approach turns out to lie between Hicks (1972 B) and Gill (1975), whose results for a 60° angle of attack give DT=1.41 D and 1.15 D, respectively.

A similar procedure was used to establish the <u>in situ</u> response of each microbead thermistor mounted in the HAT. Regrettably, it had to be based on very little data because each bead worked for only a relatively short time and a lot of recorded data has been rejected because of calibration problems and suspected salt contamination of the microbead. Most of the reliable temperature data from the Bedford tower is included in figure 7, in which the hourly averaged wind speed is plotted against the sensor response required to make Nt calculated from the 0.8 and 1.6 Hz temperature band-pass filters, equal. Clearly the response improves with wind speed. The solid line, of slope 0.90m, is an acceptable fit to all the data, implying that the microbead response, in winds up to at least 20 m/s, can

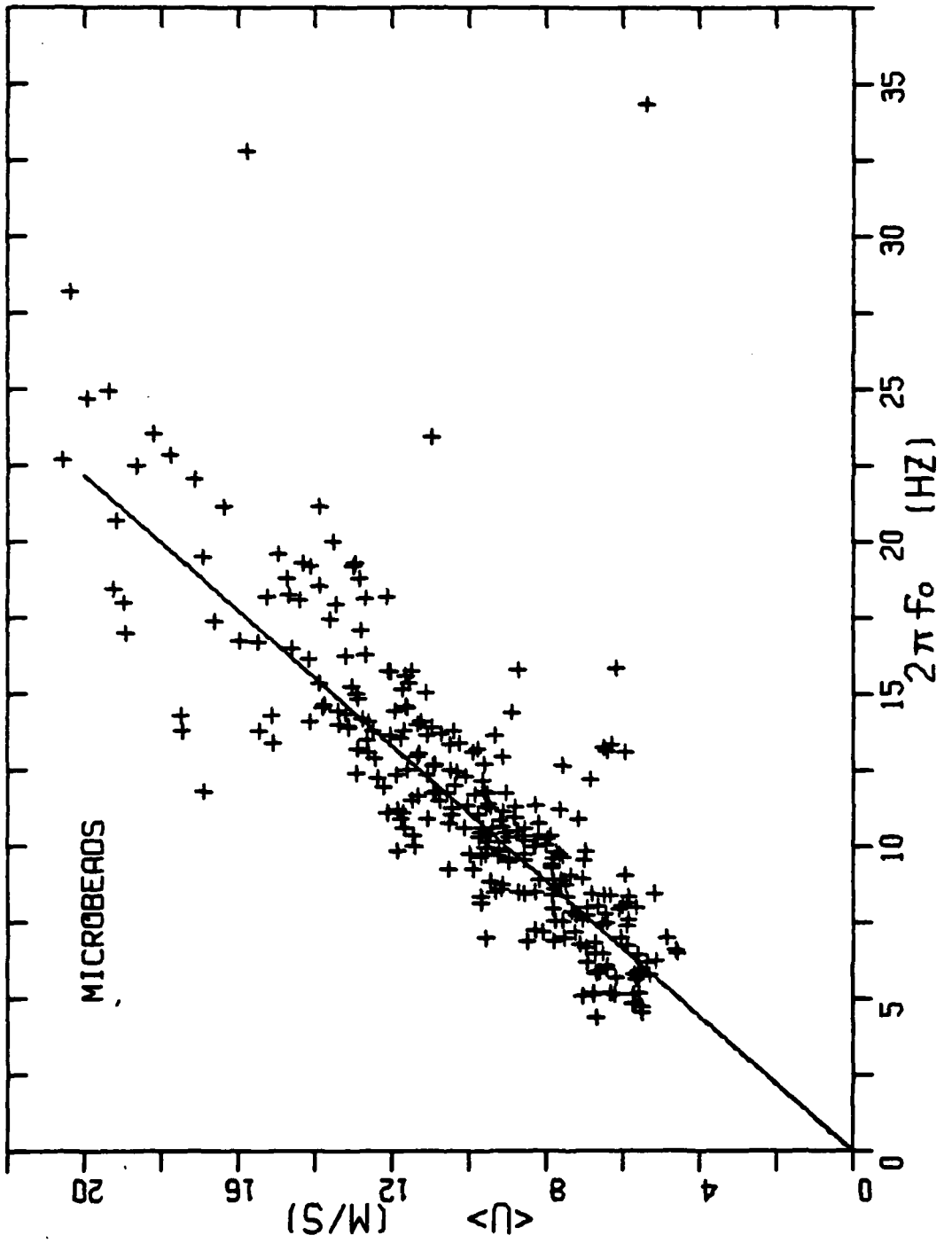

FIGURE 7: Determination of the microbead thermistor response from the 0.8 : 1.6 Hz band-pass filter ratios. The solid line has slope 0.90s.

also be described as an R-C filter with a distance constant, DB. Miyake et al. (1970 B) quote a 26 Hz response for similar microbeads at an aircraft speed of 70 m/s (distance constant about 0.4m). The lower wind speeds may give the poorer response indicated by figure 7. It is suspected, however, that the response is limited by the HAT itself and the success of a distance constant description is a consequence of the amount of air needed to flush the enclosure. Accordingly, the data from individual microbeads agree with a DB of 0.90m to within ±5%.

If the response is being treated properly, the Reynolds stress derived from each of the three band-pass filters should, on average, be equal. In figure 8 the ratios of $\epsilon^{2/3}$ (from 3.7) and equivalently (from equation 2.28) <uw> are plotted as a function of wind speed for the same data as used in figure 6. Evidently the chosen response is reasonable. Very few individual ratios differ from 1.0 by more than 10%. At the lower winds the averages of all three ratios are nearly 1.0 and in the case of the 0.8/1.6 ratio, this is true up to 20 m/s. Between 12 and 20 m/s, the 0.4 Hz band-pass filter appears to have about 5% smaller stress values (less output power) than expected. This may reflect a deviation from a purely R-C response, but more likely it is evidence of the lower portion of the filter lying, on average, below the $f^{-5/3}$ frequencies during these higher winds. At 16 m/s the distance constant formulation gives D= 0.6m, but if it were taken to be a constant 0.65m the observed 0.4/0.8 ratio would be even less, because the response correction at 0.8 Hz increases faster than at 0.4 Hz as the response is made poorer. The correction is highly non-linear

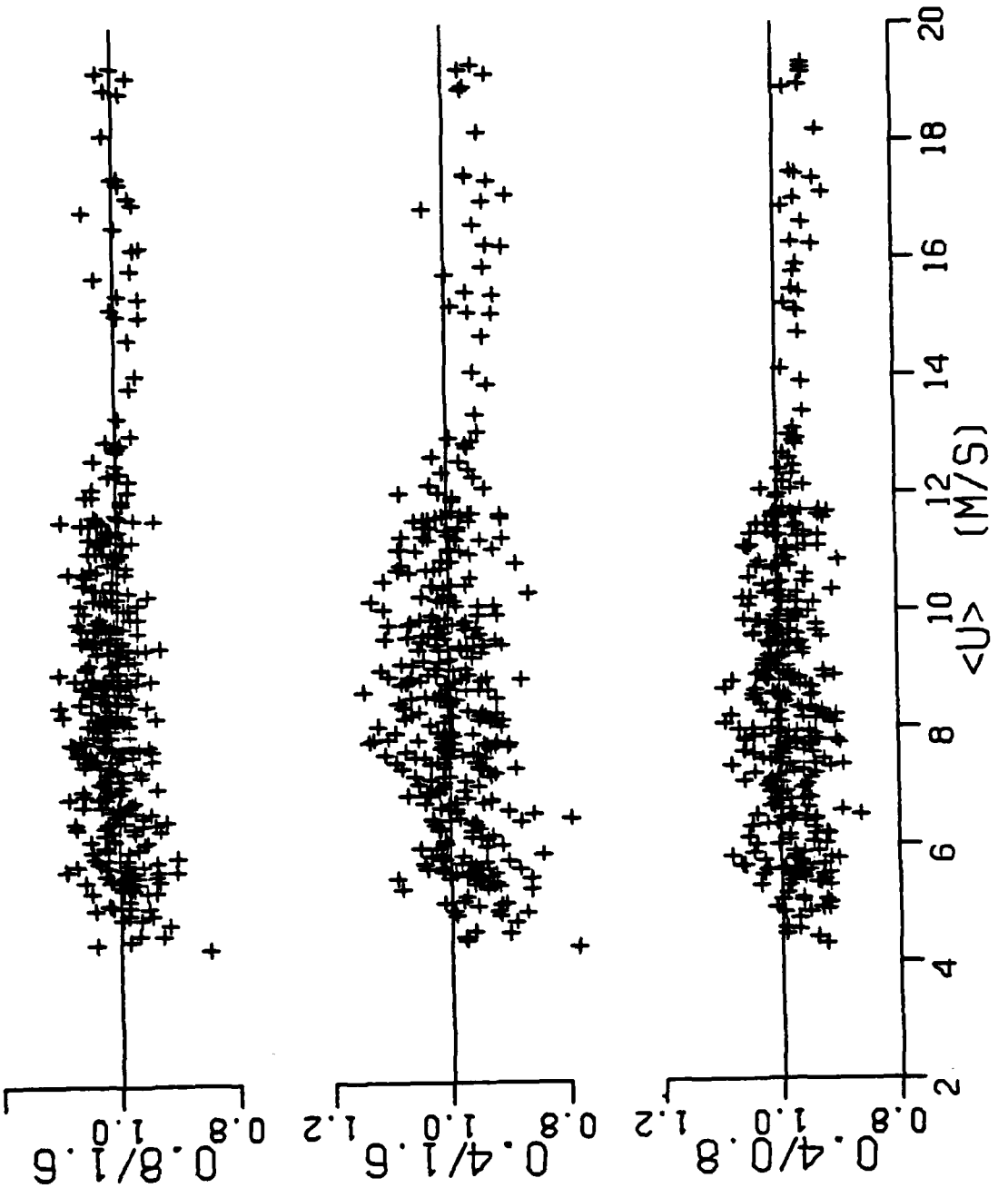

FIGURE 8: Ratios of <uw> calculated from different pairs of band-pass filters as a function of wind speed. The solid line of figure 6A gives the sensor response.

with wind speed and very different from filter to filter. Because the ratios of figure 8 vary so little, on average, with mean wind speed, it is unlikely that errors in the sensor response will produce any major spurious wind speed dependencies. A similar check on the microbead response is not feasible because both the 0.4 and 0.8 Hz band-pass filters are often not entirely in the -5/3 region of the temperature spectrum. The inevitable presence of contaminated data adds a further complication.

3.6 The Experimental Program

The Bedford tower experiment lasted from September 1976 to April 1977. A description of the tower and the results from the BIO system can be found in Smith, 1979. The tower was a floating spar buoy moored in 59m of water, which makes the site essentially a deep water wave regime (Smith, 1979). The location and a photograph of the tower are shown in figure 9. The shortest fetch to the tower site is from the west and is about 10 km, while open fetch conditions extend over a 170° range. The electronics packages can be seen on the main deck, about 3m above the sea. The Gill and HAT are at the very top alongside the BIO thrust and aerovane anemometers and microbead thermistor. The tide tables for Halifax harbour are used to find the phase and amplitude (assumed equal to half the tidal range) at the beginning of each run, from which the measurement height Z is calculated assuming a purely M2 tide, which is the

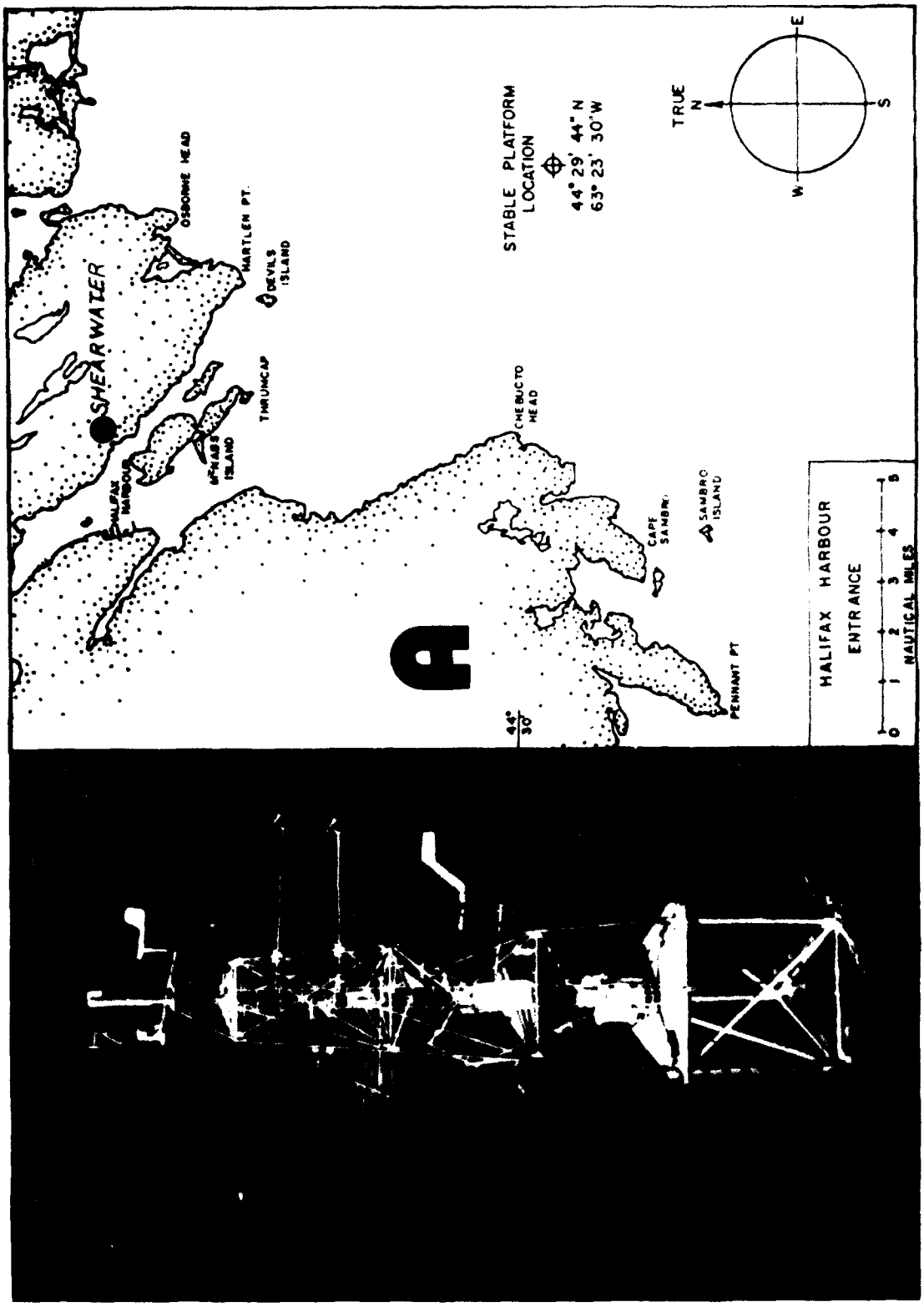

FIGURE 9 A: The Bedford tower site near Halifax Nova Scotia.
B: The instrumentation on the Bedford tower.

predominant tide in this area. The sea temperature sensor was tied to the tower about 10m below mean sea level. Surface meteorological observations, including the atmospheric pressure, PA, for air density calculations, were routinely recorded at the Shearwater "A" land station of the Atmospheric Environment Service, located about 15 km north of the tower site (figure 9).

While on the tower, the Reynolds flux system recorded the three anemometer signals plus a microbead thermistor, an open Brady humidiometer and a filtered Brady from the HAT. The switch settings of section 3.3 were employed so that flux runs of either 3 or 4 groups corresponding to 40.5 or 54 minutes respectively, can be processed. From September 15 a new record began every hour, but on the 23rd the interval was increased to 3 hours and the lower wind speed limit was set to 10 m/s. On October 4 the limit was changed to 8 m/s, then increased to 12m/s on October 6 and put back to 10m/s on February 15 where it remained until the end of the experiment. Meanwhile the dissipation system (figure 5) sampled and recorded the low-pass data from the same six signals plus a rod thermistor from the HAT and the sea temperature. The Gill-u, Gill-w, microbead and open Brady signals were selected to be band-pass filtered. The number of summations, NI, was set to 4500 to comply with a 4 minute Dt, which enabled the pair of cassettes to last for 52.5 days.

The weather ship experiment included the four patrols of CCGS Quadra between July 1977 and April 1978. During the third and fourth patrols a single propeller Gill anemometer was used with the Gill-u signal also being processed as the missing Gill-w signal. The typical mode of operation of the ship when at "PAPA" (figure 10) was to drift with the wind then return to station by steaming into the wind at less than 4 knots. During the latter operation the great bulk of good data were collected, but some useful data were also collected as the ship steamed at 7 to 12 knots while en route to "PAPA" (figure 10). The location of the sensors on the ship's foremast is shown in the photograph of figure 10. Cables were run to the electronics packages two decks below the base of the mast. With winds coming over the bow the measured tilt angles are typically only about +7°, indicating that the ship's distortion of the mean flow is not enough to upset the dissipation method. However, winds more than 30° to starboard or 60° to port were found to have greatly perturbed high frequencies, which proved to be very unfortunate because the ship drifted for many hours in such winds. In addition the foremast location received a great deal of spray so that the microbeads broke and the Lyman-alpha windows became dirty soon after the first enccunter with heavy seas. As a consequence very little temperature data and no humidity data are available from the ship. The spray also caused a great deal of pitting in the leading edges of the propellers, which they can fortunately tolerate. In a subsequent experiment (JASIN 1978), the same sensors were mounted forward of the bow of the FS Meteor so that the wind

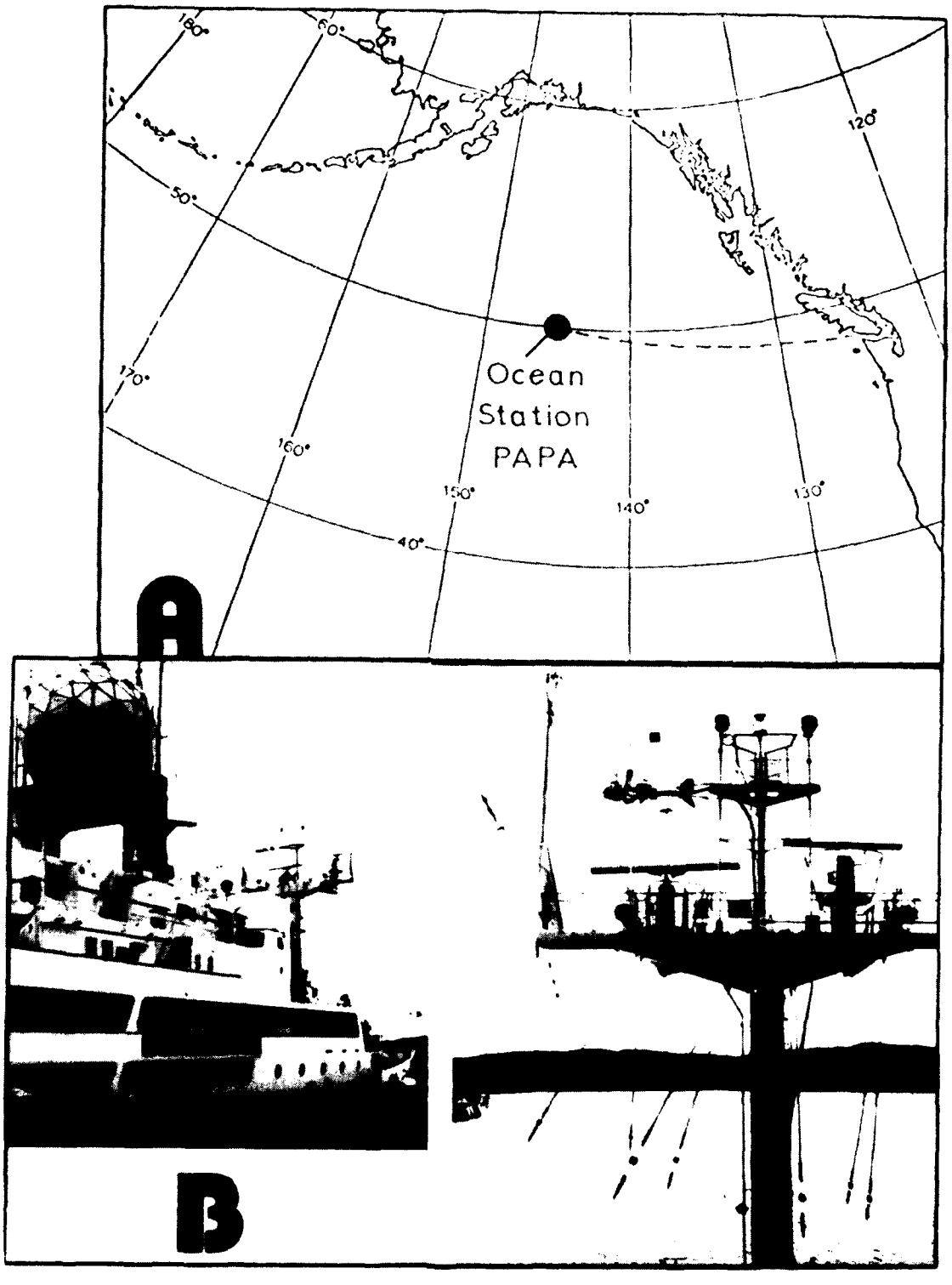

FIGURE 10 A: Ocean Weather Station "PAPA", 50°N, 145°W, and the route of the weatherships.
B: The instrumentation on the foremast of CCGS Quadra.

carried the spray away and a great deal of both temperature and humidity data were collected.

While on CCGS QUADRA, the dissipation system low-pass filtered and recorded the signals from the following sensors: a rod and two microbead thermistors from the HAT, the Gill anemometer, a Lyman-alpha humidiometer and the dewpoint system. The two Gill velocity, the two microbead and the Lyman-alpha signals were all band-pass filtered. Dt was set at 5 minutes, allowing NI to be 5800 and up to 56 days of data to be stored on the two cassettes. The Reynolds flux system was included to provide velocity and scalar spectra. It was set up as on the tower, but the Brady arrays were replaced by the dewpoint and Lyman-alpha signals. The wind speed limit was always set to at least 8 m/s so that flux records were taken throughout most of a patrol. With these switch settings it was possible to turn the systems on prior to sailing and to retrieve the data cassettes upon return seven weeks later. A sea surface "bucket" temperature and the atmospheric pressure are available from the ship's three hourly meteorological observations.

CHAPTER 4 REYNOLDS FLUX MEASUREMENTS FROM THE BEDFORD STABLE TOWER

4.1 Introduction

The Reynolds flux data set from the Bedford tower consists of 196 momentum flux runs with winds up to 20 m/s and the majority of stabilities in the range $-0.4 < Z/L < 0.1$. In most cases the fetch is unlimited, but winds from all directions, except those which put the sensors in the wake of the BIO thrust (from the east), are allowed, so some fetches are as short as 10 km. The runs are restricted to the 5 m/s or greater winds necessary to keep the tilted propeller in its linear operating range, which also ensures that the measurement height, $Z \cong 13$ m, is in the "constant flux" layer. It is very gratifying to find that in each case where simultaneous dissipation data exists, 192 runs, the band-pass data confirm the existence of a -5/3 region in the velocity spectra. Other runs are rejected because the Gill-w and Gill-u signals do not track each other properly.

All 196 runs have been considered for sensible heat flux calculations, because even 5 m/s winds are sufficient to flush the HAT. However, during many of these runs the temperature data are not available, because either the microbead was broken or very cold air drove its signal off scale. A few runs are also rejected because the mean air temperatures from the rod and microbead thermistors do not agree to within ±0.1°C. In addition many more runs have not been processed due to what is believed to be the sensitivity of a salt contaminated microbead

to humidity fluctuations as reported by Schmitt et al., 1978. This behavior is recognized by relatively little variance in the temperature spectrum below n=0.01 and in many of these cases, but not all, the dissipation data reveal that the temperature spectrum is not falling as steeply as -5/3. Only 60 of the 196 runs have been found to satisfy criteria for temperature flux calculations.

All the Reynolds flux results are tabulated in the Appendix and are referred to as runs T1 to T196.

4.2 The Stability Parameter Z/L

A stability parameter $Z/L(\Delta T)$ is calculated from equation 2.38 for each of the 196 runs. The surface temperature, TSFC, is approximated by the dissipation system's sea temperature probe, TSEA, which is assumed to have fallen linearly over a 16 hour period that was not recorded (runs T90-T93). The mean air temperature, TZ, at the measurement height, Z, usually comes from the rod thermistor of the dissipation system, but over the unrecorded gap and during periods when the rod's signal either has erratic behavior (runs T47-T55, T74-T85 and T138-T149) or is offscale, the flux system's recordings of the microbead are used. Unfortunately, during runs T102-T110, T117-T122 and T131-T133 neither temperature sensor was operational and it is necessary to use the meteorological observations from Shearwater. In figure 11B, $Z/L(\Delta T)$ is plotted against the more

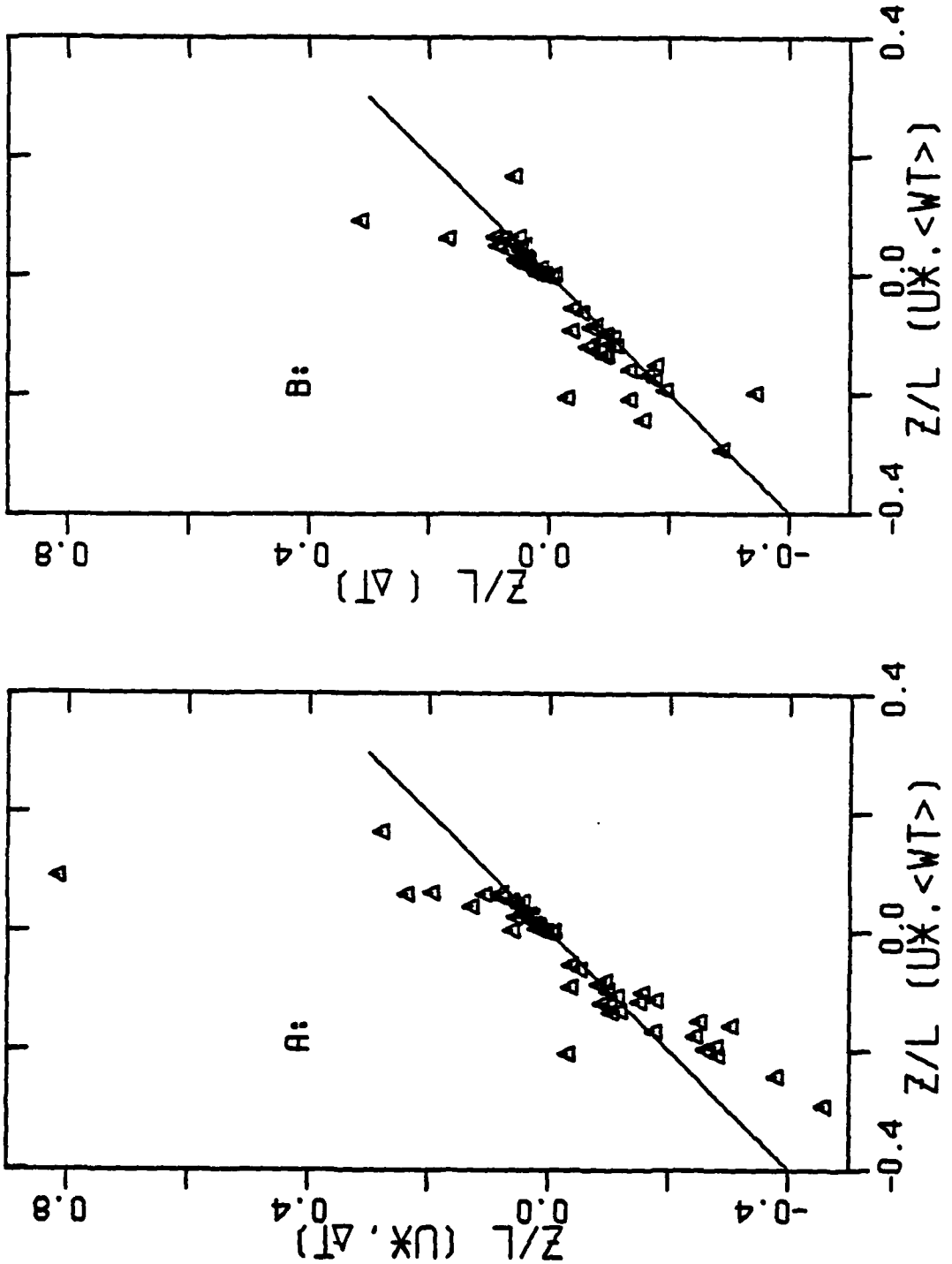

FIGURE 11 Comparison of the most complete expression for the stability parameter Z/L(u*,<wt>) to:
A: an approximate expression Z/L(u*,ΔT).
B: the bulk estimate Z/L(ΔT).

exact $Z/L(u^*,\langle wt\rangle)$ (equation 2.36) for the 60 temperature runs. The two calculations tend to agree on average and seldom differ by more than ±0.05, but occasionally the difference is substantial (more than 0.2). Since u^* is calculated for all the runs it can be used, instead of $\langle U\rangle$, to calculate a stability parameter $Z/L(u^*,\Delta T)$ from equation 2.37. However this estimate does not agree as well with $Z/L(u^*,\langle wt\rangle)$ as shown in figure 11A, where systematic departures from a 1:1 relationship are evident. Since $\langle wt\rangle$ is only available from the temperature runs it often must be approximated by $C_T \langle U\rangle \Delta T$, but evidently the associated error is partially compensated by the error in replacing u^{*2} with $C_D \langle U\rangle^2$. The bulk estimate $Z/L(\Delta T)$ is to be used exclusively, because it is the best estimate of stability that is always available, even though it may not be very accurate for an individual run.

4.3 Turbulence Spectra And Cospectra

The spectra of the fluctuating velocity components and fluctuating temperature, $\phi(f)$, provide a means of evaluating the performance of the Reynolds flux system (section 3.3).

To find a value of E for each quantity integrated by the I3 method, equation 3.5, normalized spectra and cospectra, $N\phi(n)$, are established by averaging over all available runs. All spectral values and their corresponding natural frequencies, $n=fZ/\langle U\rangle$ (186 per run), are first calculated. The $\phi(n)$ are then

multiplied by f to produce a variance preserving plot against log(n). Next the f ϕ(n) are non-dimensionalized by dividing by: u^{*2} in the case of velocity spectra and cospectra, $(\sigma t)^2$ for temperature spectra and $\langle wt \rangle = -ku^*t^*$ for w,t cospectra. Finally, the discrete normalized spectral values from M runs in a particular stability range are band averaged over n, such that $\Delta \log(n)$ remains constant, giving a mean, taken to be $N\phi(n)$, and a standard deviation, σ, for each band. A plot of $N\phi(n)$ vs. log(n) should, according to similarity theory, display a universal form, depending on stability. The normalizing factors $u^{*2}=-\langle uw \rangle$, $\langle tt \rangle = (\sigma t)^2$ and $\langle wt \rangle$ are found for each run by integrating ϕuw, ϕt and ϕwt from n=0.004 and are therefore as much as 10% small, but the error is independent of wind speed. There is a great deal of scatter in the ϕ(f)'s, not only from run to run, but between nearby frequencies of the same run, due to the inherent variability of the Fourier coefficients. The latter effect is reduced by averaging over the NG groups of a flux run. However, it is not reduced further, by averaging over Fourier bands, because this greatly increases the band-width, which should be kept as narrow as possible in order to keep $N\phi(n)$ representative of its natural frequency, especially at low frequencies where there are only a few points in each band. As a consequence, σ is extremely large and not indicative of the variability of the mean, $N\phi(n)$. Since the M runs are independent, $\sigma_m = \sigma/\sqrt{M}$ is taken as an estimation of the standard deviation of the mean. This estimation assumes Gaussian statistics, which should be approached with a large number of runs, and that the mean and σ are good measures of the

population statistics, which requires that NP, the number of points in a band, be much larger than M. This latter assumption is not strictly satisfied as NP approaches M, but because each run continues to contribute at least one point, the statistics should remain nearly Gaussian with $\sigma_m \cong \sigma/\sqrt{M}$ a reasonable approximation. Similarly, when NP becomes less than M, each point comes from a different run and $\sigma_m \cong \sigma/\sqrt{NP}$ is assumed.

In the following normalized plots $N\phi(n)$ from each band is plotted in the middle of the log(n) band and shown by a diamond with vertical bars extending up and down 1 σ_m. In the logarithmic plots the means (squares) are plotted and solid lines of -2/3 slope, indicating $\phi(f)$ proportional to $f^{-5/3}$, are drawn. The runs are sometimes split into stable and unstable groups which are averaged and plotted separately. There is no attempt to average over smaller stability ranges because the large majority of runs span only a narrow range and because of the large uncertainty in $Z/L(\Delta T)$.

Velocity Spectra

The normalized spectra of the downstream velocity component, $N\phi_u(n)$, are shown in figure 12 and there is a marked dependence on stability. The peak of the spectrum of the stable runs, figure 12B, occurs at a natural frequency more than a decade higher than that of the unstable runs (figure 12A), whose spectrum in turn has a greater proportion of its energy at lower frequencies. The spectral points below $n=10^{-3}$ come from the highest wind speed runs and their average over the natural

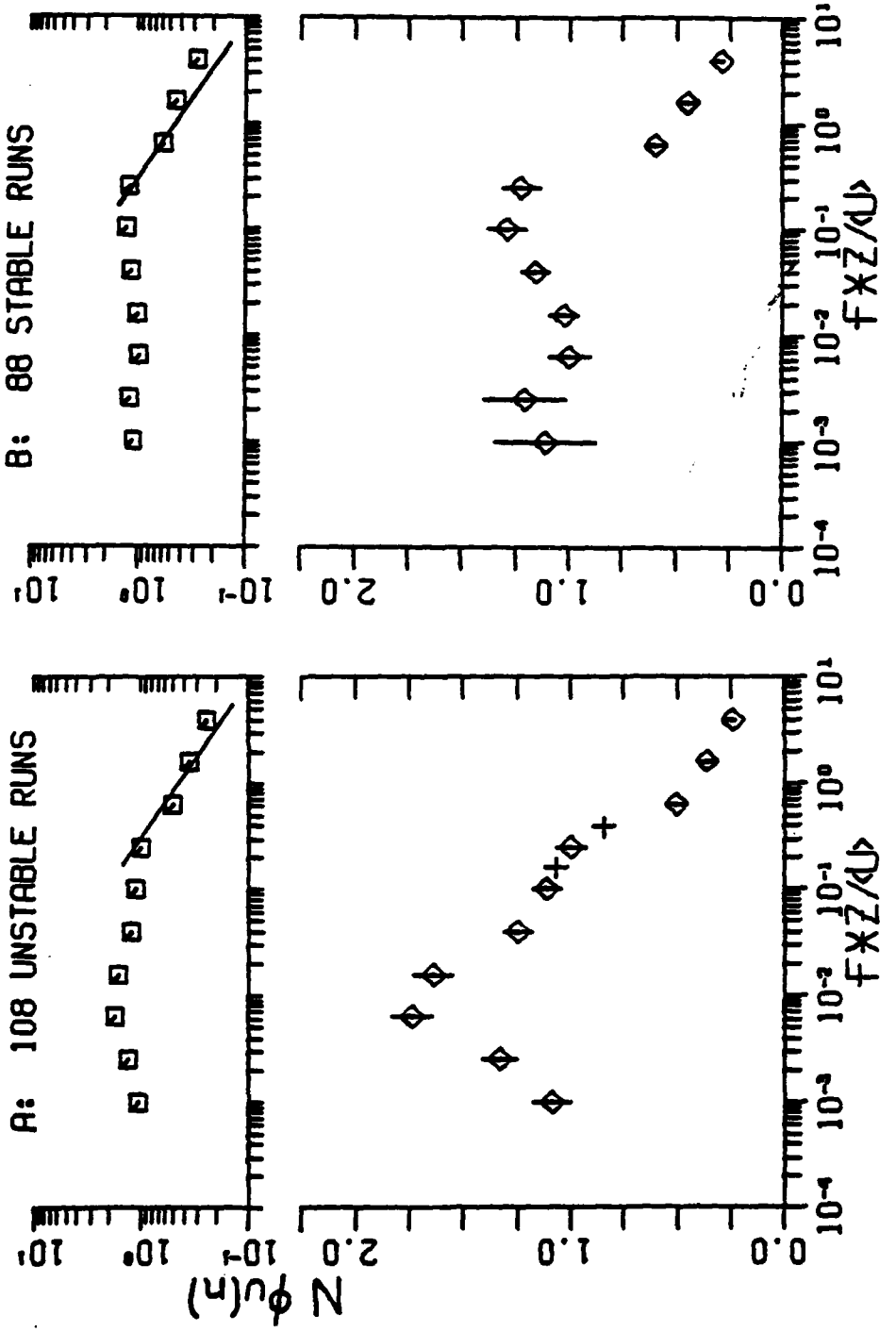

FIGURE 12 Normalized spectra of the downstream velocity component from averages of $f\,\phi_u(n)/u^{*2}$ (pluses from slow samples only). Solid line has slope -2/3. Vertical lines are ± 1 σ.
A: 108 unstable runs, B: 88 stable runs.

frequency band, log(n)= -3.21 to -3.00 is about 0.75 in both the stable and unstable case. It does appear, therefore, that a spectral gap is emerging between the fluctuating motion and the mean flow. Some platform motion is expected, but it is not evident in the spectra, perhaps because it is obscured by averaging over large frequency bands. The log-log plots of figure 12 display a similar shape and stability dependence as do the over land spectra of McBean, 1971. In contrast, the measurements over land of Kaimal et al., 1972, suggest sharper peaks.

Contributions to the bands between n=0.1 and n=0.4 come from both the slow and the fast samples depending on wind speed and the small pluses on figure 12A represent the band averages using only the slow samples. These are plotted at the average value of log(n) and not at the band center as are the overall averages. In this range (0.1 <n< 0.4) the fast sampled spectrum does, on average, match the more statistically certain spectral values found from the slow samples. There is no evidence of aliasing in the slow samples corroborating the argument that it is compensated by the 1 second time constant low-pass filter. Similar matching is not done in figure 12B because the points fall near the peak of the spectrum.

It happens that all three Gill-u band-pass filters may be utilized under all conditions encountered at the tower and at "PAPA". The logarithmic plots of figure 12 show that both the stable and unstable spectra begin to display a -5/3 region at about a natural frequency n=0.2. Above n=1.0, the Nyquist

frequency when <U>≅18 m/s, the $n\phi_u(n)$ fall above the -2/3 lines (fall less rapidly than -5/3), reflecting the expected spectral distortion due to aliasing. Figure 8 suggests that, at Z=13m, the output of the 0.4 Hz band-pass filter contains frequencies below the -5/3 range with 12 m/s and higher winds, which sets the low frequency cut-off of Hc(f) at about (0.2 12m/s/ 13m) ≅ 0.2 Hz. However, figure 8 also indicates that the stress calculated from the 0.4 Hz filter is only about 5% lower, on average, than that calculated from the other filters, for winds up to 20 m/s. Therefore, utilizing <u>all</u> three filters to find the stress should introduce a systematic error less than 2% and in return improve the statistical certainty of the estimate. The effective low frequency cut-off of the 0.4 Hz filter and prewhitener combination is $n\ \langle U\rangle/Z \cong$ (0.2 20m/s/ 13m) ≅ 0.3 Hz, the 3db down frequency of Hc(f). The tower winds are always less than 20 m/s and at "PAPA", the wind plus ship speed is always below (0.3Hz 22m/ 0.2) ≅ 33 m/s, therefore, the dissipation calculations always use the data from all three band-pass filters.

Of course, filters cannot be used in the dissipation method if they pass frequencies contaminated by the ship's motion. The horizontal velocity spectrum, $f\phi_Q(f)$, of figure 13, is an average of four Reynolds flux records taken during very rough seas and slightly unstable conditions at "PAPA". The spectral values are averaged over bands of log(f) in the manner described for the normalized spectra. The number of runs, N, is 4, so the vertical bars extend $\pm 1\ \sigma_m \cong \sigma/2$, where σ is the standard deviation about the mean $f\phi_Q(f)$ of a log(f) band. The 22 m/s

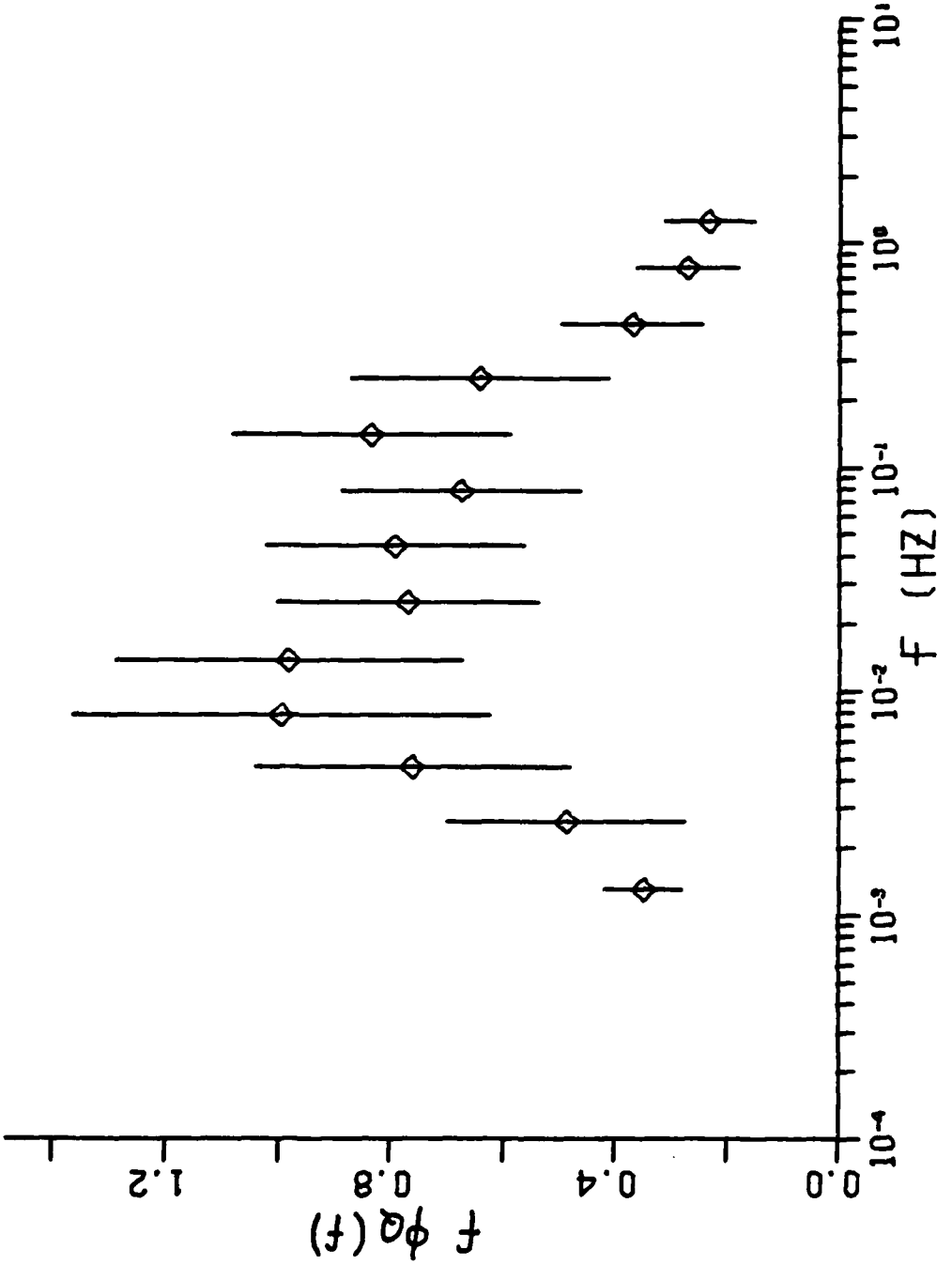

FIGURE 13 The horizontal velocity spectrum, f $\phi_Q(f)$ in Hz and $(m/s)^2$, averaged over 4 runs from CCGS Quadra in 22 m/s winds. Vertical bars extend ±1 estimation of the standard deviation of the mean.

winds make n and f very nearly equivalent and the spectrum is, accordingly, nearly the same as figure 12A except between f=0.1 to 0.3 Hz where the motion of CCGS Quadra is conspicuous. Thankfully, even under such extreme conditions, very little ship motion should be passed by the 0.4 Hz band-pass filter prewhitener combination. Nonetheless, its output while on a ship is always checked.

Figure 14 shows the normalized vertical velocity spectrum, $N\phi_w(n)$. The peaks, near n equals 1, are barely reached with the 3Hz fast sampling rate, but there appears to be a shift to a higher frequency in the stable case, which is in accord with the over land studies previously cited. The spectral shapes near the peaks must be distorted by the aliasing of a relatively large amount of high frequency variance, some of which is inevitably lost because there is only partial correction for sensor response. Again there is no evidence of platform motion. At low frequencies σ_n is very small and the low spectral levels and the observed stability dependence have also been found in other studies, indicating that the horizontal velocity is being properly removed from the tilted propeller signal. In section 3.5 the Gill-w response investigation suggested that the -5/3 range of $\phi_w(f)$ begins above $n \cong$ (0.8Hz 13m/12m/s) $\cong 0.9$, and this is consistent with the logarithmic plots of figure 14. Therefore, some restrictions have to be imposed when the Gill-w band-pass filter outputs are used in the dissipation method. On the tower, for example, the 0.4, 0.8 and 1.6 Hz outputs should definitely not be used when the wind speed exeeds (0.3 Hz 13m/1.0) $\cong$ 4 m/s, 8 m/s and 16 m/s, respectively.

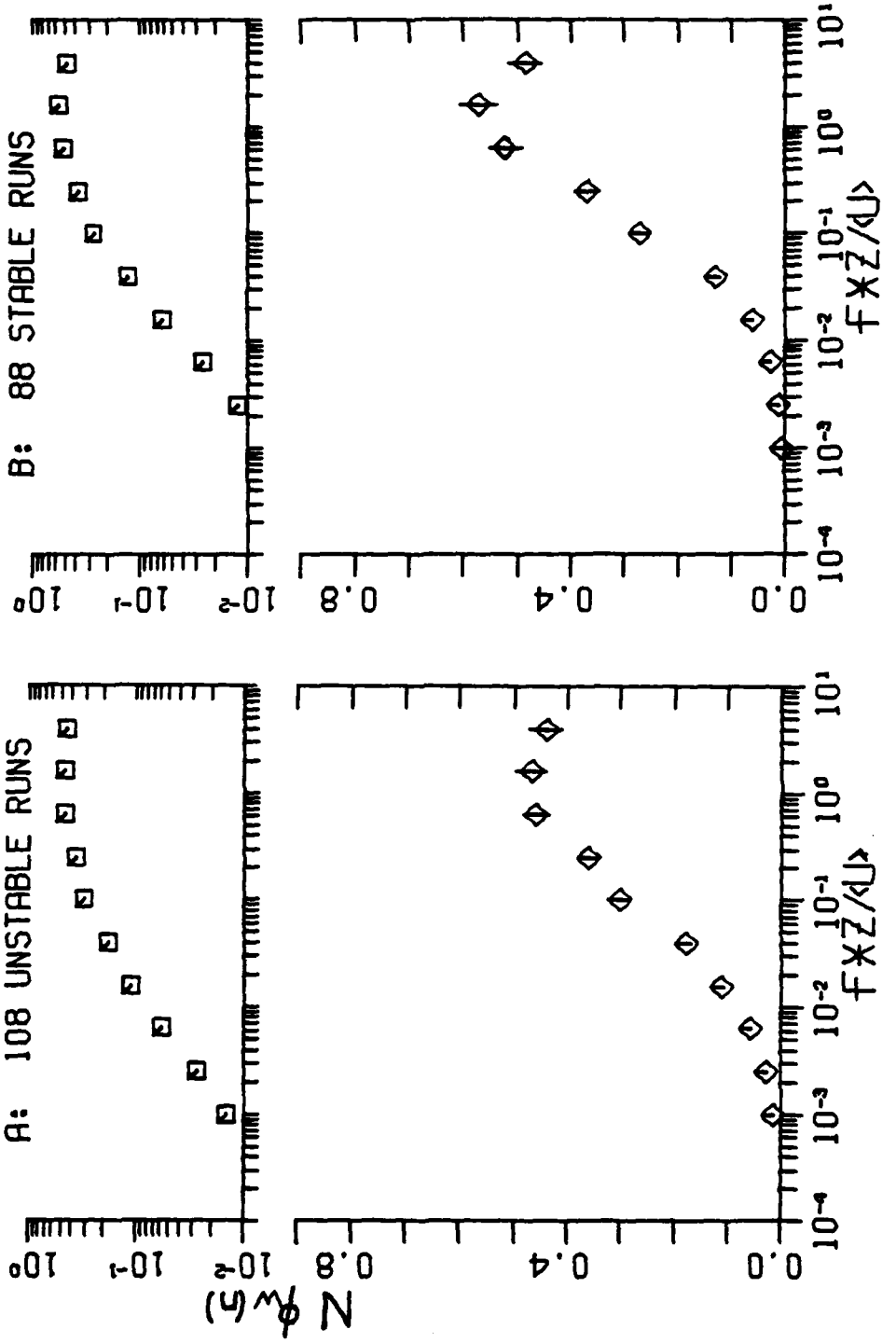

FIGURE 14 Normalized vertical velocity spectra from averages of $f\,\Phi_w(n)/u_*^2$ over:
A: 108 unstable runs B: 88 stable runs.
Vertical lines are ±1 σm.

The Temperature Spectrum

The normalized spectrum of the temperature fluctuations, $N\phi t(n)$, from all 60 temperature runs, is shown in figure 15. Individual plots for averages over the 27 unstable and 33 stable runs are not presented because they are not very different and, with so few runs, not very statistically certain. However, the majority of runs have $|Z/L| < 0.1$, so figure 15 may be representative of "near neutral" stratification. Accordingly, the spectral shape is very much like McBean's (1971) near neutral case, however the generalized temperature spectrum of Kaimal *et al.*, 1972, indicates a sharper peak at a higher frequency. An average over the $\log(n) = -3.25$ to -3.0 frequency band gives a mean of 0.15, which, despite a large standard deviation, supports the existence of a spectral gap that seemingly would emerge if more high wind speed runs were available. The two pluses plotted near n=0.2 and n=0.3 are the averages of 1524 and 402 points, respectively, from the slow samples only and their average fits the high frequency portion of the temperature spectrum quite well. The rise of the higher frequency plus may be a consequence of combining the stable and unstable runs, or due to a little aliasing, but when the microbead is suspected of responding to humidity fluctuations the peak of the spectrum is found above n=0.1 and the inclusion of only a small amount of such data could likely be the source of this feature.

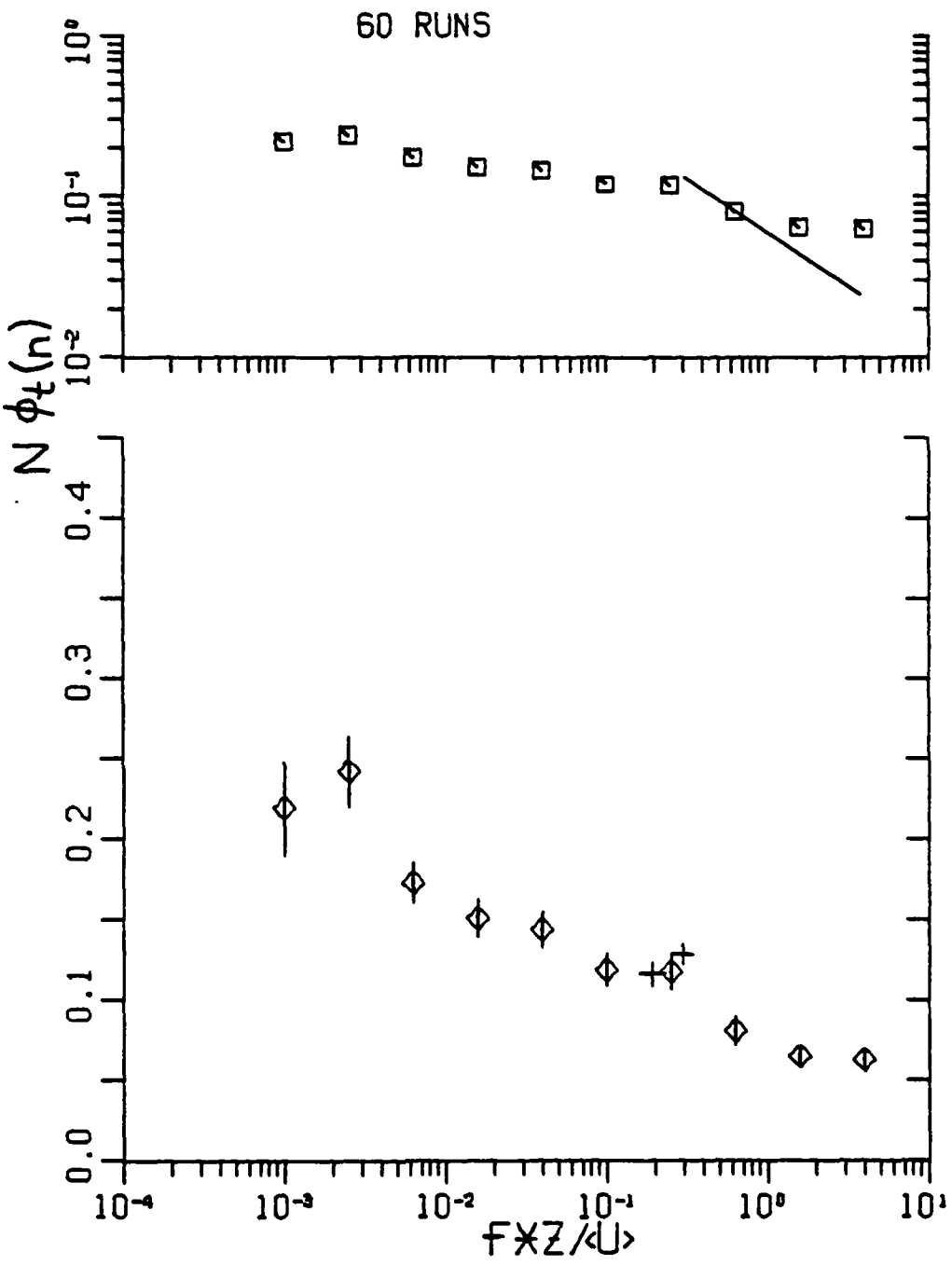

FIGURE 15 The normalized temperature spectrum from averages of $f\,\phi_t(n)/(\sigma t)^2$ over all 60 temperature runs (pluses from slow samples only). Solid line has slope -2/3 and vertical lines extend ± 1 σm.

AD-A081 392 BRITISH COLUMBIA UNIV VANCOUVER INST OF OCEANOGRAPHY F/G 4/2
THE TURBULENT FLUXES OF MOMENTUM AND SENSIBLE HEAT OVER THE OPE--ETC(U)
AUG 79 W G LARGE N00014-76-C-0446
NI

UNCLASSIFIED

2 OF 3
AD
A081392

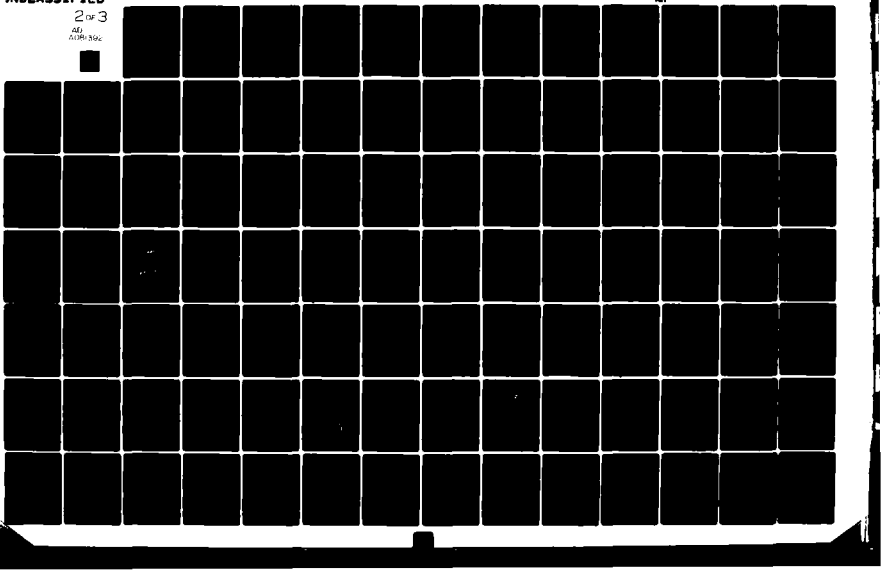

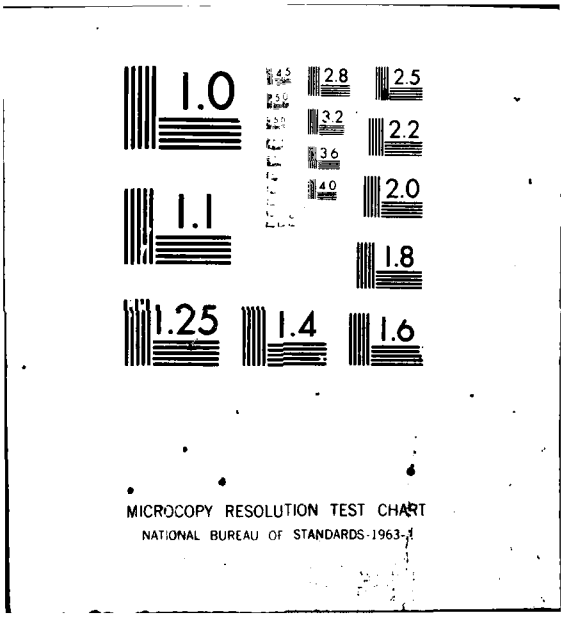
1.0
1.1
1.25
1.4
1.6
1.8
2.0
2.2
2.5
2.8
3.2
3.6
4.0
MICROCOPY RESOLUTION TEST CHART
NATIONAL BUREAU OF STANDARDS-1963-A

The logarithmic plot does not exhibit any evidence of a -5/3 region, which the San Diego results of Phelps and Pond, 1971, show to begin at about n=0.6. Here the spectrum is distorted by aliasing before it can develop, however one of the criteria for selecting the 60 temperature runs is that the ratios of the band pass filters reveal the existence of a -5/3 region above n=0.6. The 3db down frequencies of the combined prewhitener and 0.4, 0.8 and 1.6 Hz temperature band-pass filters are about 0.3, 0.55 and 1.0 Hz respectively. The implication is that the use of the temperature data in the dissipation method ought to be restricted in the following manner: the 0.4 Hz to winds less than (Z 0.3Hz/0.6) $\cong$ 6 m/s on the tower and 10 m/s on the ship, the 0.8 Hz to speeds less than (Z 0.55Hz/0.6) $\cong$ 12 m/s on the tower and 20 m/s on the Quadra and the 1.6 Hz to <U> below (Z 1.0Hz /0.6) $\cong$ 20 m/s on the tower and 37 m/s on the ship. Unluckily, at the higher wind speeds only data from the 1.6 Hz filter are useful, so there is no check on the -5/3 region.

The u,w Cospectrum

The normalized u,w cospectrum, $N\Phi uw(n)$, from the stable runs is significantly different from that found in the unstable case, as shown by figure 16. The over land results of both McBean and Miyake (1972) and Kaimal et al. (1972) are in excellent agreement with these over sea spectra. When calculating E for the I3 method of integrating u,w and w,t cospectra (page 51), the $N\Phi(n)$ are averaged over bands of $\Delta\log(n) = 0.25$. For clarity, the bands in figures 16 and 17 are

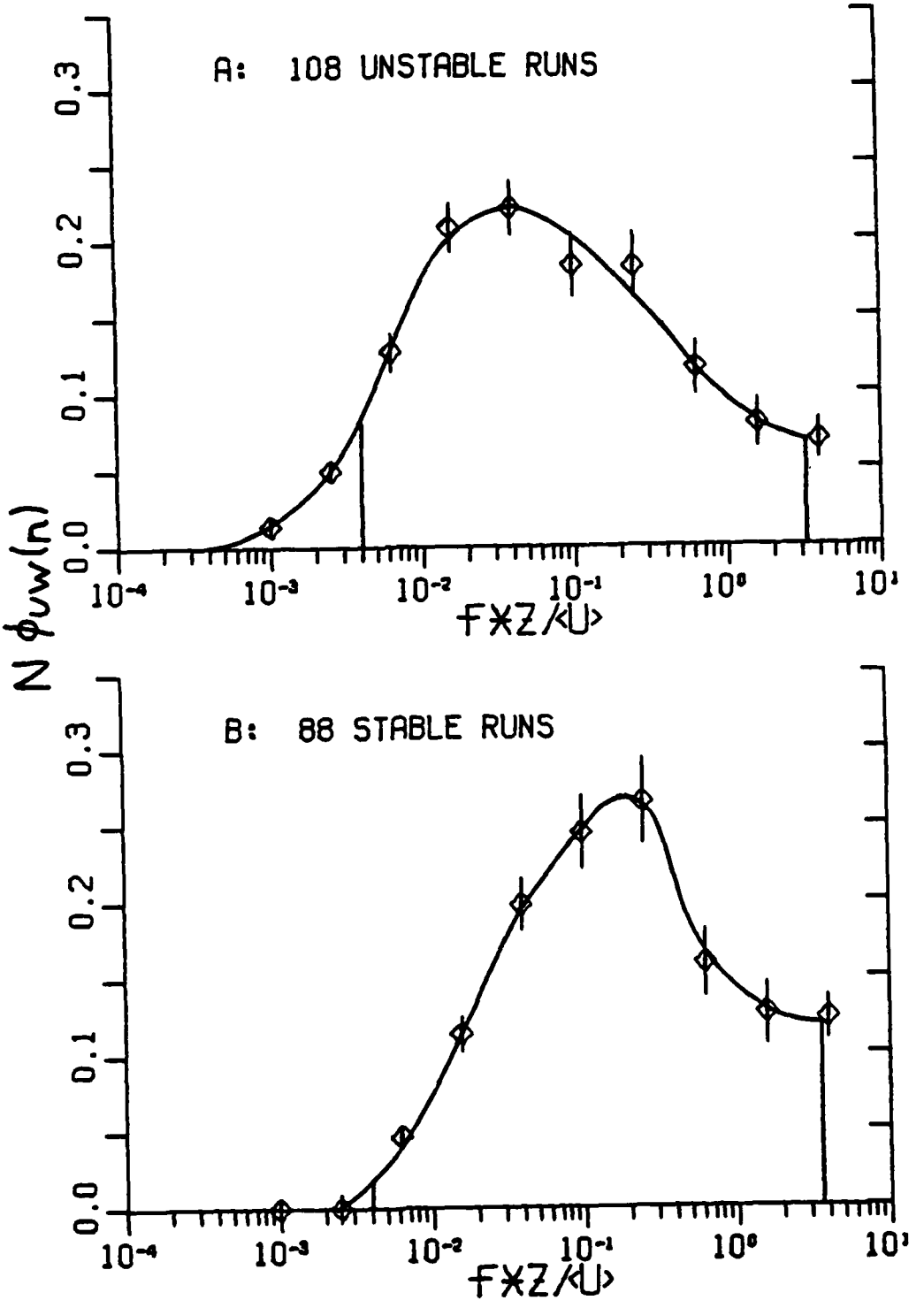

FIGURE 16 Normalized unstable (A) and stable (B) u,w cospectra ±1 σm, from averages of f φuw(n)/u*². Integration under the solid curves gives E for the I3 method.

0.40, but the solid curves trace out the approximate areas integrated. From its peak at a natural frequency n=0.03 the unstable cospectrum, figure 16A, falls steeply to lower frequencies leaving about 1% of the total covariance below $n=10^{-3}$. The more gentle fall to higher frequencies is usual, but here, as in figures 12 and 14, aliasing distcrts the shape above n=1. The highest frequency point is plotted at n=4, the band center, but the average log(n) of this band is at n=3.2, which is near the high frequency cut-off of the integration over the $\Delta\log(n) = 0.25$ bands. The total area under the curve was found to be 1.06 times the area from n=0.004. The stable cospectrum, figure 16B, shows more covariance at higher fequencies with a peak at about n=0.2. There is no covariance, on average, below n=0.002, but individual runs often display significant amounts, both positive and negative. The total area under the solid curve is only about 1.005 times the area from n=.004. The ratio E, required for the I3 method of integrating the cospectrum, turns out to be a function cf stability and Eu=1.06 and Es=1.005 are realistic values for unstable and stable cases, respectively.

The w,t Cospectrum

The normalized w,t cospectrum, $N\phi wt(n)$, behaves in a similar fashion as $N\phi uw$ and also agrees with the over land measurements. The unstable cospectrum, figure 17A, displays a broader peak at a slightly lower frequency than does the stable, figure 17B. Again there is a greater proportion of the covariance at the lower frequencies in the unstable case, where

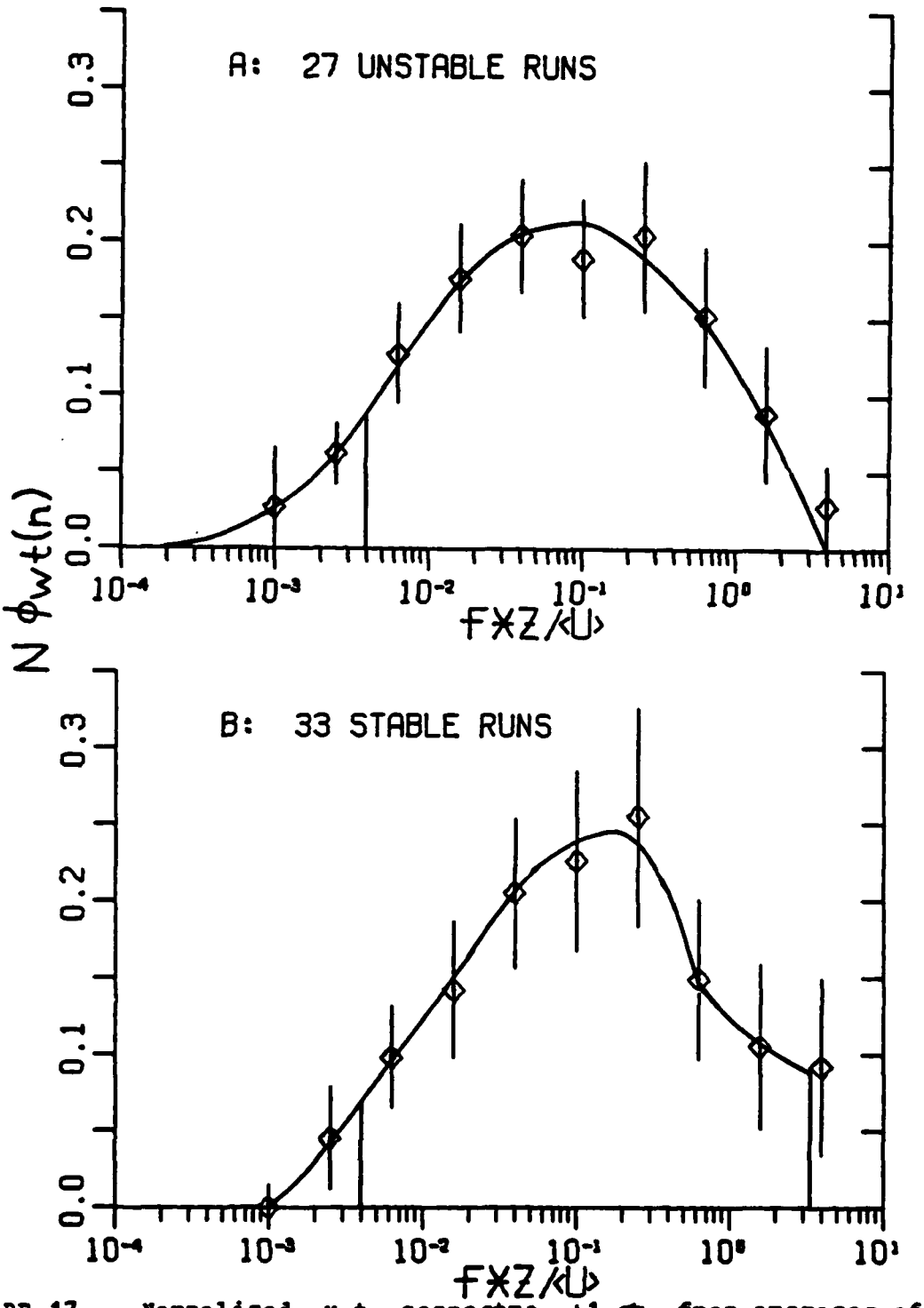

FIGURE 17 Normalized w,t cospectra ±1 σn, from averages of f φwt(n)/<wt> in (A) unstable and (B) stable conditions. Integration under the solid curves gives E for the I3 method.

the total area under the solid curve is about 1.10 times the amount from n=0.004. In the stable case this ratio is only 1.04. The suggestion is that the I3 method of integrating w,t cospectra ought to use Eu=1.10 (unstable) and Es=1.04 (stable). With only 33 stable and 27 unstable temperature runs these cospectra and integrations have more uncertainty, as reflected by the larger estimates of the standard deviation of the mean, than found for ϕ_{uw}. Humidity sensitivity of the temperature sensor is difficult to diagnose from the cospectrum, because it results in f $\phi_{wt}(n)/\langle wt \rangle$ being very similar to the average stable case, figure 17B.

4.4 Turbulence Statistics

The spectra and cospectra from each run are integrated from f=0.00065 Hz (the I1 method), to give estimates of the statistical quantities σu, σv, σw, σt and the u,w correlation coefficient $r(uw) = \langle uw \rangle/(\sigma u\, \sigma w)$. The mean, standard deviation and wind speed dependence of some of these normalized quantities are presented in table II, however there may be some stability dependence in these results. It is evident from figure 12 that this method of integrating $\phi_u(f)$ is likely to underestimate σu by more than 13% at $\langle U \rangle$=6 m/s. This effect decreases with increasing wind speed and accounts for at least half of the observed increase in $\sigma u/\langle U \rangle$ with $\langle U \rangle$. A similar behavior is expected for σv and σt, which also have significant low frequency contributions. The mean and scatter of $\sigma v/\langle U \rangle$ and

	Means of 196 runs	Standard deviation	Linear regression	Results cf Smith & Banke 33 runs
$\sigma u/\langle U\rangle$	.092	.018	.061 + .0026<U>	.094 ± .014
$\sigma v/\langle U\rangle$	.080	.031	.036 + .0037<U>	.084 ± .022
$\sigma w/\langle U\rangle$	.042	.006	.027 + .0013<U>	.048 ± .005
$\sigma w/u^*$	1.24	.10	1.18 + .005 <U>	1.47 ± .11
-r(uw)	.31	.06		.34 ± .07

TABLE II Turbulent velocity statistics from the 196 Reynolds flux runs. The means ± 1 standard deviation from Smith and Banke, 1975, are shown for comparison.

$\sigma u/\langle U\rangle$ are, therefore, quite reasonable. The values cf $\sigma w/\langle U\rangle$ and $\sigma w/u^*$ are rather less than those of Smith and Banke, 1975, perhaps because the aliased frequencies are not completely corrected for sensor response. Figure 16 shows that the I1 method should never underestimate σuw by more than 5% and that the loss of high frequency covariance should be less than half the amount of variance lost by σw. The combined error in σuw may, therefore, be about half the sum of the σu and σw errors, which is consistent with the correlation coefficient r(uw) being similar to previously reported values.

Figure 18, shows the means of $\sigma u/u^*$, $\sigma v/u^*$ and $\sigma t/T^*$ ($T^*=Kt^*$ is used to conform with McBean, 1971) band averaged over ranges of Z/L. Only 39 of the temperature runs are used in the averaging, because many runs are near neutral where large $\sigma t/T^*$

Stability range mid Z/L ±0.01	Number of runs	Standard deviations about the plotted means		
		σu/u*	σv/u*	σw/u*
-0.05	13	0.30	0.79	0.12
-0.03	17	0.25	0.41	0.09
-0.01	22	0.43	0.51	0.06
0.01	25	0.58	0.69	0.10
0.03	28	0.34	0.26	0.08
0.05	16	0.47	0.45	0.09

TABLE III Standard deviations of the turbulence statistics about the stability band means plotted in figure 18.

values occur as a result of the "noise" in σt discussed by McBean. With so few temperature runs available σt/T* at Z/L=0.077 is plotted even though only 6 runs fall in the band. Otherwise, the stability ranges are selected so that at least 10 runs fall into each band. For clarity, some standard deviations from the band averaging at small vaues of |Z/L|, are presented in table III. Typically, the standard deviations about the mean σt/T* values in figure 18 are about 0.5. The magnitude of the standard deviations in table III are comparable to the scatter in McBean's results. σw/u* exhibits the smallest stability dependence and the least scatter, perhaps because low frequency contributions to σw are minimal. Almost all the averages plotted in figure 18 fall within the scatter of McBean's (1971)

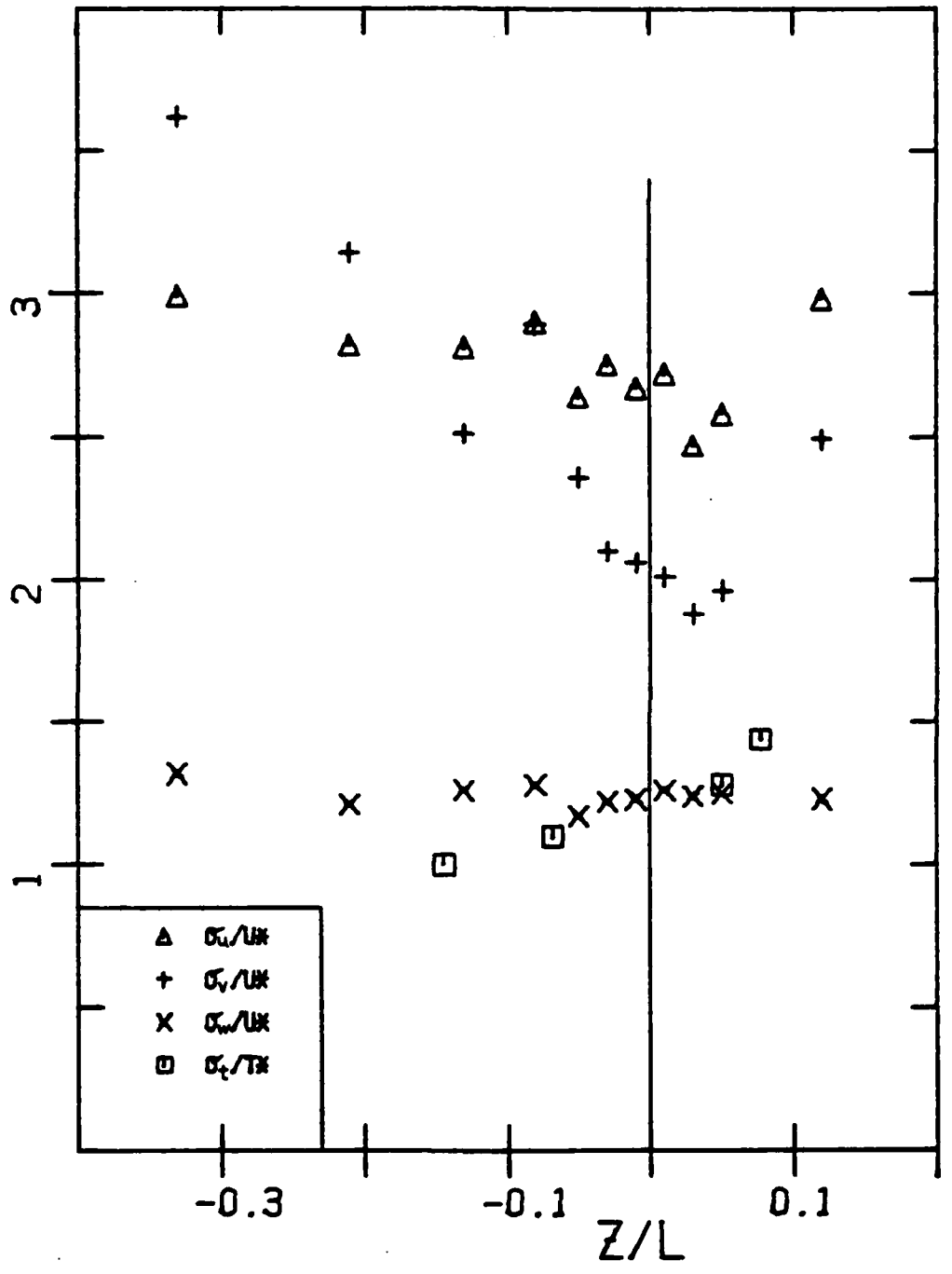

FIGURE 18 Non-dimensional turbulence statistics band averaged over stability. See table III for standard deviations about plotted means.

plots and the observed differences are not unexpected. His variances are computed as integrals from n=0.01 to 10, giving even smaller σu's, but better σw's than the I1 method. Accordingly, his $\sigma u/u^*$ values tend to be lower and his $\sigma w/u^*$'s higher than the corresponding means in figure 18. However, the wind speed ranges of the two studies are considerably different ($\langle U \rangle < 8$ m/s for all of McBean's runs), so any wind speed dependencies, such as shown in table II, complicate the comparison. In addition, both u* and T* are calculated from integrals over different frequencies. Despite these problems, $\sigma v/u^*$ and $\sigma t/T^*$ in figure 18 are generally in excellent agreement with McBean. Measurements of the sensible heat and moisture fluxes were used by McBean to find Z/L. The overall stability dependence of all the statistical quantities is very similar in both studies, which lends credence to the belief that $Z/L(\Delta T)$ is, on average, a good estimate of the stability parameter.

There do not appear to be any unexpected discrepancies between the statistical quantities and previous results. The loss of low frequency covariance can hopefully be avoided with the I2 or I3 methods of integrating cospectra. The σw values are probably too small, but because this is due to frequencies above 1.5 Hz there should be no serious consequences felt by $\langle uw \rangle$ and $\langle wt \rangle$. In conclusion the sensors and Reynolds flux system seem to be performing as expected and quite capable of providing reliable estimates of the momentum and sensible heat fluxes.

4.5 The Fluxes Of Momentum And Sensible Heat

Three methods of integrating cospectra over the uncertain low frequencies were discussed in section 3.3 and formulated in equations 3.5. I1 includes all frequencies from the slow samples, I2 adds contributions from the lower frequencies represented by the group means and I3 integrates from n=0.004 to which a stability dependent factor, E, is applied to account for the low frequencies not integrated. The ratios of <uw> from the different methods are averaged over 2 m/s wind speed bands and tabulated in table IV. The I3:I1 ratio is expected to converge systematically to 1.0 from greater values as the wind speed increases. For the unstable runs this should occur at about 13 m/s when the integral from f=0.00065 Hz begins to cover all the natural frequency range of the normalized cospectrum (figure 16A). With Eu=1.06 this does occur, but above 14 m/s the ratio is again greater than 1 possibly because these runs are nearer to neutral conditions than the average and require a lower Eu. However, the overall average of 1.00 suggests that Eu should be increased to reflect that the I1 method sometimes does miss some of the covariance. The uncertainty in Z/L makes stability adjustments to Eu impractical, but these would affect the flux by much less than the measurement error. Keeping Eu=1.06 seems reasonable and the overall I2:I3 ratio of 0.99 indicates that using this factor includes the average contribution to the covariance from the group means, which in fact usually reduces the downward momentum flux as shown by I1:I2 >1.0.

Wind speed ±1m/s	108 unstable runs Eu=1.06				88 stable runs Es=1.005			
	Points	I1:I2	I2:I3	I3:I1	Points	I1:I2	I2:I3	I3:I1
6	13	1.10	0.97	1.02	6	1.02	0.92	1.18
8	17	1.03	1.00	0.98	15	1.01	0.79	1.04
10	18	1.00	1.01	0.99	21	1.05	0.95	1.02
12	21	0.98	1.06	0.99	21	1.03	0.96	1.02
14	12	1.04	0.94	1.03	11	1.02	0.99	1.00
16	14	1.03	0.96	1.03	7	1.01	1.00	0.98
18	11	1.03	0.95	1.02	6	1.01	1.04	0.96
overall average ±1σ		1.03 .15	0.99 .14	1.00 .07		1.03 .22	0.94 .31	1.03 .14

TABLE IV Comparison of the different methods of integrating the u,w cospectrum.

At U=11 m/s the I1 method begins to integrate over the entire stable normalized u,w cospectrum (figure 16B). When averaged over <u>all</u> runs above 11 m/s the I3:I1 ratio is 1.00 and the I2:I3 ratio 0.98, showing Es= 1.005 to be appropriate. At lower speeds the I3 method does not include low frequency contributions which reduce the downward flux, making I3:I1 >1 and I2:I3 <1. These positive contributions to -<uw> were balanced in the normalized cospectrum by negative contributions (downward flux) from the higher wind speed runs. One particular

run in the 6 m/s band gives I3:I1 = 2.13 and there are not enough other runs to balance it off. Excluding this run from the band gives I3:I1 <1. It is likely then that the overall I3:I1 would be reduced if more runs were available for averaging. One stable run in the 8 m/s band has such a large positive contribution .from the group means that the total integral, <uw>, becomes positive with I2:I3= -1.56. Without this one run both the I2:I3 band average and overall average increase to 0.96, so that most of the covariance from the group means is, on average, included in the I3 method. The decrease of I3:I1 with wind speed in the stable case, suggests that if more runs and a better measure of Z/L were available Es should be made a function of stablility.

The different methods of integrating the w,t cospectrum are compared in table V. The strange results in the 12 m/s, unstable band are caused by run T111 whose group mean contribution, -0.018 °Cm/s, is larger in magnitude than and of opposite sign to the I1 integral, 0.015 °Cm/s. If this one run is excluded, the band average and overall average I1:I2 become a more reasonable 1.06 and 0.94, respectively, with the corresponding I2:I3 ratios going to 0.99 and 1.11. For the low speed unstable runs, I1:I2 less than one, suggests that there is a significant contribution to the w,t covariance at frequencies below f=0.00065 as do the results of McBean and Miyake, 1972. Without high wind speed runs it is not possible to extend the normalized cospectrum (figure 17A) below n=0.001, where it is still fairly large. The cospectrum was made to drop off to 0 at n=0.0002 so that Eu=1.10, which is a compromise. The McBean and

Wind speed ±1m/s	27 unstable runs Eu=1.10				33 stable runs Es=1.04			
	Points	I1:I2	I2:I3	I3:I1	Points	I1:I2	I2:I3	I3:I1
6	6	.79	1.36	1.01	2	1.08	1.04	.92
8	11	.96	1.06	1.05	2	.52	6.28	1.17
10	4	.99	1.00	1.01	7	1.19	0.95	1.03
12	6	-.14	.80	1.06	9	1.06	0.92	1.03
14					3	1.03	0.91	1.06
16					5	.96	1.07	0.99
18					5	.73	.52	1.01
Overall average ±1σ		.68 1.37	1.06 .39	1.04 .12		.99 .47	1.22 1.89	1.03 .09

TABLE V Comparison of the different methods of integrating the w,t cospectrum.

Miyake results indicate a more rapid drop, but the overall I2:I3 ratio of 1.06 hints that Eu should be larger. The wind speeds during unstable conditions were always too low for the I1 method to integrate over the entire normalized cospectrum making I3:I1 >1 at all speeds and the overall average 1.04.

At all wind speeds the I1 method includes the entire stable cospectrum, figure 17B, and accordingly the I3:I1 ratio shows no systematic trend with wind speed and its variability attests to the existence of random low frequency contributions to the sensible heat flux which are smoothed by the I3 method. It is suspected that more runs at the lower speeds would give an average ratio of 1.0, the same as above 15 m/s. Again there are some very anomalous runs with large group mean contributions as shown by the I2:I3 band averages of 0.52 and 6.28. Without such runs the I3 method again accounts for most of the average group mean contribution. In view of the uncertainty in table V and in figure 17B, caused by the lack of runs, a value of Es=1.04 is acceptable.

Tables IV and V exhibit evidence of large random contributions to the fluxes from the uncertain low frequencies causing a great deal of scatter in the fluxes calculated from the I1 and I2 methods. To avoid the resulting scatter, the I3 method will be adopted as the means of integrating the cospectra of all the runs. The choices for ϕ_{uw} of Eu=1.06 and Es=1.005 and for ϕ_{wt} of Eu=1.10 and Es=1.04 have some uncertainty, but they are reasonable compromises and do not appear to cause any significant systematic errors or apparent trends. The integrals will be denoted by <uw>FLUX and <wt>FLUX and the derived parameters by u*FLUX, t*FLUX and so on.

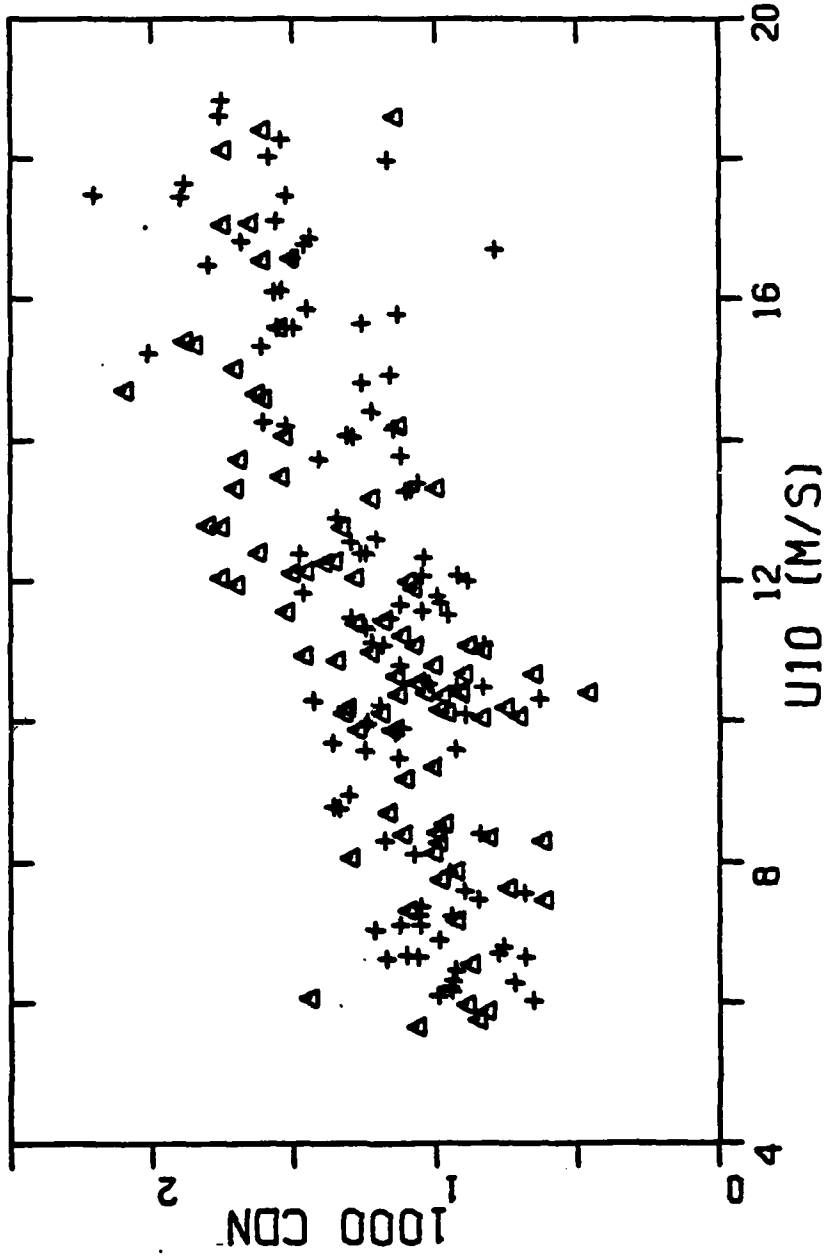

FIGURE 19 The neutral drag coefficient vs wind speed from the 196 Reynolds flux momentum runs. Triangles are the stable runs and pluses the unstable.

The Reynolds flux results are presented in figures 19 and 20 and compared with the dissipation method in Chapter 5. A more complete view of the behavior of the fluxes is offered in Chapter 6 by the more extensive dissipation data set. For the present the measured wind, UZ, temperatures, TZ and TSFC, <uw>FLUX, <wt>FLUX and Z/L(ΔT) have been put into equations 2.4 and 2.8 to give the roughness lengths, Zo and Zot, and into 2.11 and 2.10 to give a wind speed, U10 an air temperature, T10, and a drag coefficient, C10, at 10 meters. A neutral drag coefficient, CDN, is derived from Zo with equation 2.12. The plot of CDN vs. U10, figure 19, looks identical to the BIO tower results in Smith, 1979, from which a regression of 120 near neutral C10 values on U10, gives $0.44 + 0.063\ U10 = 10^3 C10$ as compared to $0.46 + 0.069\ U10 = 10^3 CDN$ from figure 19. Since there is nearly an equal partition between stable (triangles) and unstable (crosses) runs in figure 19, a regression of C10 on U10, $0.43 + .069\ U10 = 10^3 C10$, is not very different. The higher coefficients at the higher wind speeds are commonly observed, but overall these values are distinctly smaller than those at similar wind speeds in Garratt's, 1977, review. In figure 19 the stable (triangles) and unstable (pluses) data do not separate into distinguishing patterns. Throughout the small stability range found over the sea, average stability effects appear to be small.

In figure 20 <wt>FLUX is plotted against U10(TSEA-T10) for the 52 temperature runs with $|\Delta T| > 0.5^{o}C$, so that a line from any point to the origin has a slope equal to CT10, equation 2.10. The solid line represents the parameterization of Friehe

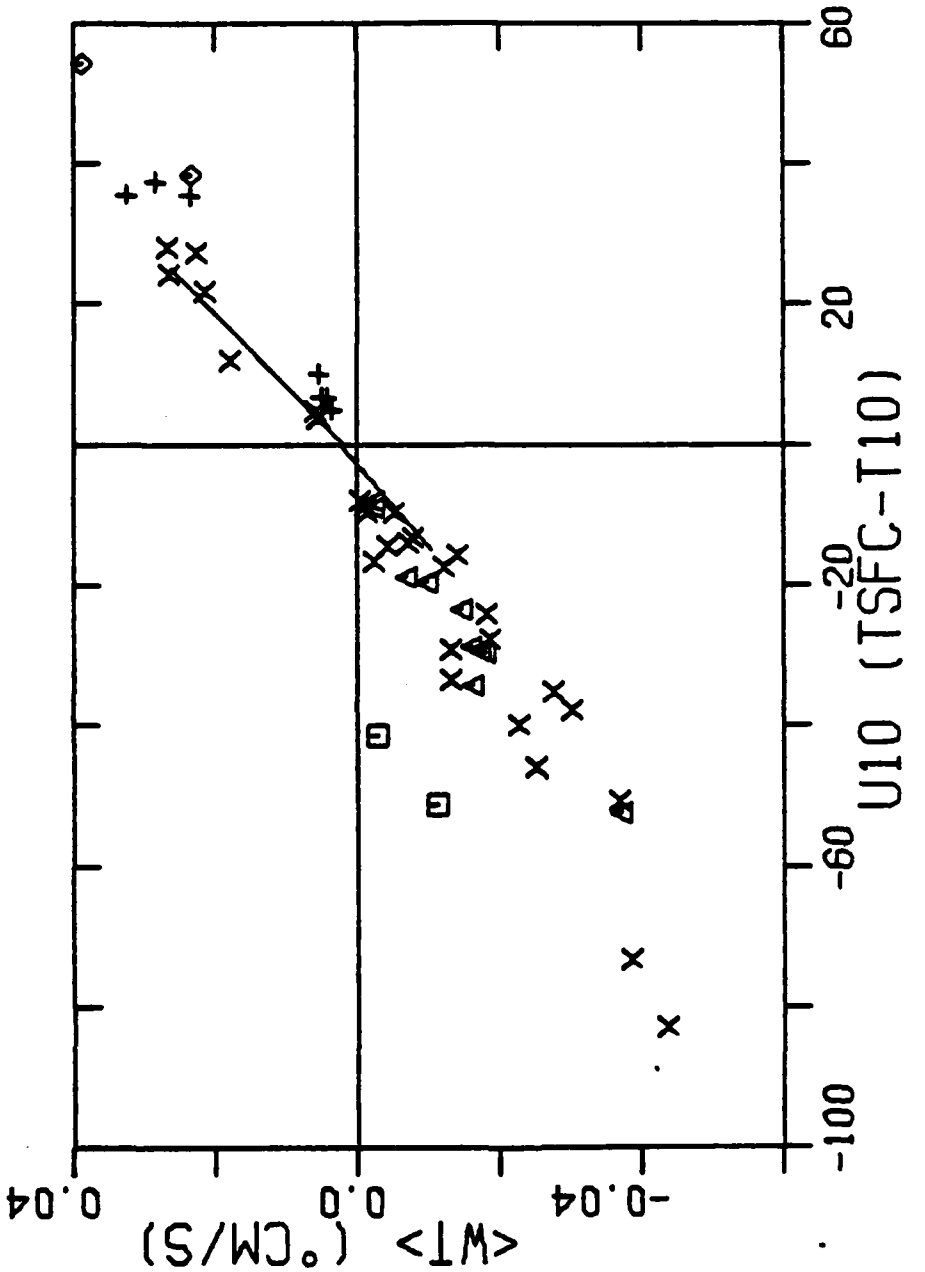

FIGURE 20 <wt> vs. U10(TSFC-T10) in °C and m/s for the 52 temperature runs with |ΔT| >0.5°C. Stability ranges: △, Z/L >0.05; ×, -0.1 <Z/L< 0.05; +, -0.2 <Z/L< -0.1; ◇, Z/L <-0.2. Solid line is from Friehe and Schmitt (1976).

and Schmitt, 1976, which fits quite well for $-10 < U10\,\Delta T < 25°Cm/s$. The data do not support an increase in CT10 above this range, which Friehe and Schmitt suggest on the basis of Smith and Banke's, 1975, measurements on the beach at Sable Island. The BIO tower results (Smith, 1979) span $|\langle U\rangle \Delta T| < 150°Cm/s$ and indicate slightly higher CT10 values than do either Friehe and Schmitt or figure 20, in both the unstable and stable cases. Smith (1979) finds $10^3\langle wt\rangle = 3.2 + 1.10\ U10\ \Delta T$, for $\Delta T > 0$ and $-0.1 + 0.83\ U10\ \Delta T$, for $\Delta T < 0$, from regressions of $\langle wt\rangle$ on $U10\,\Delta T$. All three studies show the stable coefficient to be smaller than CT10 in unstable stratification. There is not a great deal of scatter in figure 20, except from two runs (plotted as squares), during which very warm air moved over a cold sea. Such conditions greatly influence the average sensible heat flux and are discussed in section 6.3, when the corresponding dissipation data is presented. Near neutral runs ($|Z/L| < 0.05$), plotted as crosses, are much the same as the more stable (triangles), but the more unstable (pluses, Z/L 0.05 to 0.25 and diamonds, $0.25 < Z/L$) seem to give smaller CT10s, however there are far too few data to be conclusive as there are wind speed, fetch and other effects to consider.

CHAPTER 5 INTERCOMPARISON OF THE REYNOLDS FLUX AND DISSIPATION METHODS

5.1 Introduction

The Bedford tower experiment provides an excellent opportunity to establish, by comparison with both the Reynolds flux and BIO results, a dissipation method that is valid over a wide range of open sea conditions. The dissipation system recorded data during 192 Reynolds flux momentum runs and all 60 temperature runs and the results are tabulated with those of their corresponding flux runs in the Appendix. The stability, $Z/L(\Delta T)$, and ϵ give a $u^*DISS = (\langle uw \rangle DISS)^{1/2}$ from each of the four methods of manipulating the turbulent kinetic energy equation and velocity profile, equations 2.28. Similarly $\langle wt \rangle DISS$ is obtained both by including and excluding the stability effect on the temperature profile, equations 2.32. The "best" momentum and sensible heat flux dissipation methods are to be determined by comparison with u^*FLUX and $\langle wt \rangle FLUX$ from the direct eddy correlation measurements. However, the dissipation and Reynolds flux systems are not entirely independent, because they share the same sensors. In order to complete the intercomparison of the methods, u^*DISS is also checked with eddy correlation measurements of u^* from the BIO system.

It is essential to the intercomparison that the runs be as nearly simultaneous as possible. The dissipation runs are chosen to begin between 0 and 4 minutes before the start of the flux run and in most cases the starts are within 2 minutes. They last for 56 minutes if the flux run consists of four, 13.5 minute, consecutive groups and for 44 minutes in the few cases that only three groups comprise the run. These times become the averaging periods, < >. The dissipation, ϵ, is taken as the average of the three individual values obtained by substituting the average power, <P>, from each Gill-u band-pass filter, into equation 3.7. The separate values never differ from their average by more than 15% and a difference of more than 10% is found in only 10 runs. With both ($\phi u(fc)$ $fc^{5/3}$) and u^{*2} proportional to $\epsilon^{2/3}$ (equation 2.23), their average values differ from those derived from a single band-pass filter by less than 10% and usually by less than 7%. The deviation in ($\phi u(fc)$ $fc^{5/3}$) is probably due to the spectrum's fluctuations about a -5/3 line and the average ϵ should be a good measure of the molecular dissipation. Values of the dissipation of temperature fluctuations are calculated from equation 3.6 using only filters that lie entirely in the -5/3 region of $\phi t(f)$. Thus, Nt is often an average of only 1 or 2 separate estimates and therefore may not be as reliable as ϵ. In order for the calculated ($\phi t(fc)$ $fc^{5/3}$) values to agree with individual band-pass filters to within 10%, the average, Nt, must not differ from each individual estimate by more than 10% (equation 2.23). Equation 2.33 shows that 10% deviations in both $\phi t(f)$ and $\phi u(f)$ will produce a 10% deviation in the calculated <wt>.

5.2 The Momentum Flux

At neutral stability all four momentum flux methods are equivalent and in non-neutral conditions methods 2, 3 and 4 simply adjust the neutral approximation, method 1, by a function of Z/L, figure 1. u*DISS1, equation 2.24, is the simplest calculation and it is plotted against u*FLUX in figure 21. There is generally good agreement between the two calculations from the 192 simultaneous runs, for which Z/L is usually between -0.45 and 0.20. A 20% deviation in the u* estimations from a 1:1 relationship is indicated by the dashed lines, which satisfy the equation

$$|x-y| \; / \; [(x+y)/2] = 0.2 \; , \qquad (5.1)$$

with x=u*FLUX and y=u*DISS. In view of the errors in <u>both</u> methods, deviations of this magnitude are expected. Points at the higher u* values rarely fall outside the dashed lines. It appears, therefore, that the neutral dissipation method provides a very good estimate of momentum fluxes greater than about $u^{*2}=0.16 \; (m/s)^2$, which occur at wind speeds above about 11 m/s. The smaller fluxes span a greater stability range and the cluster of points lying above the upper dashed line, with u*<0.4 m/s, come from the most stable runs. Apparently, the assumptions of dissipation method 1, cause a systematic error in stable conditions, which tends to make u*DISS1 significantly greater than u*FLUX.

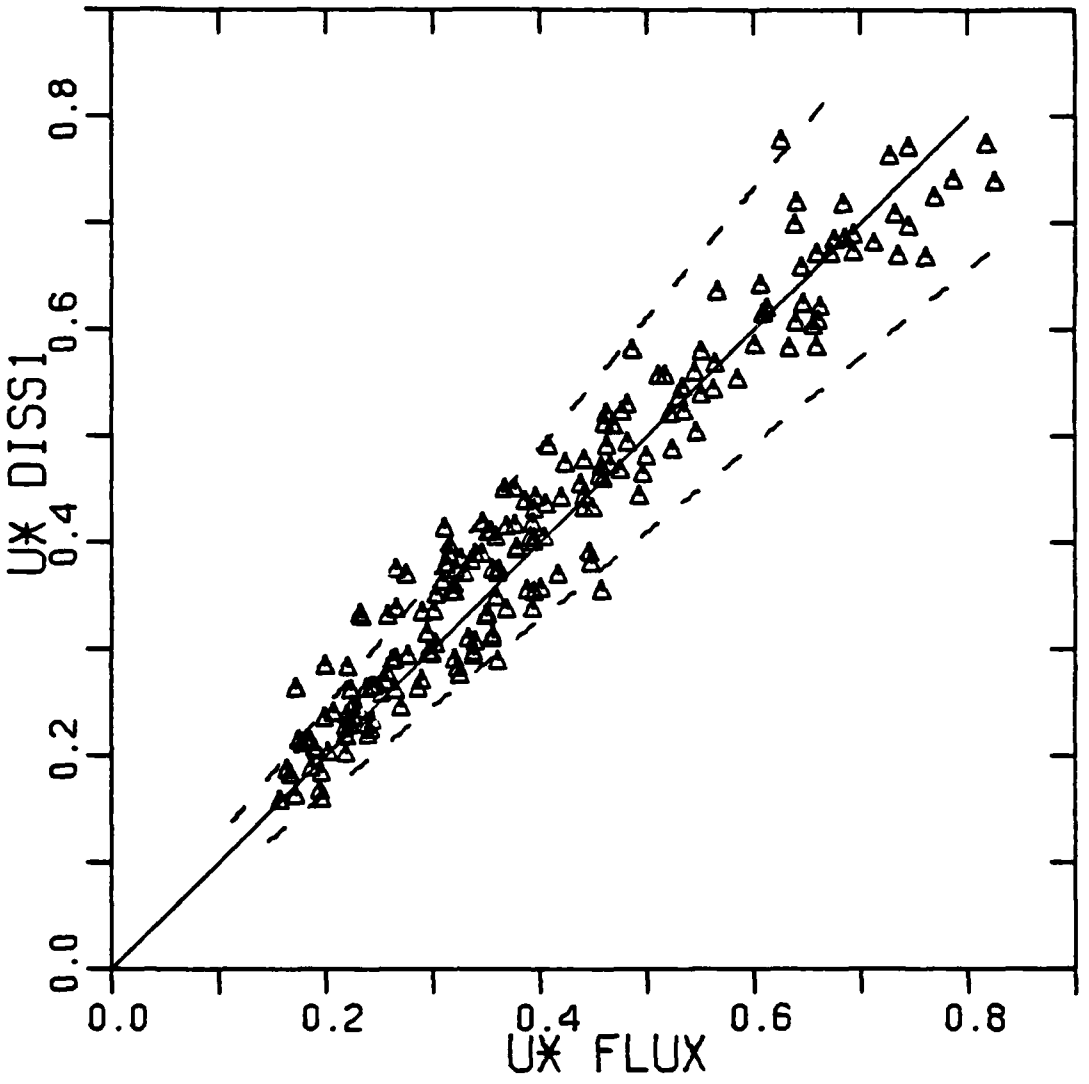

FIGURE 21: Comparison of u* in m/s from the neutral dissipation method and the Reynolds flux method for all 192 simultaneous Bedford tower runs. Dashed lines indicate a 20% deviation from the solid 1:1 line.

Method 1 should be valid over a range of "near neutral" stabilities where the buoyancy and two vertical divergence terms of the turbulent kinetic energy equation and the effects of Z/L on the velocity profile are either small or tend to cancel one another. The extent of such a regime is investigated by grouping the simultaneous runs according to Z/L(ΔT) and seeing over what range u*DISS1 and u*FLUX agree on average. On the stable side it is observed to extend to Z/L=0.05 as shown by figure 22A. The solid triangles, representing the runs with 0.04 <Z/L< 0.05, are still showing reasonable agreement. For Z/L>0.10 every run gives u*DISS1 greater, often by more than 20%, than u*FLUX and a stability correction that reduces u*DISS is necessary. On the unstable side, figure 22B shows that down to Z/L =-0.10 use of the neutral equation is acceptable. The agreement is evident in the runs with -0.1 <Z/L< -0.05 (solid triangles). Runs in the -0.3 <Z/L< -0.1 range are not included because u*DISS1 tends to be smaller than u*FLUX by an average of about 10%. However, in more unstable conditions the two calculations again tend to agree. A combination of figures 22A and 22B shows that in a "near neutral" regime, -0.1 <Z/L< 0.05, u*DISS1 gives a very good estimate of the momentum flux without an explicit knowledge of the stability. Extension of the unstable limit down to at least Z/L=-0.4, introduces very little error. This is a useful result, because open ocean conditions are often within this range and because an accurate Z/L is not always available. It is only in rather stable, Z/L>0.05, and perhaps in very unstable stratification, that the neutral approximations cause appreciable errors.

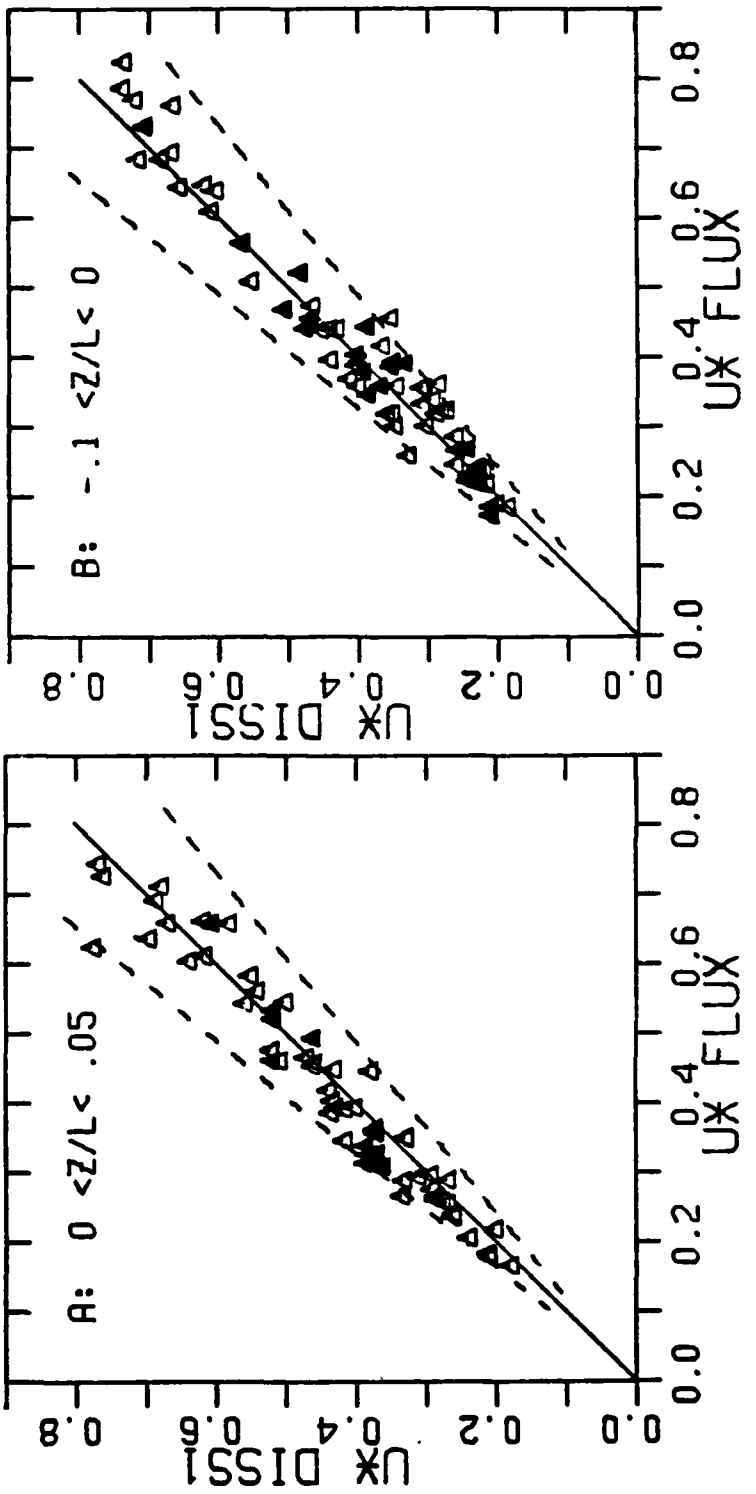

FIGURE 22 Investigation of the "near neutral" momentum flux (u* in m/s) regime for;
A: 61 stable runs (solid triangles 0.04 <Z/L< 0.05).
B: 70 unstable runs (solid triangles -0.1<Z/L<-0.05).

Fortunately, estimates of $Z/L(\Delta T)$ are available for all the simultaneous runs. Under stable conditions the buoyancy term of the turbulent kinetic energy equation (2.19) is a sink, so there is actually more production than is lost through dissipation alone and the larger production gives larger u* estimates. Another effect of stable stratification is to reduce the amount of flux associated with a given velocity profile, so the u* estimates become smaller. Method 4 (equation 2.27) incorporates the buoyancy term and method 3 (2.26) the effect on the profile, while method 2 (2.25) does both, with the profile effect dominating. Thus, in stable conditions, u*DISS4> u*DISS1> u*DISS2> u*DISS3, as is clearly shown by figure 1. It is observed that in the stable runs u*DISS1 tends to be greater than u*FLUX, so only methods 3 and 2 can provide the proper adjustment. The u* estimates from both these methods are plotted against u*FLUX for all 88 stable runs in figure 23. Both dissipation methods appear to give equally good agreement, establishing that the local production nearly equals dissipation, on average, with both the divergence and buoyancy terms of equation 2.19 being small. However, method 2 is preferred because it does account for buoyancy, its adjustment is smaller and its assumption, that the two divergence terms balance, is supported by McBean and Elliot's, 1975, observations.

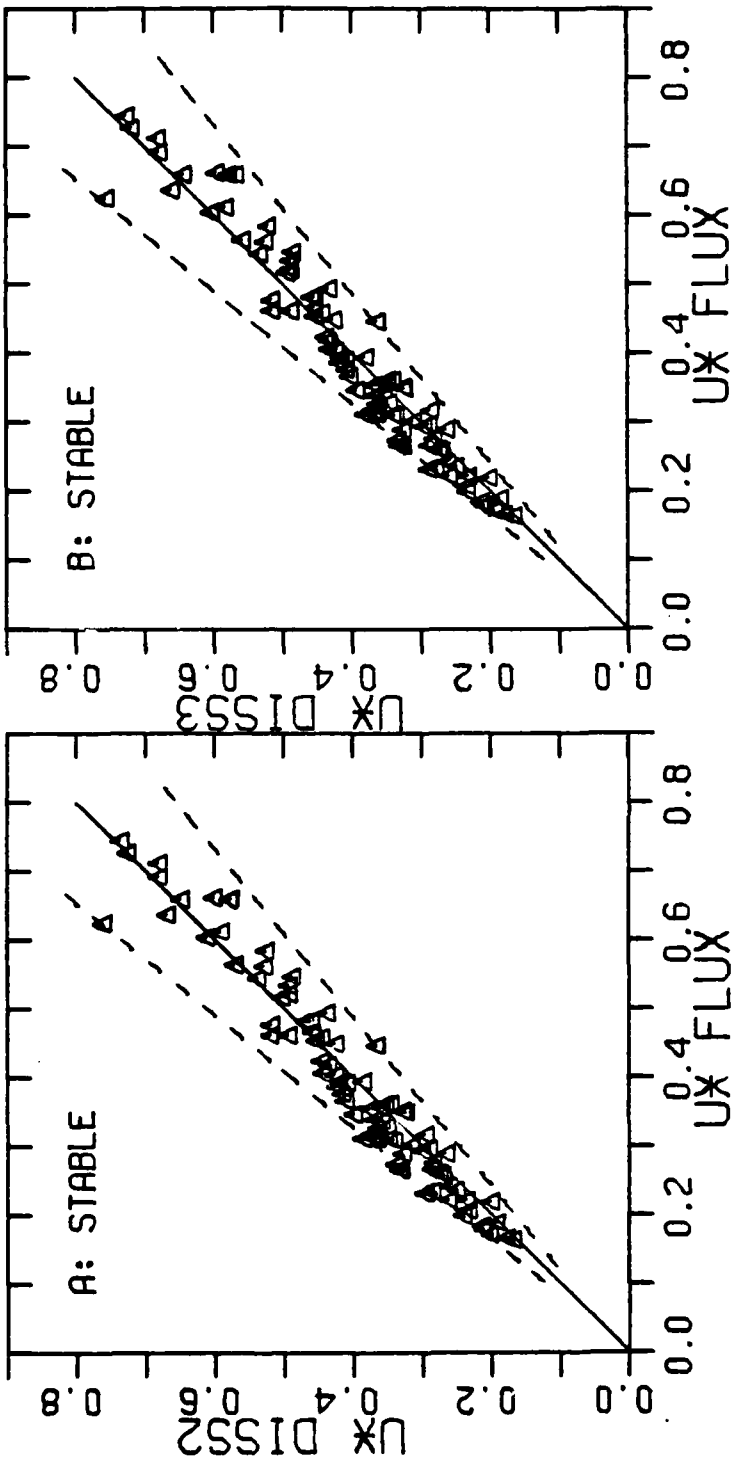

FIGURE 23 Comparison of 88 stable Reynolds flux runs to
A: dissipation method 2 (u* in m/s)
B: dissipation method 3 (u* in m/s).

During unstable conditions the roles of buoyancy and the stability modified profile, on the dissipation estimates are reversed, with u*DISS3> u*DISS1> u*DISS4. Figure 1 shows that in method 2 the effect on the profile still dominates down to Z/L=-0.1, when the buoyancy finally becomes an important source of turbulent kinetic energy. At about Z/L=-0.4, u*DISS2 becomes less than u*DISS1. Throughout the unstable range of the runs, u*DISS2 differs from u*DISS1 by less than 10% and qualitatively it is the only method that provides the appropriate stability refinements. Method 3 clearly gives far too large a u* in the more unstable cases. The u* estimates from methods 4 and 2 are plotted against u*FLUX for the 104 simultaneous unstable runs in figure 24. The agreement of method 2 is excellent and the scatter is very evenly distributed about the 1:1 line. This result indicates that the divergence terms also tend to cancel in unstable conditions as suggested by McBean and Elliot's findings. Because u*DISS1 also gives a reasonable estimate throughout -0.4 <Z/L< 0.05, the effect of stability on the profile must nearly balance the buoyant production. Pond et al., 1971, calculated u* up to 0.3 m/s using method 4, which is seen to be acceptable, but not applicable to higher u*values.

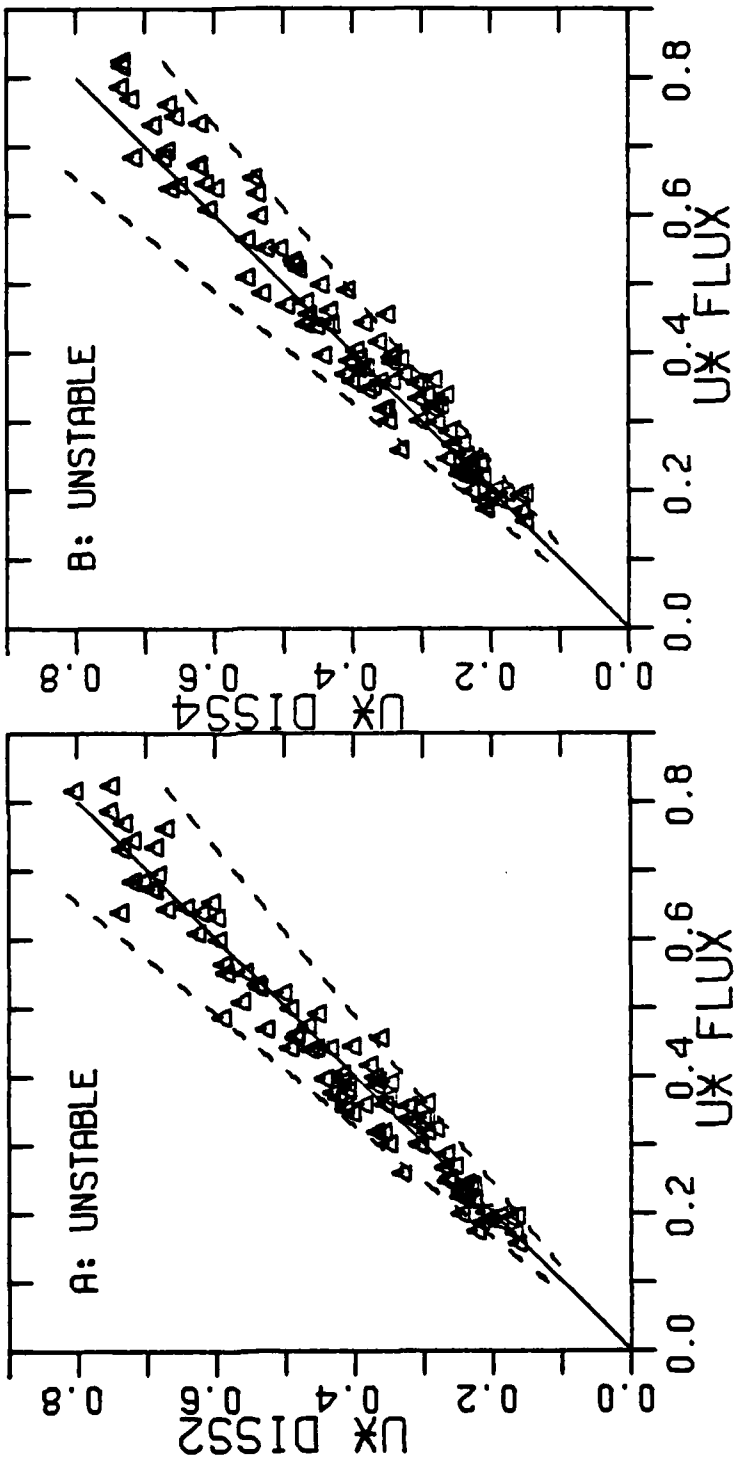

FIGURE 24 Comparison of 104 unstable Reynolds flux runs to
A: dissipation method 2 (u* in m/s)
B: dissipation method 4 (u* in m/s).

Whenever Z/L is available it is evident that, over the stability range of the intercomparison, method 2 gives the "best" estimates of u*, henceforth u*DISS and <uw>DISS will be calculated using this method. Figure 25 is a plot of u*DISS vs u*FLUX from the 192 simultaneous runs and a comparison with figure 21 illustrates the overall effect of the stability correction. In the region 0.15 <u*FLUX< 0.4m/s, the reduction of u*DISS from the most stable runs greatly improves the agreement, but u*DISS still tends to be greater than u*FLUX. As a consequence, the average of regressions of u*DISS and u*FLUX,

$$u^*DISS = 0.96\ u^*FLUX + 0.025\ m/s,$$

has a positive offset and the overall average u*DISS:u*FLUX ratio, 1.03 (standard deviation 0.10), is greater than 1.00. The two techniques differ by at most 28% and usually by less than 20% in u*, which is about the amount of scatter expected. A 20% error in <uw>DISS and a non-compensating 20% error in <uw>FLUX give a 20% deviation in u* estimates. It is doubtful that the u* agreement would be so good if a major systematic error had arisen from the propeller response correction because it is of fundamental importance to u*DISS, but only secondary to u*FLUX. Conversely, the non-cosine behavior of the Gill propellers is a potential source of substantial error in Reynolds flux measurements, but not to the dissipation estimates, thus the good agreement indicates that it too is being treated properly. Similarly, it appears as if the low frequency covariances are being handled satisfactorily.

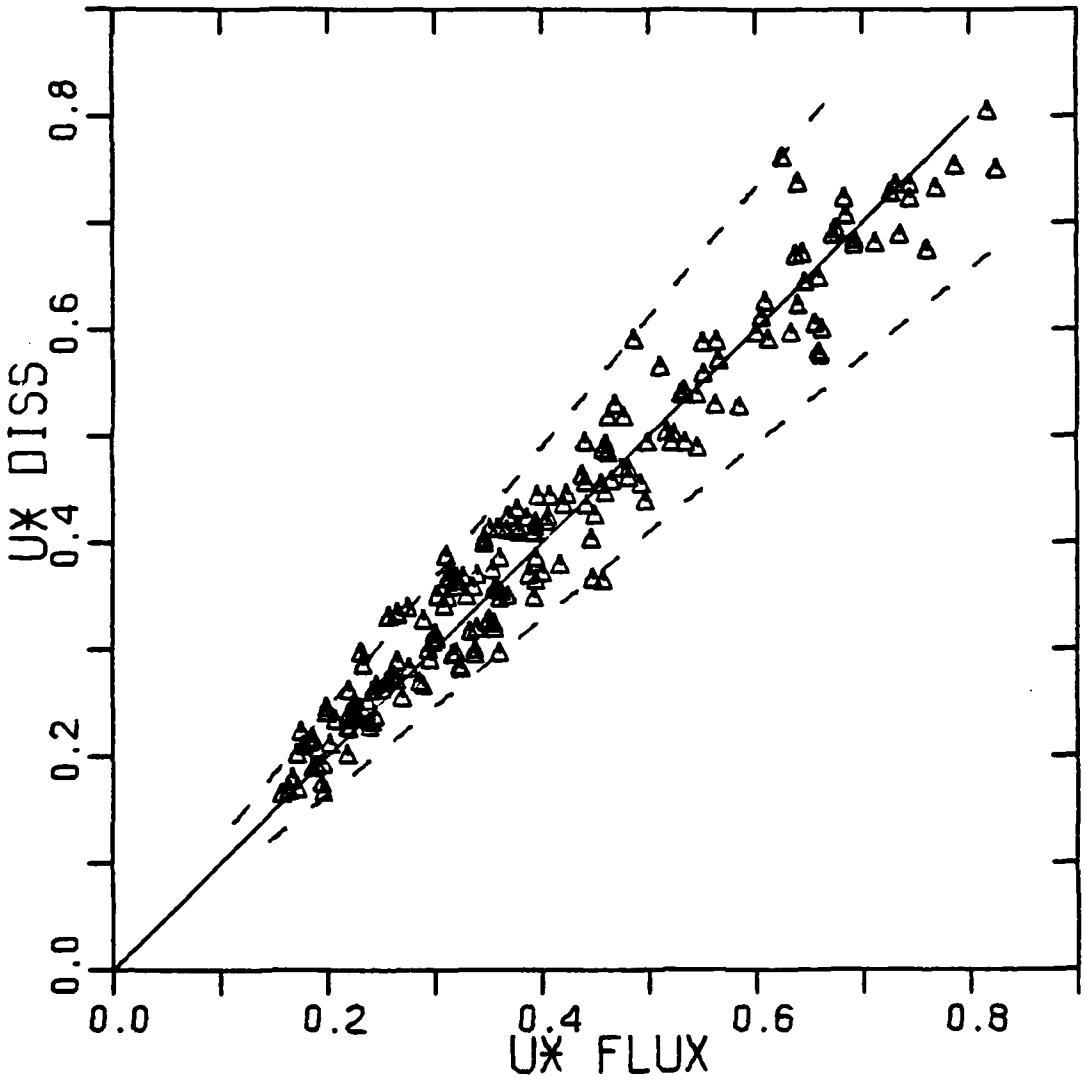

FIGURE 25: Intercomparison of u* in m/s from the "best" dissipation (2) and the "best" Reynolds flux (I3) method for all 192 simultaneous runs.

Wind speed range (m/s)	Number of points	<uw>DISS / <uw>FLUX Mean	Standard deviation	Minimum	Maximum
6 - 8	27	1.10	0.14	0.82	1.42
8 - 10	25	1.02	0.21	0.68	1.49
10 - 12	54	1.14	0.23	0.68	1.58
12 - 14	32	1.05	0.16	0.79	1.34
14 - 16	18	0.97	0.13	0.76	1.23
16 - 18	17	1.00	0.09	0.79	1.10
18 - 20	9	1.01	0.14	0.83	1.36
Overall 4 - 20	182	1.05	0.17	0.68	1.48

TABLE VI Ratio of dissipation to Reynolds flux estimates of the momentum flux band averaged over 2 m/s wind speed intervals.

The momentum flux and drag coefficient are proportional to <uw>, so trends in the <uw>DISS:<uw>FLUX ratio are investigated by averaging the ratio over wind speed and stability bands in tables VI and VII, respectively. In order that the band means are not unduly weighted by individual runs with atypical ratios, only those runs whose ratios fall within ±2 standard deviations about a complete band average are used to calculate the means, standard deviations and ranges in tables VI and VII. In table VI, the overall average of 1.05 and standard deviation, σ, of 0.17, are quite acceptable. A σ of 17% is comparable to the

Stability range Z/L		Number of points	<uw>DISS / <uw>FLUX			
			Mean	Standard deviation	Minimum	Maximum
-.45	-.30	9	1.08	0.23	0.77	1.48
-.30	-.15	15	0.97	0.14	0.72	1.31
-.15	0	74	1.04	0.17	0.68	1.36
0	0.05	59	1.06	0.17	0.76	1.40
0.05	0.10	18	1.16	0.17	0.92	1.53
0.10	0.20	6	1.34	0.33	0.87	1.65

TABLE VII Ratio of dissipation to Reynolds flux estimates of the momentum flux band averaged over stability ranges.

expected error in each method and the mean is less than $\sigma/3$ greater than the desired overall average of 1.00, despite the large ratios that occur during lower winds when stability has its greatest range. Otherwise there is no systematic trend with wind speed, although the range of the ratio seems to decrease with increasing speed. At the higher wind speeds where stability should always be near neutral the band means are about 1.00. Therefore, it seems likely that any wind speed dependency of the drag coefficient observed in dissipation results would also be found in corresponding eddy correlation measurements. Table VII shows that, as expected, the stable runs produce the largest average ratios. Figure 1 shows that switching to dissipation method 3 would not greatly alter this result (4% in

the 0.10 <Z/L< 0.20 band). It is possible that the higher ratios are caused by underestimating <uw>FLUX with the I3 method. As Z/L increases, the proportion of covariance at high frequencies and, hence, the amount lost through incomplete sensor response corrections also increases, but the effect should not exceed 5%. It has been shown in section 4.5, that, on average, Es=1.005 treats the low frequency covariance adequately, but the four runs that give such a large average to the most stable band of table VII occurred nearly sequentially (runs T174, T175, T176 and T178), so the band does not neccessarily reflect average conditions. Since there are no fluctuating temperature data from these runs, Z/L(ΔT) could be underestimating Z/L and causing overestimates of u*DISS.

In order to complete the intercomparison of methods it is important to show that the observed agreement of figure 25 does not depend on using the same sensors. Dr. S.D. Smith of the Bedford Institute of Oceanography has kindly allowed some of his eddy correlation measurements of u*, u*BIO, from the tower (Smith, 1979) to be compared to simultaneous dissipation measurements. The runs overlap as do the Reynolds flux runs and are typically about 44 minutes in duration. The BIO mark 6.4 thrust anemometer operated from October 7 to December 8, 1976. In figure 26, u*DISS is plotted against u*BIO for all 20 simultaneous runs from this period. On average, the agreement is excellent and the scatter is no larger than expected considering the addition of calibration errors and the separation of the anemometers by about 2 m. A direct comparison of u*FLUX and u*BIO values is not possible, because simultaneous

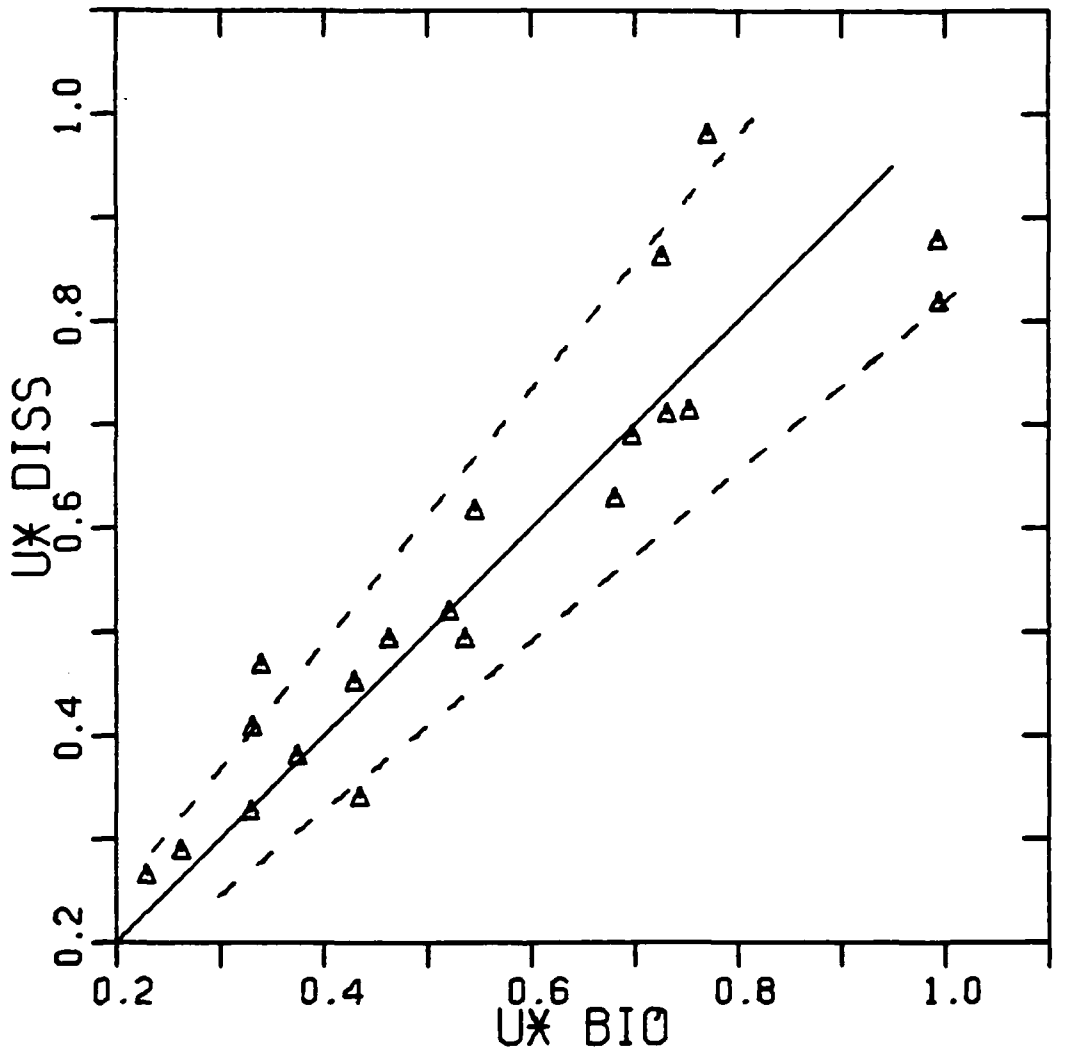

FIGURE 26: Comparison of u* in m/s from the dissipation system and from the BIO eddy correlation system from 20 runs on the Bedford tower.

measurements are rare, however the dissipation intercomparison gives a favourable indirect one. These conclusions ought to be qualified by noting that there are disagreements with the mean winds from later BIO data which are still to be resolved. The u* comparison of these data shows u*DISS to be greater than u*BIO (often by more than 20%) in 28 of 30 runs.

5.3 The Sensible Heat Flux

The sensible heat flux is estimated using the two dissipation methods for the 60 simultaneous temperature runs and these are compared to <wt>FLUX in figure 27. The dashed lines satisfy 5.1 with x=<wt>FLUX and y=<wt>DISS, indicating a 20% deviation of the actual fluxes from the solid 1:1 line. <wt>DISS, the neutral approximation, is clearly, on average, more negative than <wt>FLUX (figure 27A). Method 2 applies a rather large correction for the influence of stability on the temperature profile, but figure 2 shows the adjustment to be in the proper sense in both stable and unstable conditions. A regression of <wt>DISS2 against <wt>FLUX (figure 27B) gives

$$\text{<wt>DISS2} = 1.04\ \text{<wt>FLUX},$$

with a correlation coefficient of 0.99. The agreement is remarkably good considering the errors in both methods and the sensitivity of <wt>DISS2 to the rather uncertain $Z/L(\Delta T)$. These results suggest that the turbulent transport term in the

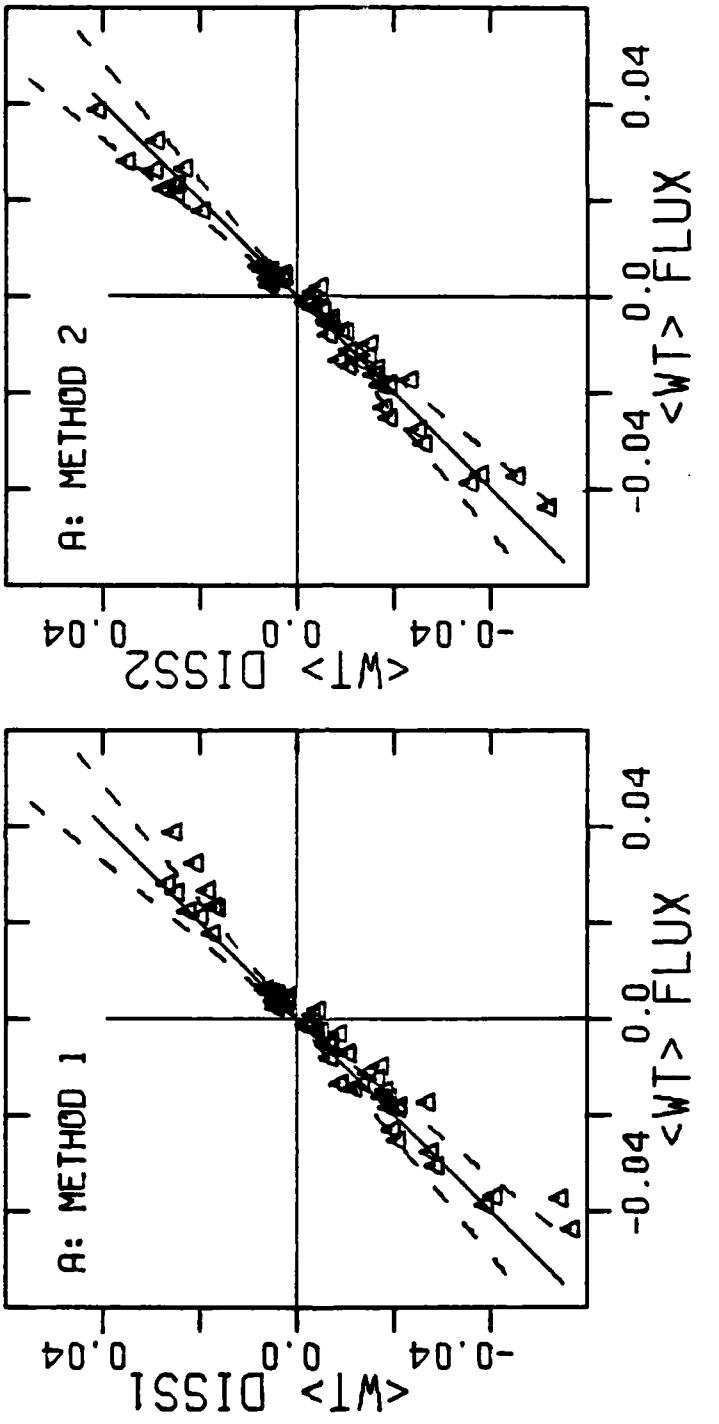

FIGURE 27 Comparison of the 60 simultaneous sensible heat flux calculations in °Cm/s.
A: <wt>DISS1 vs. <wt>FLUX
B: <wt>DISS2 vs. <wt>FLUX.

temperature variance budget is itself small and that it cannot compensate for changes in the local production of temperature variance due to stability. In the range -0.03 <Z/L< 0.05 the correction to <wt>DISS1 is less than 10% and, if necessary, method 1 could be used to estimate the sensible heat flux without an an explicit Z/L. However, method 2 gives the better estimate and will always be used to calculate <wt>DISS. The two points in the fourth quadrants of figures 27A and 27B illustrate an inherent difficulty in finding small fluxes with the dissipation method. <wt>DISS is calculated from equation 2.32 and the sign of the square root is chosen so as to force <wt> to have the same sign as ΔT = TSFC-TZ. However, it is commonly observed in eddy correlation measurements that <wt> is between 0 and +0.05 °Cm/s when ΔT is slightly negative. There have been very few measurements of large sensible heat fluxes over the sea, but the excellent agreement in figure 27B, when the magnitude of the flux is large, strongly suggests that this measurement may be done using the dissipation method.

The low and high frequency temperature fluctuations affect the sensible heat flux calculations in the same manner as the velocity variations affect the momentum flux. Similar arguments regarding non-cosine behavior, sensor response and low frequency covariance lead to the conclusion that the temperature elements of both the Reynolds flux and dissipation systems must be performing properly in order to achieve the observed agreement. With no large systematic errors in evidence, <wt>DISS and <wt>FLUX should both be giving representative estimates of the sensible heat flux.

As previously noted many temperature runs have not been processed because of suspected salt contamination of the microbead. In a few of these cases the temperature band-pass filters unexpectedly display a -5/3 drop to within 10%. The band-pass filter check is, therefore, a necessary, but insufficient test for this behavior. This is unfortunate because it restricts dissipation temperature measurements to periods when the temperature spectrum can be obtained from the Reynolds flux system. A possible means of overcoming this problem would be to average the output of another band-pass filter centered at about n=0.02 for comparison with the outputs of the filters in the -5/3 range. It is also interesting to note that <wt>DISS and <wt>FLUX are in good agreement in some unstable contaminated runs, albeit both seem to be somewhat high.

It is expected that the largest dissipation errors are in the constants and the assumptions. The fact that there are no major persistent errors, suggests that the combined errors in the constants is not very large. This is suppcrted by equations 2.29 and 2.33 which show <wt>DISS to be proportional to

$$(KZ)^{1/3} \quad (Bt')^{-1/2} \quad u*DISS .$$

If, for example, the Kolmogoroff constant, Bt', was greatly in error, u*DISS would be expected to be more accurate than <wt>DISS and hence, in better agreement with Reynolds flux calculations. The results, figures 25 and 27B, do not support this. Similarly, K and Z appear to be reasonable. Of ccurse

there could be major offsetting errors, or the constants may be highly variable, but it seems more likely that it is the assumptions which are the most uncertain aspect of the dissipation method. It is also probable that much of the scatter in the u* and <wt> intercomparisons originates with the Reynolds flux values.

On average, the Reynolds flux and dissipation methods give nearly the same momentum and sensible heat fluxes. In addition, both the dissipation and Reynolds flux systems appear to be functioning as expected. With the possible exception of u* from the most stable cases (Z/L> .05), the estimates of <uw> and <wt>, by both techniques, should be reliable and free of major systematic errors. It is, therefore, possible to have confidence in the dissipation system when it is operating on a ship where the Reynolds flux method is not practicable.

CHAPTER 6 DISSIPATION MEASUREMENTS FROM THE BEDFORD STABLE TOWER AND CCGS QUADRA

6.1 Introduction

The dissipation system has provided a great deal more data from the Bedford tower than the Reynolds flux system, because it continuously records and has proved to be more reliable. In addition, a considerable amount of dissipation data has been collected at "PAPA". In total 1086 hours of momentum flux measurements from the tower and 505 hours from the weathership are found to satisfy a variety of criteria for data reliability. Only 237 hours of tower data and 23 hours from CCGS Quadra are found to be suitable for sensible heat flux calculations. There are several long periods of continuous recording which make it possible to investigate the time histories of the fluxes, winds and temperatures.

Only data from the horizontal, Gill-u, propeller are used to find the dissipation, ϵ, and hence momentum flux. Because of the greater uncertainty, it is not worthwhile including the moderate wind speed measurements from the tilted, Gill-w, propeller that are available from the few periods when the horizontal propeller failed. The tower analysis is limited to wind speeds greater than 4.0 m/s. At lower winds the Gill-u propeller is still in its linear regime, but the sensor response corrections become very large and it is not impossible for the thickness of the "constant flux" layer to fall below the anemometer height. On CCGS Quadra the measurement height is

nearly twice as high, so the limit is set at 8.0 m/s. A further restriction requires the stability to be in the range -0.6 <Z/L< 0.15. At Z/L=0.15 dissipation momentum flux calculations require a correction for stability of about 25% (figure 1). This adjustment is supported mainly by the Reynolds flux intercomparison, where Z/L is greater than 0.15 for only three runs, and also by McBean and Elliott's, 1975, measurements, that include only three stable runs with the highest at Z/L=0.12. It is, therefore, dangerous to extrapolate these findings beyond Z/L=0.15, where the correction becomes even larger. On the unstable side there are 21 runs in the McBean and Elliot study and 104 runs in the section 5.2 intercomparisen, with the most unstable at Z/L=-0.3 and -0.45, respectively. At Z/L=-0.6 the stability adjustment is still less than 10% so it should be all right to extend dissipation method 2 at least this far. This criterion effectively sets the outer limits of sensible heat flux calculations, because they require ϵ from Gill-u. The stability corrections to <wt>DISS are 1.8 at Z/L=-0.6 and 0.75 at Z/L=0.15 (figure 2) and although these are substantial, they are strongly supported by the work of Wyngaard and Coté, 1971, which consists of runs from Z/L=-1.1 to Z/L=0.4, and the intercomparison of section 5.3. Temperature data are also rejected if there is any evidence of salt contamination of the microbead or if the rod and bead thermistors do not agree, on average, to within ±0.1°C.

In processing a dissipation momentum [temperature] run from either the ship or tower, 20 minute averages of all Gill-u [temperature microbead] band-pass filters in the -5/3 range of $\phi u(f)$ [$\phi t(f)$] are used to find independent values of the dissipation of turbulent kinetic energy [temperature fluctuations] from equation 3.7 [3.6]. These individual values are averaged together to give the ϵ [Nt] necessary for the calculation of the momentum flux [sensible heat flux] from equation 2.28 [2.32]. However, if any separate band-pass value differs from ϵ [Nt] by more than 15% [10%] the run is rejected. This criterion ensures that the spectral values at the frequencies used fall within 10% of the average -5/3 slope of the input spectrum and that fluxes calculated from individual filters are within 10% of the value found from the average. The 20 minute averages could be used to produce time series of the fluxes and related parameters, but in practice hourly averages are employed because it is felt the longer averaging time increases the reliability of the dissipation method. In order to obtain the hourly averages, three sequential 20 minute flux estimates are averaged and then used to calculate the related parameters. Hereafter, these hourly averages from the dissipation system will not be specifically denoted, but referred to simply as <uw>, <wt>, u* t*, CD, CT and so on. For dynamic flux calculations the air density ρ is found from equation 2.35, using the atmospheric pressure from the meteorological observations from Shearwater and CCGS Quadra.

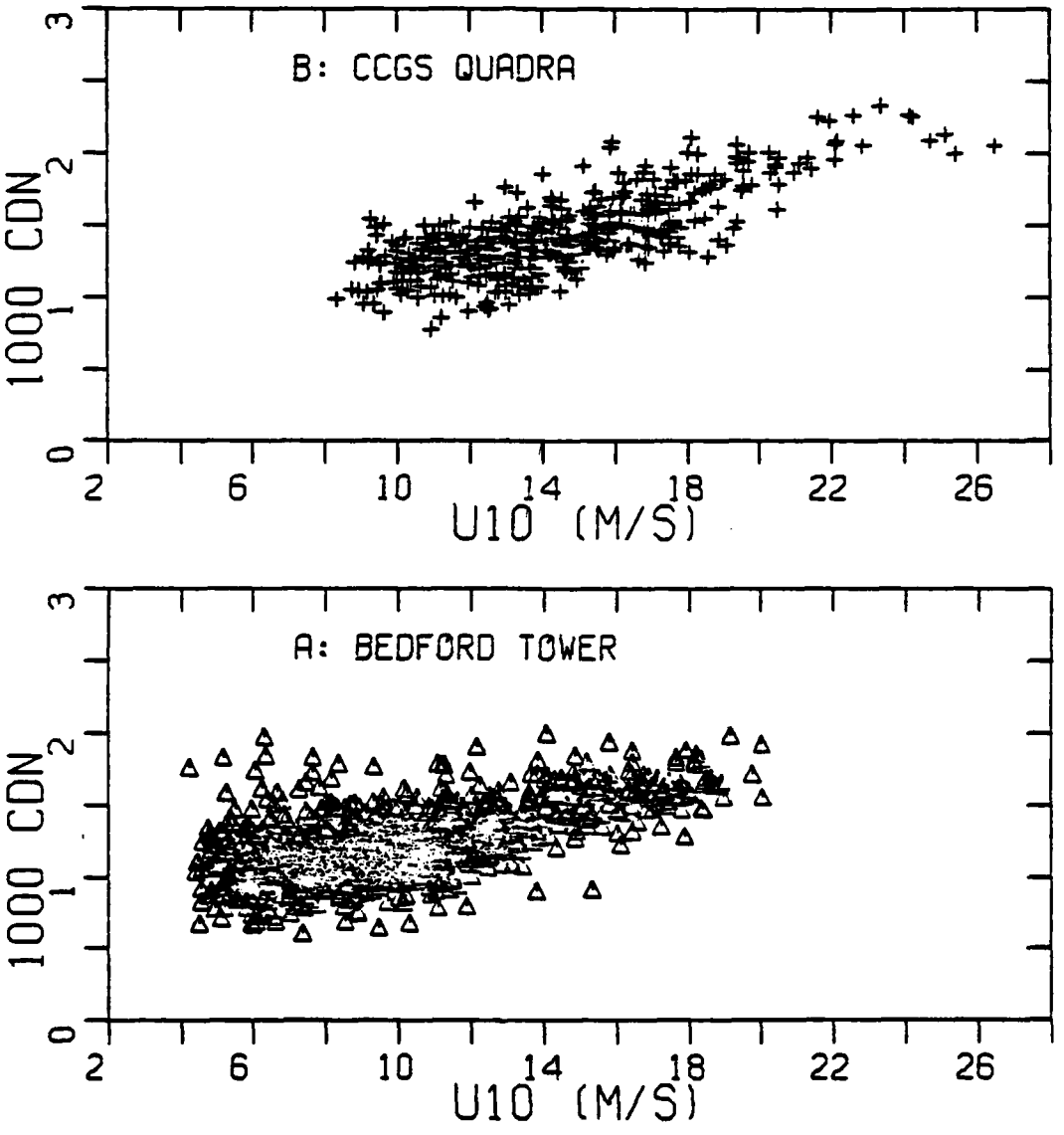

FIGURE 28 The neutral drag coefficient as a function of wind speed from:
A: 1086 hourly averages from the Bedford tower.
B: 505 hourly averages from the CCGS Quadra.

6.2 Bulk Aerodynamic Parameterization Of The Momentum Flux

Hourly averages of u* and UZ and Z/L are used to calculate U10 from equation 2.11 and the neutral drag coefficient, CDN, from 2.8 and 2.12. These are plotted separately for the tower and ship data in figure 28. There are very few extreme values and most points are obscured by the concentration about a mean CDN value. Between U10 =4 to 11 m/s the scatter is uniform with only a few values of 10^3CDN outside the range 0.65 to 1.5. At higher wind speeds a tendency for higher values develops and there appears to be less scatter. Above U10=20 m/s there are few points, so these data may not fully reflect average conditions. Fortunately, in the region 8 <U10< 18 m/s, there is a very good overlap of tower and ship results which allows the two situations to be compared.

In figure 29, CDN is averaged over 2 m/s intervals of U10, provided there are at least 10 runs in a band, and the means plotted with vertical bars extending up and down 1 standard deviation. For clarity, tower results (triangles) are just to the left of band center and the ship points (pluses) to the right. Over the range 8.5 <U10< 20.5 m/s, the band averaged CDN's from one platform are seen to differ by less than one standard deviation (but usually less than 1/2 σ) from the other platform's mean. No systematic errors, such as in the choice of Z, appear to have been introduced in moving the dissipation system from the tower to CCGS Quadra. The drag coefficient agreement also establishes that the tower site is, in fact, representative of open sea conditions, at least up to 20 m/s

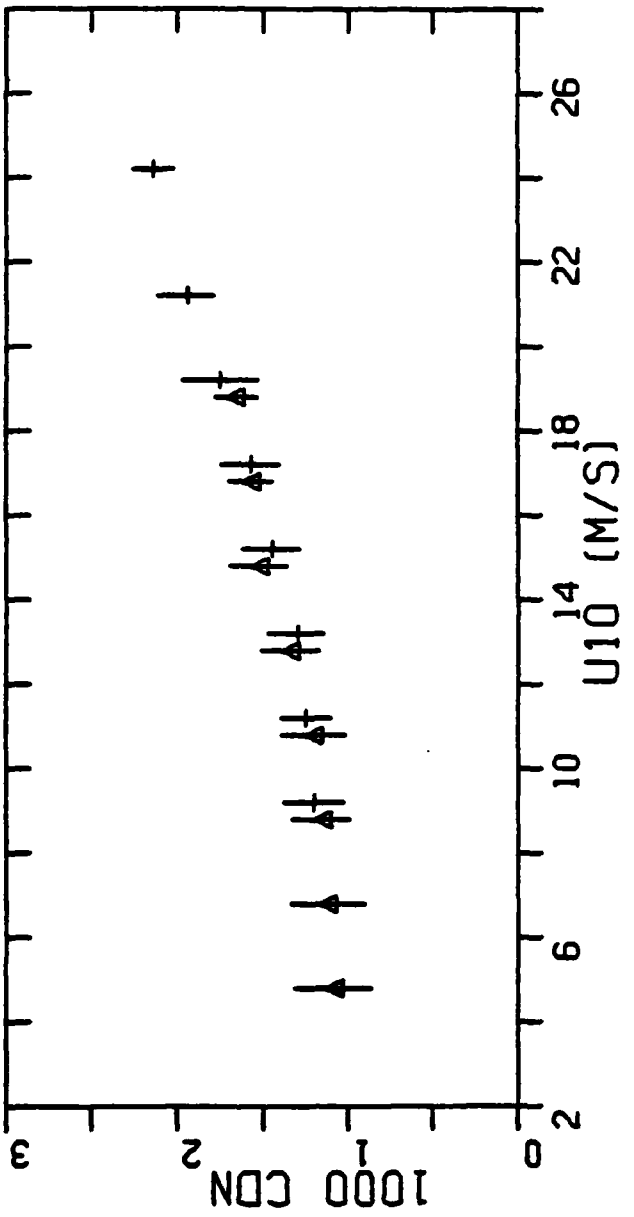

FIGURE 29 Comparison of the ship (pluses) and tower (triangles) neutral drag coefficients. Vertical bars extend ± 1 σ about plotted band averages.

winds. This allows the tower and ship results to be combined into a single data set of nearly 1600 hours from about 16 months of operation between September 1976 and April 1978.

Fetch Effects

The tower data of figure 28A include some runs from limited fetches, whose inclusion in the overall data set must be justified. Up to about 10 m/s, CDN from the tower does not vary appreciably with wind speed, therefore data in this range are used to investigate the influence of fetch on the drag coefficient. The results are shown in table VIII, where the neutral drag coefficient, CDN, from measurements about 13m above

Fetch (km)	Number of hours	Mean 10^3CDN ±1 standard deviation	10^3CDN Min	10^3CDN Max	Azimuthal range (° True)
10 - 20	200	1.14 ±.18	0.75	2.03	253 - 393
20 - 100	54	1.10 ±.22	0.73	1.87	246 - 253 33 - 65
100 - 200	85	1.13 ±.24	0.64	1.76	235 - 246
Unlimited tower	263	1.13 ±.22	0.62	1.75	67 - 235
Unlimited tower+ship	291	1.14 ±.21	0.62	1.75	
Tower all fetches	590	1.13 ±.21	0.62	2.03	0 - 360

TABLE VIII Variation of the neutral drag coefficient with fetch for winds between 4 and 10 m/s.

the sea, does not exhibit any dependency on fetches greater than 10 km and, in view of the overall scatter, the means are very consistent. This conclusion depends on using CDN, since the mean C10 from the 10-20 km fetch range is 17% larger than from the unlimited fetch runs, presumably because the offshore winds tended to be more unstable. The indication is, that for winds below 10 m/s, fetch effects are not important if the aspect ratio, Z/fetch, is at least as small as 10^{-3}. There is also an indirect implication that the surface roughness, Zo, does not depend strongly on surface wave parameters that are not fully developed by 10 km during 10 m/s winds. The data compiled by Wiegel (1964, p 216), for fetch limited waves, show the significant wave height and the phase speed from a 1000 km fetch (fetch $g/\langle U\rangle^2 \cong 10^3$) to be, respectively, 10 and 5 times greater than expected with a 10 km fetch. The necessity of extracting the wind speed dependency from CDN complicates extending the investigation above 10m/s, but as the aspect ratio stays the same, there should not be a sudden fetch dependency. Tower data from all fetches are, therefore, grouped together in all subsequent analyses. The better statistics resulting from the additional data should more than compensate for any small fetch effects.

Stability Effects

Equation 2.12 defines CDN as a function only of Zo and 2.8 implies C10>CDN for Z/L<0, C10<CDN for Z/L>0 and C10=CDN at neutral stability. Table IX indicates that CDN and hence Zo are independent of Z/L in the unstable case. At Z/L<-0.3, C10 values are clearly higher than the average, but reduction to neutral stability gives no systematic trend to the mean unstable CDN's, which are reasonably consistent in view of the scatter. Extraneous effects seem to influence the stable runs to a much greater degree. When reduced to neutral, the average stable

Z/L(ΔT) range		Number of hours	CDN * 1000 Mean ±1σ	CDN * 1000 Max Min	C10 * 1000 Mean ±1σ	C10 * 1000 Max Min
-.60	-.45	25	1.06 ±.12	0.80 1.31	1.22 ±.14	0.91 1.52
-.45	-.30	35	1.12 ±.19	0.77 1.73	1.26 ±.22	0.86 1.98
-.30	-.15	77	0.98 ±.16	0.67 1.38	1.07 ±.18	0.70 1.54
-.15	0	166	1.09 ±.20	0.68 1.74	1.12 ±.21	0.68 1.83
0	+.05	104	1.19 ±.18	0.62 1.85	1.16 ±.18	0.60 1.81
+.05	+.10	122	1.21 ±.19	0.64 1.79	1.13 ±.17	0.60 1.64
+.10	+.15	61	1.23 ±.28	0.75 2.03	1.11 ±.24	0.68 1.80

TABLE IX The stability dependency of the drag coefficients from the 4 < U10 < 10 m/s data of table VIII.

CDN's are larger than the overall mean and they seem to increase with stability. However, the large drag coefficients responsible for this feature are found to be associated with rapid changes in wind direction following a storm. Such a sequence of events may possibly influence parameters important to Zo and merely coincide with stable stratification. A time series showing the development of these high, low wind speed, stable drag coefficients is presented later (figure 31). The data suggest that the stability dependence of the drag coefficient is well described by similarity theory with Zo independent of Z/L and that sea surface conditions are the source of the trend in CDN with Z/L found in table IX.

Wind Speed Dependency

In figure 30 the 1591 neutral coefficients from all the data are band averaged over 2 m/s intervals and plotted at the U10 mean (vertical bars show ± 1 σ). The mean C10 values are similar, because of the almost equal numbers of stable and unstable runs. A smooth curve (concave up) with CDN increasing with U10 could be made to fit these points. However, below about 10m/s, the slight increase of the average CDN's should be adequately described by a constant. The higher wind speed points show a more rapid rise of CDN with U10, that is approximately linear from 10 to 26 m/s. In order to quantify this behavior, all 618 hourly CDN values with $U10 \leq 10$ m/s are averaged and all 973 with $U10 > 10$ m/s are regressed against U10 (correlation coefficient 0.74). All the band averages are very well described by the resulting solid line of figure 30:

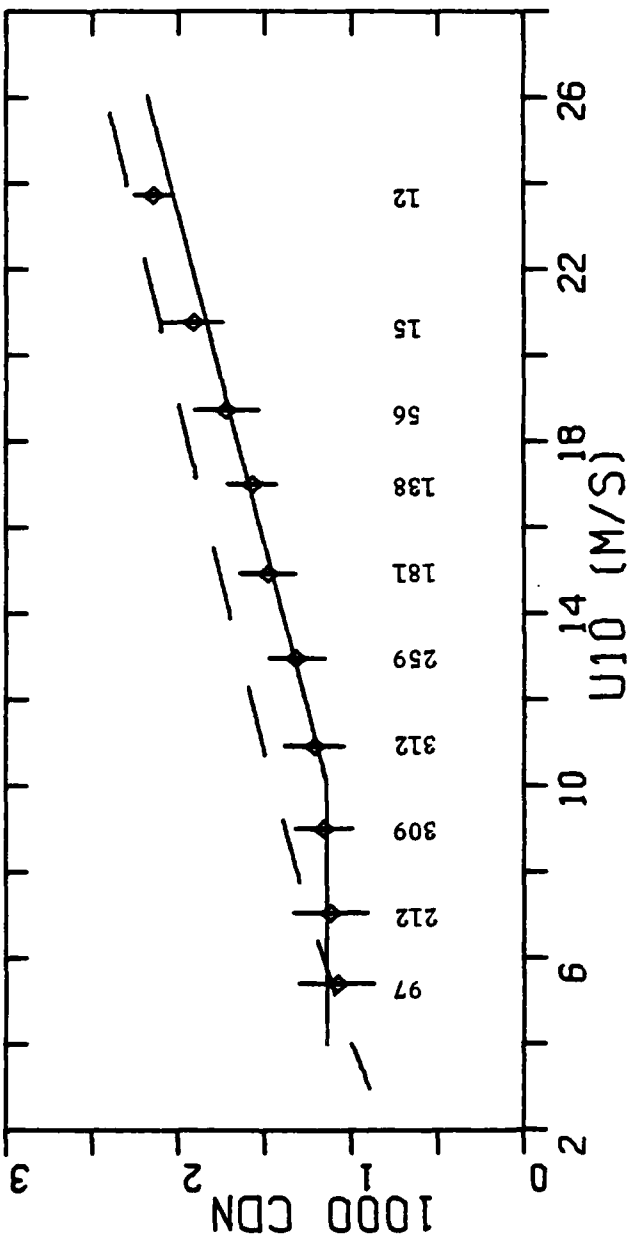

FIGURE 30 The neutral drag coefficient averaged over wind speed bands. Vertical bars indicate ± 1 σ and the number of points in band is shown below each average. Lines show the Charnock representation with α= 0.0144, K= 0.41 (dashed) and equations 6.1 (solid).

$$10^3\ CDN = 10^3\ C10 = 1.14 \qquad 4 < U10 \leq 10\ m/s$$

$$10^3\ CDN = 0.49 + .065\ U10 \qquad 10 < U10 < 27\ m/s \tag{6.1}$$

$$10^3\ C10 = 0.46 + .068\ U10\ ,$$

where the C10 results are included for comparison. The exact numerical values of 6.1 depend slightly on the somewhat arbitrary choice of a lower wind speed limit for the regression. Conveniently, with the choice of 10 m/s, the line segments happen to match. The behavior of CDN described by 6.1 is distinctly different from the dashed curve of figure 30, which is the Charnock representation with $\alpha = 0.0144$, $K = 0.41$ (or $\alpha = 0.016$, $K = 0.4$), as suggested by Garratt (1977). Equations 6.1 fit Smith's (1979) eddy correlation data from the Bedford tower site extremely well. For winds below 10 m/s, his average 10^3CDN is 1.11 from 14 runs (1976-1978) and about 1.24 from 11 near neutral runs (1968-1969). A regression of all 120 runs (1976-1978) between 6 and 22 m/s yields $0.44 + 0.063\ U10 = 10^3 C10$. However, the Sable Island results of Smith and Banke (1975) are significantly higher, suggesting that the Sable Island site with its surf zone and perhaps other shallow water locations: Lough Neagh at 8 to 15 meters (Sheppard et al., 1972), Lake Flevo at 4 meters (Wieringa, 1974), the 10m Caspian Sea location of Kitaigorodski et al. (1973) and the Spanish Banks site of Miyake et al. (1970 A) and Weiler and Burling (1967), may not be representative of the open ocean situation. Unfortunately, almost all the measurements above 14 m/s (and many at lower speeds), that were available to Garratt came from

these shallow water locations. A number of open sea measurements contributed to his 10 to 11 m/s band average, which very nearly lies on 6.1. It also seems likely that excluding the results of Sheppard et al. would give band averages in the 3 to 7 m/s range that would be adequately described by 6.1. In the range 7 to 10 m/s, the band averages of Garratt generally run about 20% (less than 1 σ) higher than equations 6.1.

Open ocean measurements used by Garratt (1977) are in better agreement. From the Argus Island tower, a site similar to the Bedford tower, the overall average of 69, near neutral, Reynolds flux CD's at 7.5m is 1.24×10^{-3} for wind speeds from 4 to 10 m/s (De Leonibus, 1971). The corresponding value of C10 is about 1.17×10^{-3}. Brocks and Krügermeyer (1970) present C10's from 152, near neutral, 15 minute profiles over the Baltic and North Seas and the Equatorial Atlantic measurements (787, near neutral, 10 minute profiles) of Hoeber (1969). Equations 6.1 are within the scatter, but generally lower by 10 to 15%. The overall average 10^3C10 from Hoeber (5 to 11 m/s) is 1.23±0.25 and his band averages agree very well with those of figure 30, except between 5 and 6 m/s where an average of only 11 points is 1.48. With 2/3 of his profiles unstable, CDN may average a few percent less. Averaging the Baltic and North Sea data (4 to 12 m/s) gives 10^3C10 = 1.30±0.18, but there is a slight trend with wind speed. The Bass Strait site of Hicks (1972 A) ought to be representative of the open sea, however his wind speeds are reduced by u* to account for surface drift. If the eddy correlation drag coefficients are reduced by about 7%, they then conform to the CDN's of figure 28 and the 30 values between 3

and 8 m/s then average 1.13×10^{-3}, however 6 runs from 8 to 10 m/s average about 1.4×10^{-3}. Garratt also uses the 18 eddy correlation runs (3 to 11 m/s) from Hasse (1970), quoting an average of $10^3 C10 = 1.21 \pm 20\%$.

The two data sets used by Garratt that remain to be discussed are open sea studies from R/V FLIP, however, they are not independent. Because of flow distortion due to FLIP, Paulson et al. (1972) use an empirical correction factor chosen so that their average <uw> (from profiles) and the average of corresponding eddy correlation measurements from Pond et al. (1971), are equal. The latter data (20 runs) give an average CD at about 8 meters of 1.52×10^{-3} in winds between 4 and 8 m/s and slightly unstable conditions. The equivalent average CDN is expected to be about 1.3×10^{-3} with a 20% variability. Accordingly, Paulson et al. find $10^3 CDN = 1.32$ for 19 runs.

It appears as if the major source of the disagreement between the data of figure 28 and the data used by Garratt (1977) is that the latter includes measurements from onshore and shallow water (less than 15 meters) sites. Equations 6.1 are consistent with most of the deep water (more than 50 meters) drag coefficients to within possible measurement error. The discrepancies suggest a slightly higher drag coefficient at wind speeds below 10 m/s. In contrast, recent measurements (10 hours) in Bass Strait (Antonia et al., 1978) in winds between 5 and 10 m/s and $-0.1 < Z/L < 0$ give an average $10^3 CD$ at 5 meters of 1.05 and 1.25 (about 0.9 and 1.1 at 10 meters) from the Reynolds flux and dissipation methods, respectively. Since a constant

CDN is a good fit to most individual data sets, it is likely to remain a good description of the overall open ocean situation below about 10 m/s. The "best" constant to use is debatable, but it should be in the range 1.1×10^{-3} to 1.3×10^{-3}. The average $10^3 C10$'s (neutral or near neutral) from all the discussed open ocean; eddy correlation, dissipation and profile measurements in winds less than 10 to 12 m/s are about; 1.17 (178 runs), 1.14 (626 hours) and 1.24 (958 profiles, 188 hours), respectively. The overall average is 1.20, but only 1.17 if the results from Hoeber and from Brocks and Krüggermeyer are weighted by 1/6 and 1/4, respectively, to make them comparable to hourly values. At the higher wind speeds, the vast majority of the open sea drag coefficients come from Smith (1979) and figure 28, which are both well described by 6.1. It is an interesting feature of 6.1, that an extrapolation to 50 m/s fits the hurricane and wind flume data compiled by Garratt (1977) as well as a continuation of the Charnock line of figure 30.

The Variability Of CDN And Zo

It may be possible to describe turbulence and the drag coefficients with a variable Zo, although this is expected to be difficult and there are no measurements of surface conditions available. The wind speed dependence of CDN above 10m/s shows that a constant Zo is not applicable. A Charnock representation with $\alpha = 0.0123$ ($K = 0.40$), passes within ±1 standard deviation of all the band means of figure 30, but its predicted low wind speed behavior is not observed. A Charnock line with $\alpha = 0.008$ fits the region from U10 = 11 to 17 m/s fairly well, but then

falls off much too quickly to account for the values up to 26 m/s. The CDN's to 50 m/s in Garratt (1977), require α to be about 0.016. CDN is very nearly a constant, 0.00114, for 4 <U10< 10 m/s, as is the average of C10. This behavior may be a consequence of highly variable sea surface conditions tending to make Zo increase with decreasing wind speed and balancing, on average, the tendency of lower u* values to make it smaller. Above 10 m/s, the important parameters seem to change character, so that Zo varies with wind speed, producing the observed near linear rise in CDN with U10. It may be possible to describe Zo by a Charnock formulation with α an experimentally determined function of various surface parameters.

To explore the influence of the sea surface on the turbulence above it, it is useful to examine the time histories of the winds and fluxes. An example, with hourly averages, is run D33C, figure 31. The drag coefficient is seen to vary quite smoothly with time, such that the random variability about a running average over a few hours is only about 10%. The increase with wind speed is evident from hour 6 to 21. In addition, CDN is seen to behave very differently on the rising wind than it does when the wind speed is dropping. The falling wind is also accompanied by an almost complete reversal in direction and it is this situation that gives rise to the high drag coefficients at low wind speeds. The picture of lower than average drag coefficients on the rising wind and higher ones on the falling wind is also supported by runs D29D and D31F, figures 32 and 33. Denman and Miyake (1973) observed that drag coefficients tended to increase on the leading side of a storm,

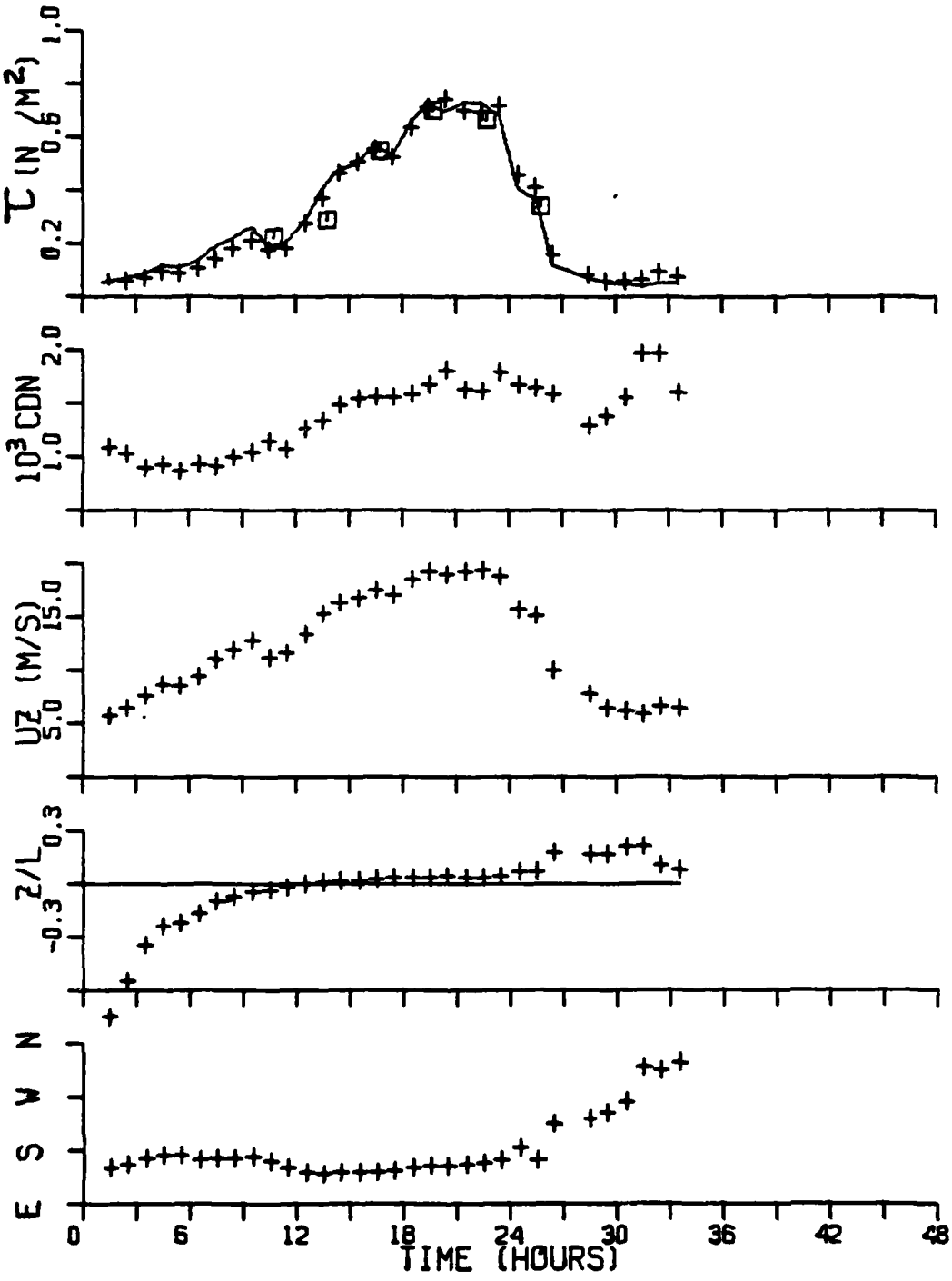

FIGURE 31 Time series of the momentum flux from run D33C, starting at 4:40 GMT December 7, 1976. Momentum fluxes are from the dissipation (pluses), Reynolds flux (squares) and bulk (solid line) methods.

then either remain constant or decrease slightly. This is also a very apt description of the time series in figures 31, 32 and 33. The scaling arguments of section 2.1 predict that the difference between the 10m and surface momentum flux should be greater (giving lower coefficients), on the falling wind. Apparently the increase in Zo in this situation is more than enough to overcome this loss. It is possible to speculate that Zo depends on surface parameters that, as the wind speed falls, remain near their "old" values produced by the previously higher winds. If α were dependent on the total wave generating force and hence U10-Cw (section 2.3), where Cw is the component of the wave speed in the $\vec{i}$ direction, it would be very sensitive to sudden changes in wind direction, because these would tend to make Cw smaller and perhaps even negative. It appears likely that some of the observed scatter in drag coefficients is due to the influence of the past history of the wind as "remembered" by the sea surface. With access to wave spectra, Denman and Miyake (1973) concluded that the drag coefficient was dependent on the nature of the wave field to the order of 20%.

In order to examine their influence on the average CDN, tower data from various wind conditions are presented in table X. Unfortunately, above 15 m/s there are too few data for meaningful averages. Winds of "constant speed" and "constant direction" are allowed to have 4 m/s and 30 degree ranges respectively. Data used in the "after direction changes" category are from the six hours following a change in direction of at least a 60 degrees in less than two hours. Peak winds are included in the rising winds. The suggestion is, that either a

Wind conditions (number of hours)	Regression and correlation	WIND SPEED BANDS (M/S) 4.5-7	7-9	9-11	11-15
All tower data (1086)	.79 +.043 U10 .59	1.11 (176)	1.13 (264)	1.17 (259)	1.33 (247)
Constant speed and direction (253)	.71 +.049 U10 .60	1.03 (31)	1.13 (68)	1.14 (79)	1.31 (59)
Rising winds (167)	.64 +.054 U10 .70	1.01 (22)	1.11 (33)	1.14 (31)	1.25 (49)
Rising wind steady direction (81)	.60 +.055 U10 .67	1.08 (3)	1.11 (15)	1.10 (18)	1.24 (29)
Falling wind (111)	.94 +.036 U10 .51	1.40 (3)	1.25 (12)	1.28 (24)	1.38 (49)
Falling wind steady direction (80)	1.05+.025 U10 .36	1.31 (2)	1.28 (8)	1.29 (18)	1.34 (29)
After direction changes (60)		1.18 (22)	1.34 (12)		1.60 (16)

TABLE X Mean 10^3CDN of wind speed bands in different wind conditions. Bracketted values are the number of hours contained in an average or regression of CDN against U10.

direction change or a falling wind tends to produce higher than average drag coefficients. Table X also indicates that if observations were available only during rising winds with constant direction, as may be the case in some data sets, the average CDN value for 7 <U10< 11 m/s, would be about 4% lower than given by 6.1. The observations of CDN during rising winds

show a systematic rise with wind speed and a regression of CDN against U10 gives 10^3 CDN= 0.64+ 0.054 U10 with a correlation coefficient of 0.70. Thus, if only these data were available one could easily conclude that the average drag coefficient increases linearly with wind speed even below 10 m/s. Such a trend may also emerge even if data with constant speed and direction are included. Similar effects are expected at the higher speeds too, so in order to arrive at a realistic mean drag coefficient for all wind speeds it is imperative that measurements be made during all likely wind conditions. It is, therefore, possible that drag coefficient formulations may vary with location and time of year, with the break from a constant to a linearly increasing CDN being quite variable.

The tower data is also sorted into monthly groupings in table XI. There is no trend in the September data and the average CDN's are lower than those of the other months. There is a reasonably significant trend in the October data throughout the entire wind speed range. The high CDN's at low winds are evident in the December results, while March seems tc reflect average conditions, table X. The results of experiments conducted at different times of the year may, therefore, be considerably different, possibly because wind conditions vary throughout the year. It would be desirable to include data from every month in any drag coefficient formulatien. Unfortunately, no measurements from May through August are available from either the tower or the weathership, but the high wind speed formulation should not be affected as these are not the months with the greatest winds.

Wind conditions (number of hours)	Regression and correlation	WIND SPEED BANDS (M/S) 5-7	7-9	9-11	11-15
September (241)	1.05+.001 U10 .008	1.07 (94)	1.04 (79)	1.05 (47)	1.06 (21)
October (131)	.83 +.047 U10 .65	1.11 (28)	1.16 (25)	1.30 (28)	1.45 (34)
December (251)	.78 +.044 U10 .62	1.22 (20)	1.14 (42)	1.14 (53)	1.33 (73)
March (271)	.77 +.044 U10 .65	1.12 (24)	1.18 (49)	1.17 (96)	1.31 (70)

TABLE XI Mean $10^3 C_{DN}$ of wind speed bands for different months. Bracketted values are the number of hours contained in an average or regression of CDN against U10.

The Empirical Drag Coefficient

The investigation of the tower data has shown that neither stability nor fetch (greater than 10 km) have a significant effect on the average neutral drag coefficient. It has been demonstrated that much of the variability in CDN measurements, not only between individual data points, but between entire data sets, may be due to the influence of the surface wave field. However, it appears as if the measurement of the important surface parameters could possibly be more complicated than direct momentum flux measurements. An important parameter that can be practically incorporated into a neutral drag coefficient formulation is the wind speed.

The empirical CDN formulation of 6.1 gives bulk estimates of the momentum flux from the wind speed, UZ and stability, $Z/L(\Delta T)$, following the procedure outlined in section 2.3. An iterative technique is used to solve equation 2.15 for U10. For the first pass $U10' = UZ/[1 + 0.1\,K(Z,Z/L)]$ is assumed ($CDN^{1/2}/K \cong 0.1$), giving a CDN' from 6.1. On subsequent iterations (never more than 3) U10' is found from 2.15 using the CDN' of the previous pass until successive U10' values change by less than 1%. CDN' from the final pass is substituted into 2.14 to give a CD, which gives the momentum flux through 2.9. Bulk estimates are to be compared to direct estimates in later time series that include data with $-1.0 < Z/L < 0.3$. The stability need not be included in the U10 calculation, because the maximum stability of the ship data is only 0.08 and on the tower, where stabilities are higher, the reduction is only from 13 to 10 meters, therefore, (section 2.3) the worst error is less than 2% in U10 and about 1% in CD and $\langle uw \rangle$. The error in $Z/L(\Delta T)$ (section 4.1) introduces an error in CD of about 5%. A 2% error in UZ becomes 4% in $\langle uw \rangle$. The large standard deviations in figure 30 and the range of previous measurements, suggest that any CDN formulation has at least a 10% uncertainty. The combined error in bulk estimates from equation 2.9 are, therefore, greater than 15% as are the errors in direct estimates. Although individual bulk estimates may differ from direct dissipation or Reynolds flux measurements by 50% or more, there should be reasonable agreement on average, albeit the necessary averaging period may vary with time and place.

Comparison Of Methods

In all the time series presented, figures 31 to 34, the momentum flux or Reynolds stress, (in N/m^2 or pascals, Pa) is calculated from the dissipation method (pluses), from the Reynolds flux method (squares) and from the bulk formula of 6.1 (solid line). Run D29D, figure 32, is a typical September situation. During the unstable conditions of the rising wind (to hour 22) the bulk formula gives a total momentum input of 2.23 $N\text{-}hr/m^2$, which is 34% higher than found from the dissipation calculations. Upon reaching the peak winds the two methods are in much better agreement and the deviation over the whole run is reduced to 18%. A front is passing the tower in D33C (figure 31) and a similar situation occurs, but with the rising and falling wind effects balancing, the overall deviation is only 1%. In D29D the falling wind and changing direction effects are not great enough to make the average stress from the two methods equal. It would be expected that these influences are strongly felt after the passage of low pressure systems, because as centers pass the winds quickly fall, then regain velocity as the direction changes after which they drop off slowly. A low pressure center is passing to the west of the tower, from south to north, in D31F, figure 33. Unfortunately the earlier winds from the east were obstructed by other instrumentation on the tower. Stability is always very nearly neutral or slightly stable and should not have been a factor in causing the large observed stresses that give a total momentum input over the period shown of 6.5 $N\text{-}hr/m^2$, which is 12% higher than given by the bulk calculations. A run from March 1977,

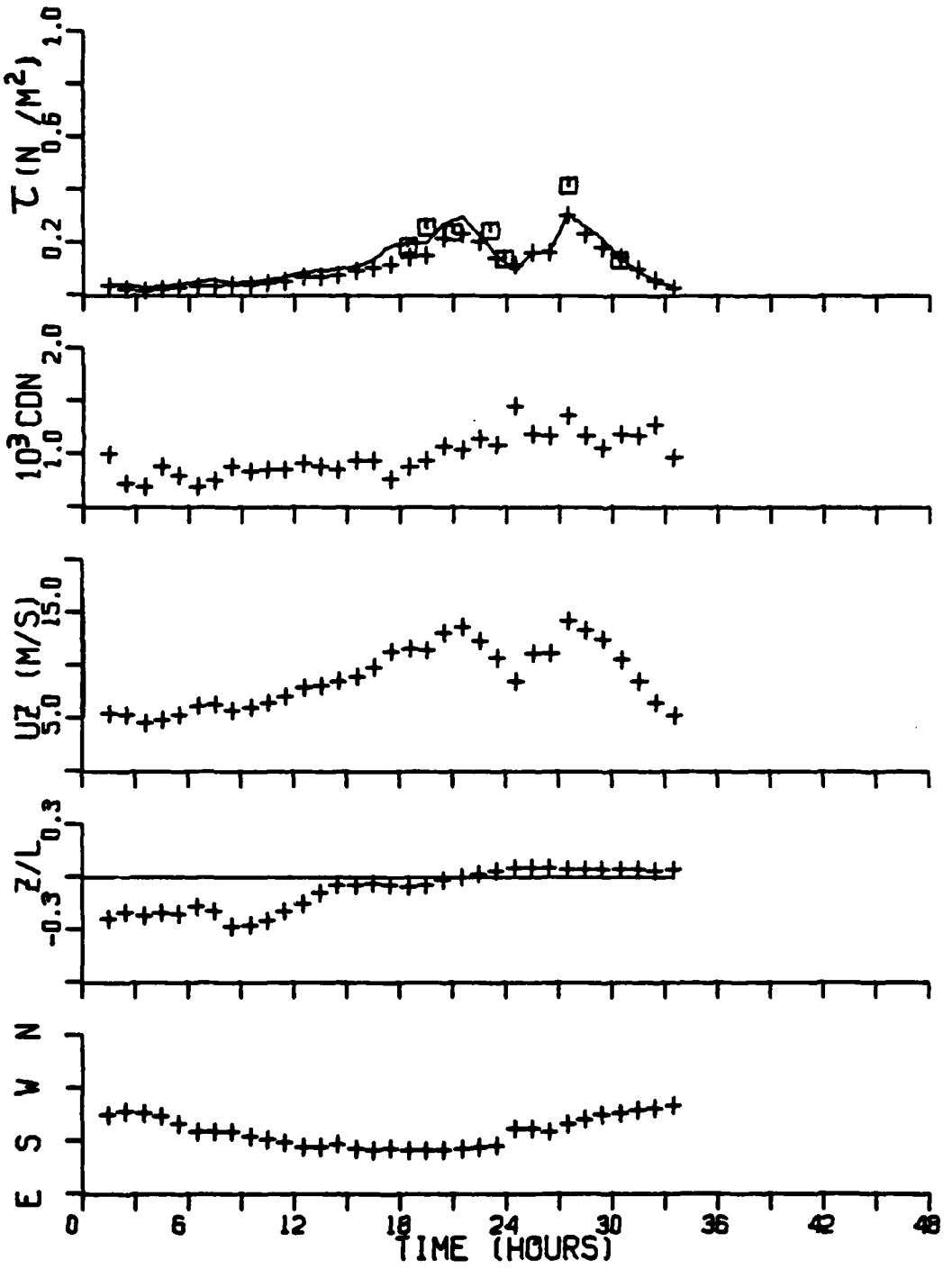

FIGURE 32 Time series of the momentum flux from run D29D. Time is from 17:00 GMT September 26, 1976, and symbols are the same as in figure 31.

D38B, figure 34 shows that all three methods can be in excellent agreement over a long period of time provided the wind is reasonably steady. Over this period of nearly two days, the cumulative momentum input from the dissipation calculations is less than 3% higher than that found from the bulk formula.

In general the Reynolds flux method verifies the dissipation calculations, but an exception is found at hour 28 of run D29D, figure 32. The flux run, T61, is an average of only 3 groups (40 minutes) starting 15 minutes after the beginning of the hour 28 dissipation average. In this 15 minute interval there was a sudden 4 m/s increase in wind speed, which the hourly averaging smooths. The simultaneous dissipation run does agree with T61 (Appendix), illustrating that identical time intervals are required for intercomparisons. The flux run, T112, at hour 14 of run D33C (figure 31) is also found to be in much better agreement with its simultaneous dissipation run than with the hourly average. Run D33C discloses a sampling problem associated with the tower operation of the Reynolds flux system. Most of the low wind speed runs were collected in September when the drag coefficients tend to be low. Later, when the more variable winds seem to produce some very high coefficients at wind speeds below 10 m/s, the Reynolds flux system was prevented from recording by the wind speed limit setting. Thus the Reynolds flux data set (figure 19) tends to be biased toward small CD's, relative to 6.1, at the low wind speeds and to exhibit a trend with wind speed over the whole range of measurements. Above the maximum wind speed limit setting (12 m/s) 6.1 fits the data of figure 19 very well.

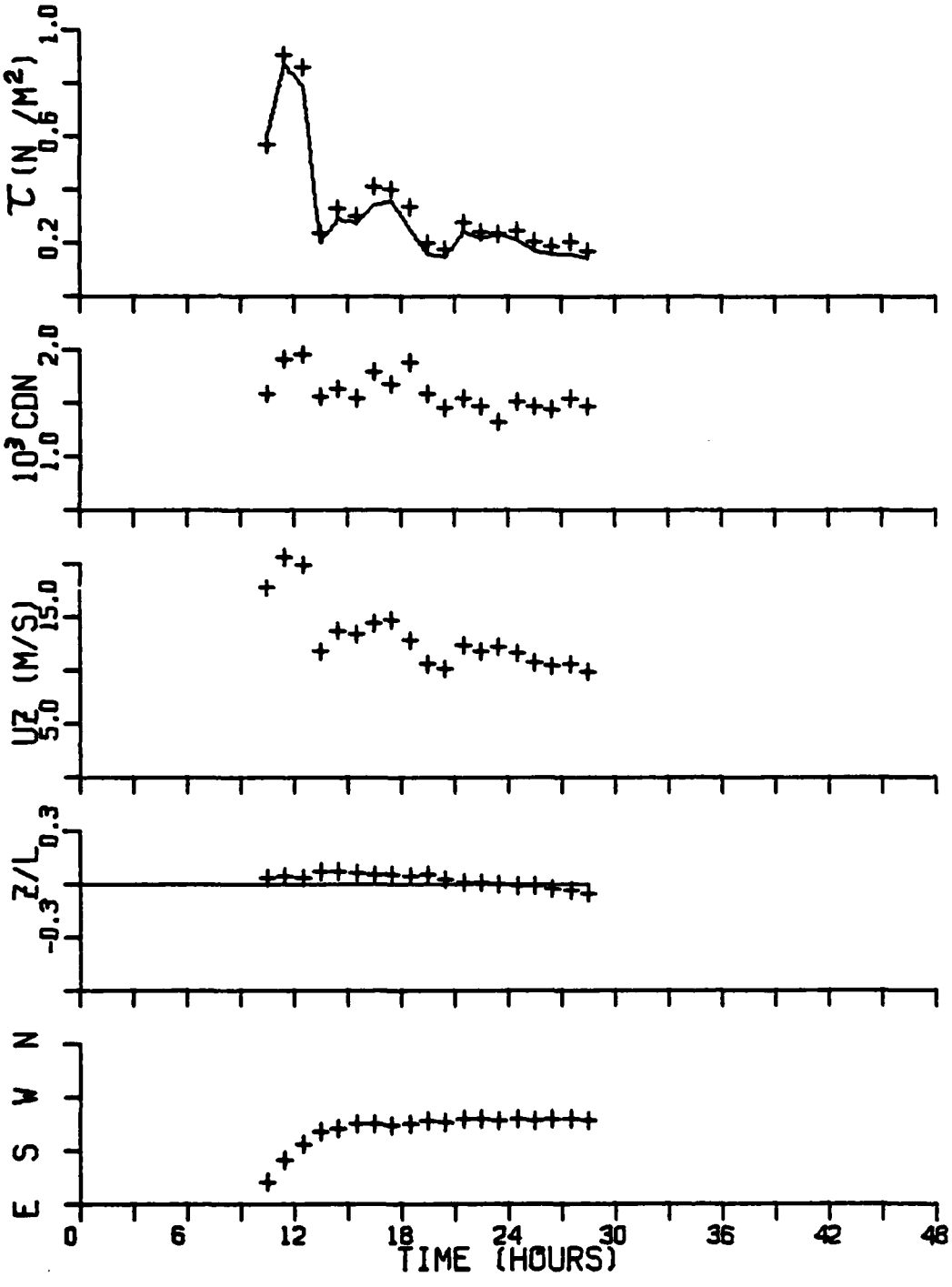

FIGURE 33 Momentum flux time series from run D31F. Starting time is 4:00 GMT October 20, 1976. The solid line represents the bulk estimates of τ.

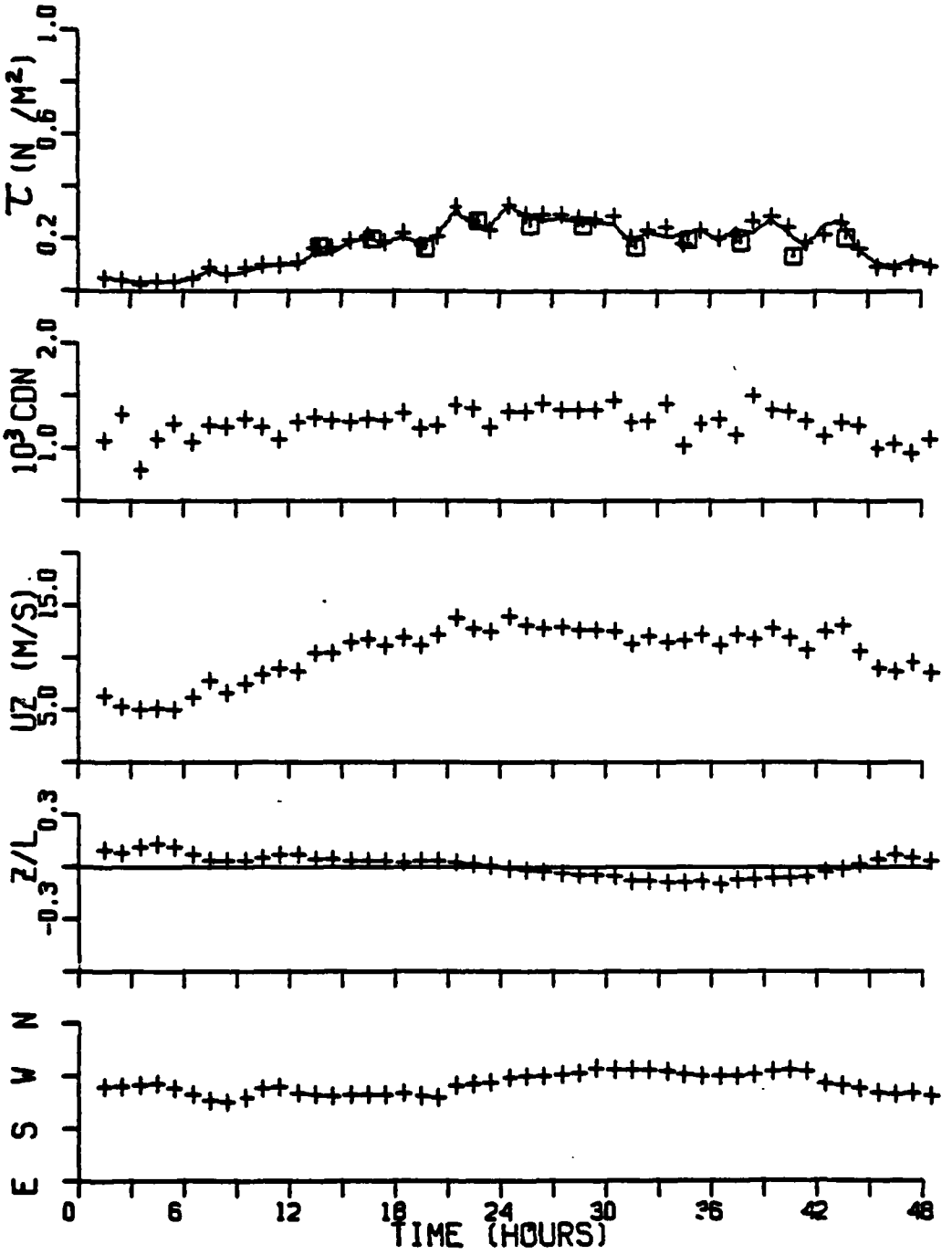

FIGURE 34 Momentum flux time series from D38B. Time is from 16:00 GMT March 12, 1977 and symbols are the same as in figure 31.

It appears that the bulk aerodynamic method gives good estimates of the total momentum input or average stress over periods of a few days or more. The bulk estimate should improve if measured or approximated stability conditions are included. It has been shown that in steady winds the hourly bulk estimates are good measures of the stress, but with more variable winds they may consistently differ, over periods up to a day, from dissipation estimates. With comparable error in both methods, it is not obvious which is the more accurate. It is conceivable that the varying winds are producing systematic errors in one or more of the dissipation method's assumptions and causing the discrepancies. However, if this occurred it is likely that the overall scatter of figure 28 would be greater than the scatter in drag coefficients calculated from other methods, which is not observed. It is felt that, since at least some of the scatter in measured drag coefficients at the same wind speed is real, dissipation measurements, although subject to random errors, ought to follow changes in the real stress more closely than bulk estimates. A bulk formula based on long term averages may not be strictly applicable to short term phenomena, such as wave development during a rising wind or the deepening of an inlet's upper layer following a switch from down to strong up inlet winds. In such cases, it may be possible to devise an appropriate formulation cabable of providing good hourly stress values with minimal measurement error. A possible means of incorporating variable wind effects would be to allow the drag coefficient to depend on the past history of the wind.

6.3 Bulk Aerodynamic Parameterization Of The Sensible Heat Flux

The sensible heat flux is parameterized in terms of a surface - air temperature difference. The mean air temperature at 10m, T10, is obtained from the average temperature at the measurement height, TZ, through equation 2.11. At the Bedford tower the surface temperature, TSFC, is approximated by a sea temperature, TSEA, measured about 10m below the mean sea level, where the heating and cooling of the surface by radiation and heat exchanges with the atmosphere may not be followed exactly. On CCGS Quadra a surface "bucket" temperature was recorded as part of the 3-hourly meteorological observations. These are interpolated to give hourly TSEA values, which may be a problem, because the ship was steaming through large sea surface temperature gradients during the one run that useful temperature measurements were recorded. At any time then, TSEA may differ substantially from a representative surface temperature. As a precaution that the Stanton number, CT (equation 2.9), is not too adversely affected, data used in the parameterization are restricted to conditions with $|TSEA-TZ| > 1.0°C$, even though the flux measurements may still be reliable.

Figure 35 is a plot of $\langle wt \rangle$ against U10 ΔT ($\Delta T = TSEA - T10$), for all 129 hours of unstable temperature data, and a regression line (the average of $\langle wt \rangle$ against U10 ΔT and U10 ΔT against $\langle wt \rangle$). The 23 hours of data from the weathership (plotted as pluses) show considerable scatter, but no systematic departure from the tower results (triangles). The regression is

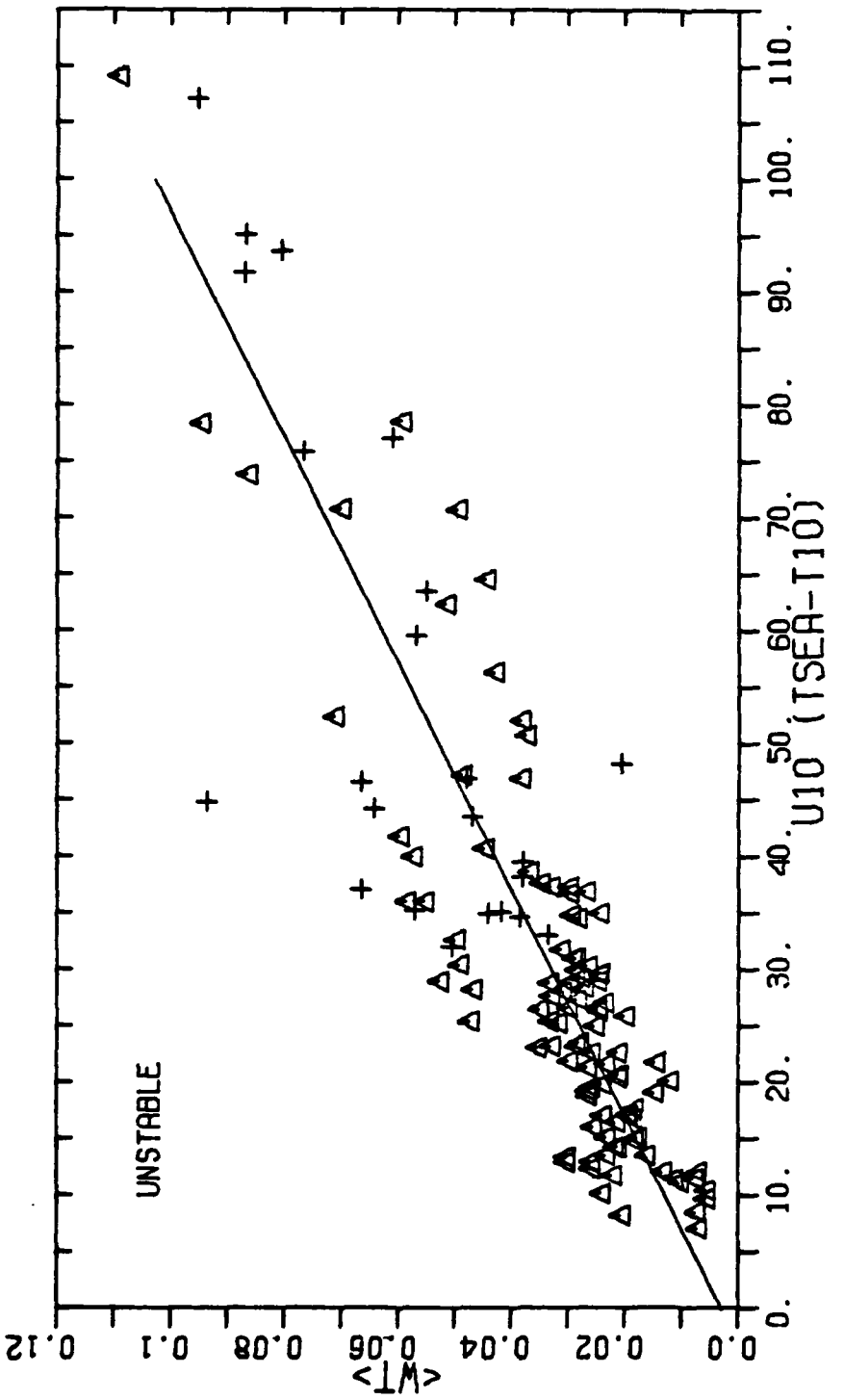

FIGURE 35 Parameterization of the sensible heat flux in °Cm/s in unstable stratification. Triangles represent tower data and pluses are from CCGS Quadra.

$$\langle wt \rangle = 0.00100\ U10\ \Delta T + 0.0029\ ^{\circ}Cm/s$$

$$10^3\ CT10 = 1.00 + 2.9\,(^{\circ}Cm/s)\ /\ (U10\ \Delta T)\ , \qquad (6.2)$$

with a correlation coefficient of 0.86. This is almost identical to the formula given by Friehe and Schmitt, 1976, for $0 < U10\ \Delta T < 25\ ^{\circ}Cm/s$ only. Restricting the parameterization to data with $|\langle wt \rangle| > 0.004^{\circ}Cm/s$, U10 >4.0 m/s and $|\Delta T| > 1^{\circ}C$ eliminates low heat flux and small U10 ΔT situations, but a positive heat flux is still predicted at U10 $\Delta T = 0$, although the value of 0.002 °Cm/s given by Friehe and Schmitt, who used mostly small heat flux data, is probably more realistic. The additional data at higher sensible heat fluxes indicate that a single parameterization is acceptable from U10 $\Delta T = 0$ to possibly more than 100 °Cm/s. Again this result is in accord with the BIO tower data of Smith, 1979, but the average coefficient is much lower than found by Smith and Banke (1975) from a limited number of Sable Island measurements.

The sensible heat flux time series from run D33C, figure 36, shows that seemingly very small Stanton numbers arise during a rapid increase in air temperature, just after ΔT first goes negative. Fortunately, Reynolds flux measurements (squares) are also available over this period and their good agreement with the dissipation method verifies the treatment of equation 2.21. Temperature spectra from the Reynolds flux recordings do not display any evidence of salt contamination, so it is felt that the $\langle wt \rangle$ values from this period are reasonably accurate. However, it is possible that they are significantly less than their surface values. The loss of sensible heat flux with

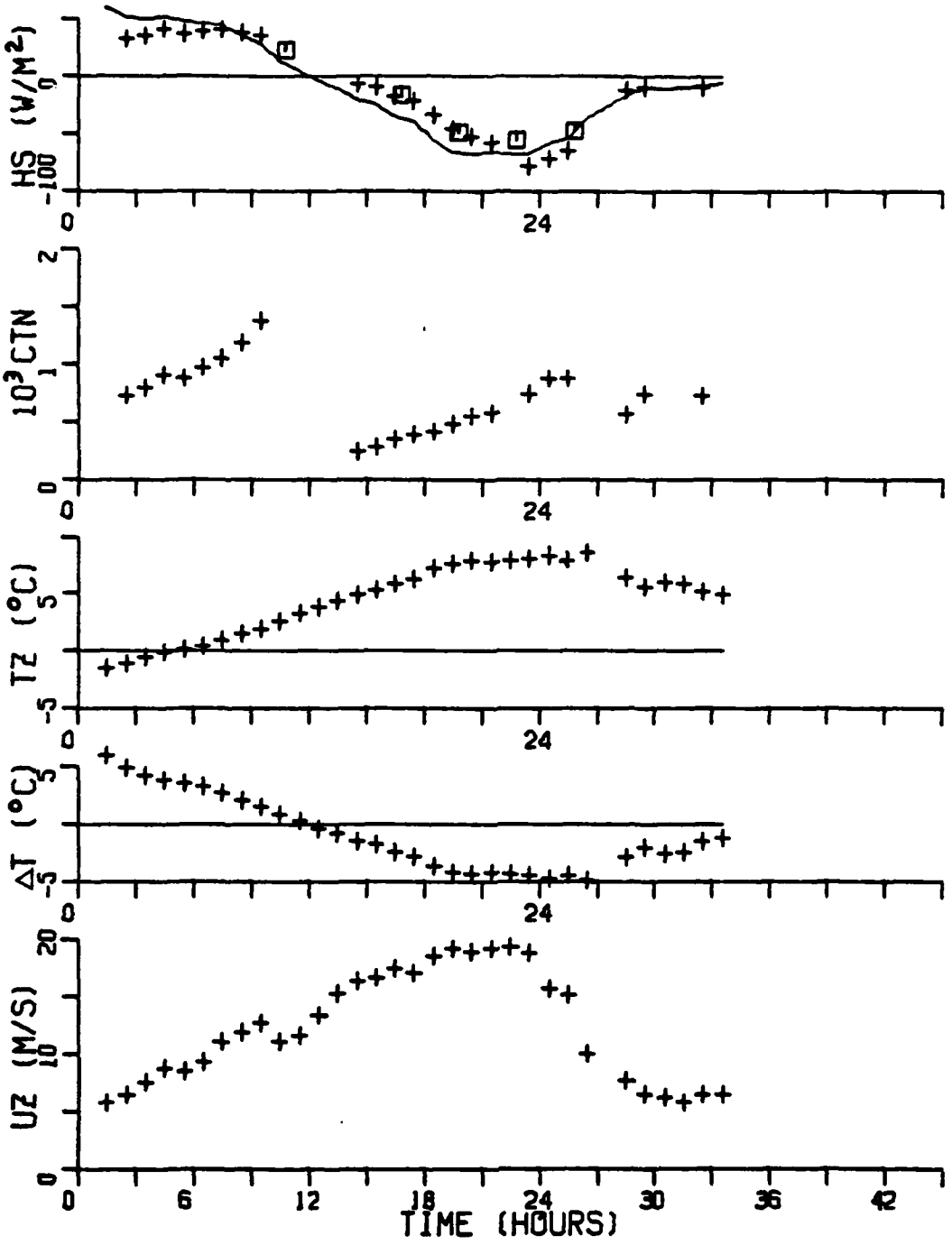

FIGURE 36 Time series of the sensible heat flux from run D33C (figure 31). Time is from 4:40 GMT December 7, 1976. Hs is from the dissipation (pluses), Reynolds flux (squares) and bulk (solid line) methods.

height was discussed in section 2.1 and if the 0.5°C/hour heating were due solely to the vertical flux divergence, then a 40% loss in flux at 13m would be expected. Qualitatively the low CTN values observed can be explained by speculating that <wt> was measured above the "constant sensible heat flux" layer, since if this were the case, the percentage of the loss should decrease as the magnitude of the surface flux increases and no loss should be evident after the peak temperature. However, there is probably a great deal of heating due to horizontal advection, which would mean less loss of flux with height. There are other situations of rising temperature which do not seem to be affected to such a great degree so possibly the measured <wt>'s do not differ from the surface flux by as much as the low CTN's would suggest. Another possibility is that TSEA at a depth of about 10m is not tracking the surface temperature. In the 12 hours prior to run D33C there was very little wind and the air temperature was below -15°C, giving a huge ΔT of about 20°C. It appears as if the surface temperature, TSFC, may have become much colder than TSEA during this time, because as the air warmed and the wind increased, presumably mixing the unstable water column, TSEA actually decreased from 3.9 to 3.5°C. It is not impossible that the surface heating produced by the later high air temperatures was prevented from mixing down to the sea temperature probe by the then stable upper water column. In this situation TSEA could become less than TSFC by enough to produce the observed behavior of D33C and to upset the parameterization of the sensible heat flux. There was only one other similar situation at the tower

and even lower Stanton numbers were calculated, but these data were rejected on the basis of abnormal temperature spectra. Despite the preceding arguments, lower than average CT values may occur in the circumstances described, but they are not likely to occur over the open sea, so this period of D33C is not included in the parameterization and analysis of the stable sensible heat flux.

Figure 37 is a plot of $-\langle wt \rangle$ against $-U10(TSEA-T10)$ from 131 hours of stable stratification with the suspect D33C results plotted as crosses. The regressions of $-\langle wt \rangle$ against $-U10\,\Delta T$ and $-U10\,\Delta T$ against $-\langle wt \rangle$ for the 123 triangles have a correlation coefficient of 0.93 and when averaged yield

$$\langle wt \rangle = 0.00075\ U10\ \Delta T + 0.0020\ ^{\circ}Cm/s$$
$$10^3\ CT10 = 0.75 + 2.0\,(^{\circ}Cm/s)\ /\ (U10\ \Delta T)\ , \qquad (6.3)$$

which is also plotted on figure 37. Again a positive heat flux of about 0.002 °Cm/s at $U\ \Delta T=0$ is indicated even though there is no data with $|U\ \Delta T| < 5^{\circ}Cm/s$. Inclusion of the suspect D33C data lessens the slope to about 0.00065. Friehe and Schmitt only considered data with $U\ \Delta T > -15^{\circ}Cm/s$ and their suggested formula differs from 6.3 by only 10% at $U\ \Delta T = -15^{\circ}Cm/s$. There are only a few data points beyond $U\ \Delta T = -35^{\circ}Cm/s$ that contribute to 6.3, which, therefore, cannot be expected to be representative of more negative $U\ \Delta T$'s. The BIO tower results (Smith, 1979) contain more, large negative heat flux runs and suggest a larger CT10 of about 0.00083. Although the BIO regression differs from 6.3 by about 13% at $U\ \Delta T = -100$ °Cm/s, the data points overlap

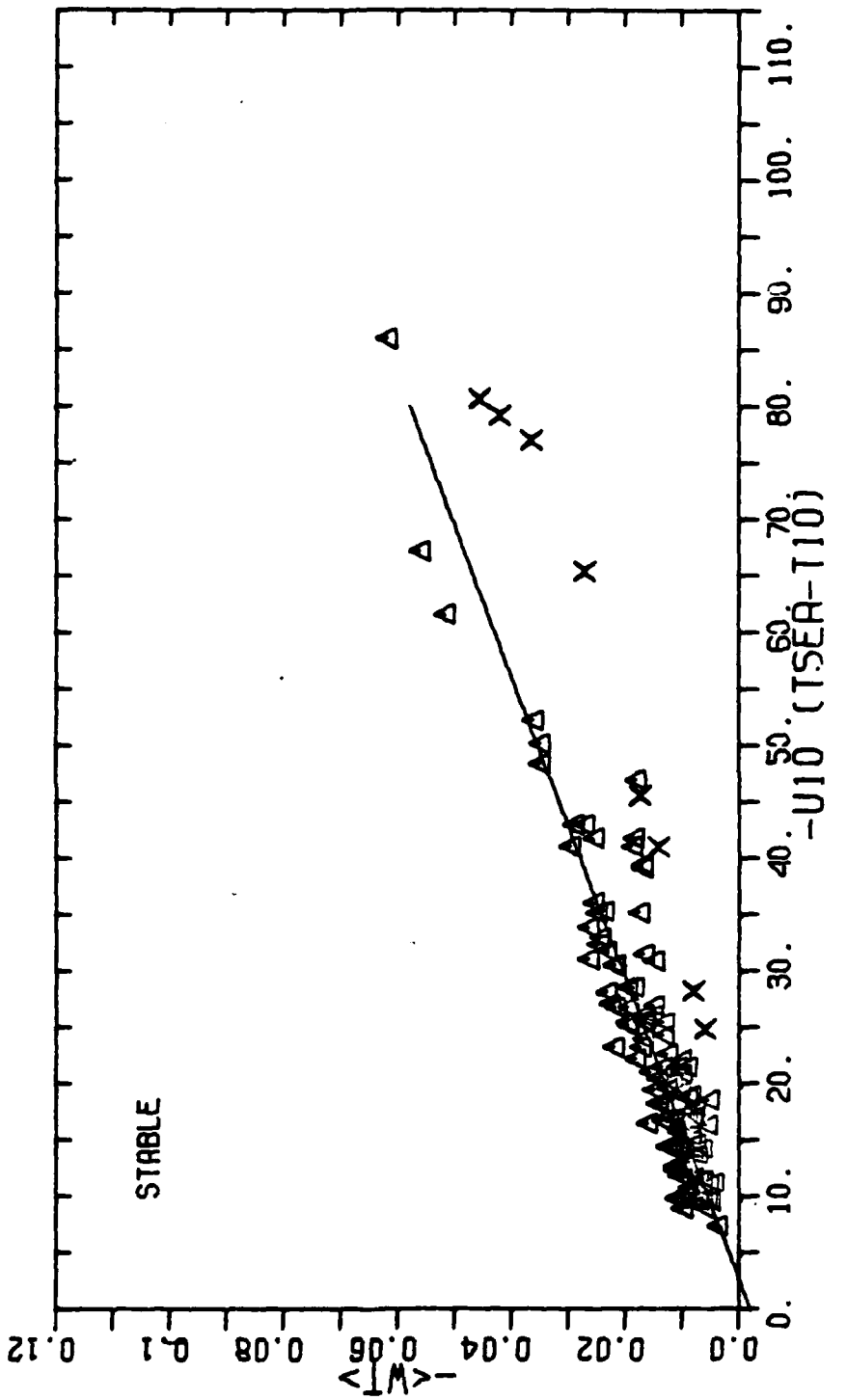

FIGURE 37 Parameterization of the sensible heat flux (°Cm/s) in stable stratification. Crosses are from D33C. Solid line is a regression of the triangles only.

very well. A single parameterization of the sensible heat flux in stable stratification should adequately describe all the measurements, but it appears to differ from the unstable case.

It is felt that the uncertainty in U10 ΔT is perhaps greater than in <wt>, so band averaging is carried out over bands of <wt> and the results are tabulated in table XII. The band averages are reasonably well described by 6.2 and 6.3 over the entire range of measurement, thus linear fits to the data of figures 35 and 37 are appropriate. The ratio of the averages gives a CT10 for each band and the unstable values are clearly higher than the stable ones. The individual points are far too few and scattered for any trends to be seen. For example, the 10^3CT10 value of 1.21 in the 0.05 to 0.07 °Cm/s band, becomes 1.04 if U10 ΔT is increased by only 1/2 a standard deviation.

Stability Effects

The stability dependence of the neutral Stanton number is examined in figure 38, where CTN, equation 2.12, is plotted against Z/L. The solid lines represent the overall averages:

$$\begin{aligned} &123 \text{ stable} \quad 10^3 \text{ CTN} = 0.69 \\ &129 \text{ unstable} \quad 10^3 \text{ CTN} = 1.08 , \end{aligned} \tag{6.4}$$

about which the standard deviations are 0.16 and 0.36, respectively. There is not a great deal of data on which to base definitive conclusions, but it appears as if CTN and Zot are reasonably independent of Z/L in stable and unstable

Range of <wt> °Cm/s	Average <wt> ±1 standard deviation	Average U10ΔT ±1 standard deviation	10^3 CT10 ratio of averages	Number of runs
0.09, 0.11	.098 ±.007	84.9 ±30	1.15	4
0.07, 0.09	.080 ±.007	79.0 ±16	1.01	7
0.05, 0.07	.058 ±.005	47.9 ±16	1.21	15
0.03, 0.05	.038 ±.007	35.5 ±13	1.07	38
0.01, 0.03	.023 ±.005	22.0 ±8.2	1.05	58
0.006, 0.01	.007 ±.001	9.86 ±1.7	0.71	7
-.01, -.004	.008 ±.002	13.7 ±3.6	0.59	43
-.02, -.01	.014 ±.003	22.4 ±8.4	0.62	55
-.03, -.02	.025 ±.003	34.0 ±6.0	0.74	19
-.05, -.03	.035	50.3	0.70	3
-.07, -.05	.057	71.6	0.80	3

TABLE XII Parameterization of the sensible heat flux by band averaging U ΔT over ranges of <wt>.

stratification separately. However, the discontinuity in the mean CTN at Z/L=0, implies a dramatic change in Zot. This feature could be incorporated into the theory by relating Zot to a parameter that changes character abruptly at neutral stability, but that otherwise has very little stability dependence as is indicated by the relative constancy of the

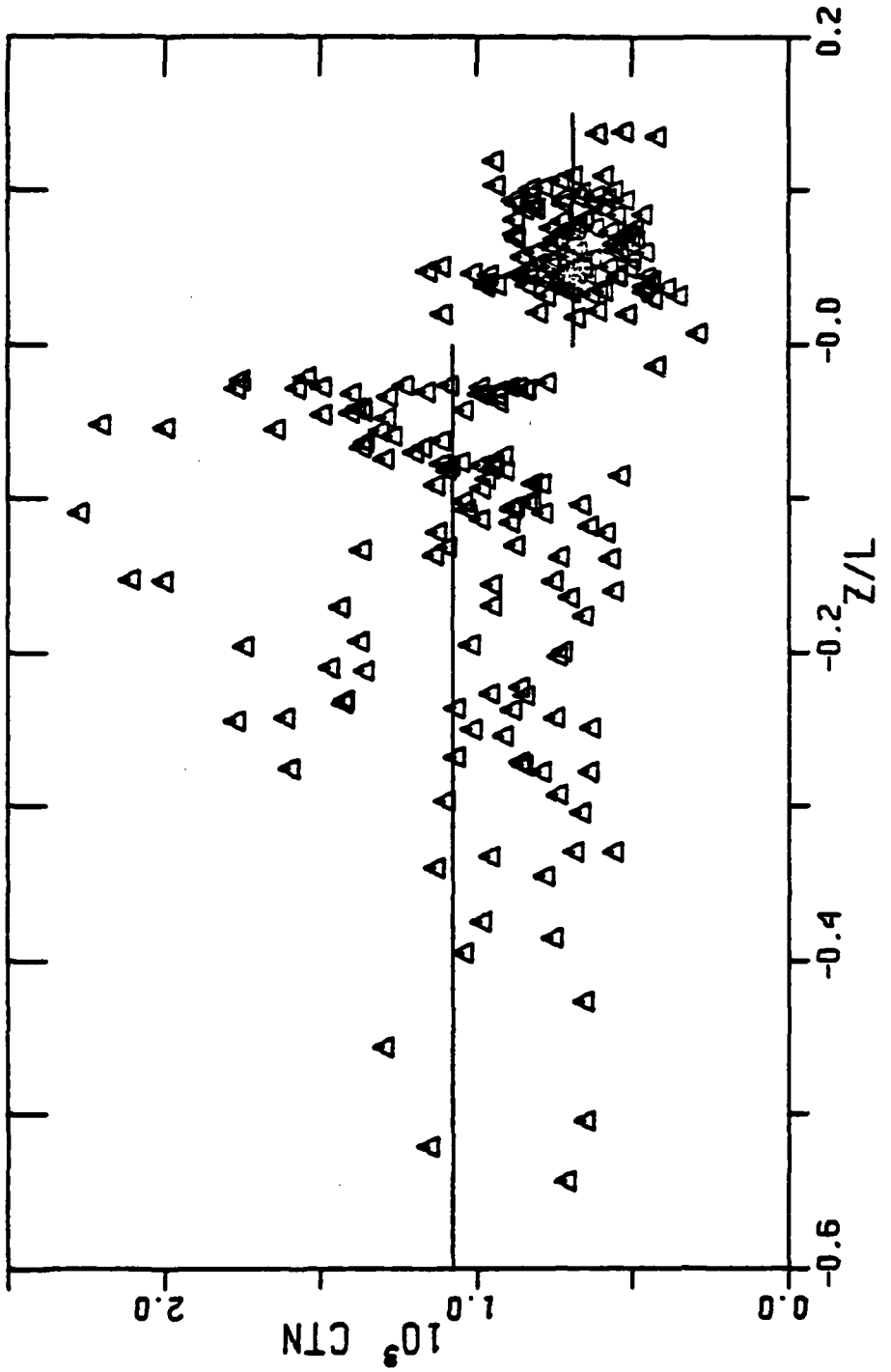

FIGURE 38 The neutral Stanton number as a function of stability. Solid lines represent the mean in both stable and unstable stratification.

average CTN away from Z/L=0.

There is a great deal of scatter in figure 38 and it should be reiterated that microbead contamination by salt particles could only be checked at the few, sometimes infrequent, times for which spectra were available from the Reynolds flux system. It is therefore possible that some contaminated data has escaped notice and is responsible for some of the high CTN values at Z/L<0. Similarly, because temperature and humidity are oppositely correlated in stable stratification, contaminated data may be responsible for some low CTN's at Z/L >0. The high CT10 values following hour 40 of run D38B (figure 39) are quite likely a result of bead contamination, because a Reynolds flux run at about hour 44 was rejected on the basis of a lack of low frequency variance in the temperature spectrum and the run at hour 41 was a borderline case.

Wind Speed Effects

Equation 2.12 relates CTN to Zo, indicating that it should increase with wind speed above 10 m/s, if Zot does not counteract the increase in Zo. The situation may be complicated by the observed dependency of Zot on Z/L, which correlates with wind speed. The effect of wind speed on CTN is investigated for the stable and unstable case in tables XIII and XIV respectively. In the stable case there is no indication of an increase in CTN with wind speed. In fact above 10 m/s where CDN begins to increase, there is a hint, albeit not significant, that CTN decreases. In table XIV the means are scattered, but

Wind speed range (m/s)	Number of runs	Mean 10^3CTN ±1 standard deviation	Minimum	Maximum
6 to 8	19	0.71 ± .18	0.43	1.12
8 to 10	39	0.73 ± .17	0.47	1.61
10 to 12	25	0.65 ± .14	0.36	0.98
12 to 14	26	0.69 ± .13	0.44	0.88
14 to 18.2	14	0.62 ± .20	0.29	0.88

TABLE XIII Averaged neutral Stanton number as a function of wind speed in stable stratificatien only.

again there seems to be no obvious wind speed dependency. However, nearly all of the data in table XIV above 18 m/s come from CCGS Quadra, which did not really yield enough data at the lower wind speeds to fully intercompare the ship and tower results. There is a suggestion in table XIV that the unstable CTN increases from U10 = 10 to 18 m/s. Larger CTN values are reported over shallow water by Francey and Garratt, 1978, who find an increase with wind speed given by 10^3CTN = 0.083 U10 + 0.48. The contention that CTN increases with U10 is apparently supported by run D33C, figure 36, where the increase in UZ from 10 to 13 m/s (hours 7 to 10) is accompanied by a sharp rise in CTN from about 1.0 to 1.4×10^{-3}. The rise in CTN with winds above 10 m/s appears to be greatly perturbed by the transition to stable stratification and although the following stable data are suspect, the rise seems to subsequently continue. No

Wind speed range (m/s)	Number of runs	Mean 10^3CTN ±1 standard deviation	Minimum	Maximum
5.5 to 8	32	1.13 ± .47	0.56	2.28
8 to 10	29	0.94 ± .28	0.54	1.47
10 to 12	25	1.06 ± .34	0.64	2.21
12 to 14	11	1.13 ± .24	0.71	1.38
14 to 18	13	1.31 ± .24	0.43	2.01
18 to 22	13	1.14 ± .28	0.78	1.76
22 to 26	6	0.90 ± .06	0.85	0.99

TABLE XIV Averaged neutral Stanton number as a function of wind speed in unstable stratification only.

definite conclusion is possible because of the lack of data and the strong influence of stability. For example, if the suspect D33C data were included in the 14 to 18.2 m/s range of table XIII, the band average would decrease giving a smaller CTN at the highest speed, even though these additional CTN's increase with wind speed.

These results do not, therefore, rule out the possibility that CTN follows the wind speed dependency of Zo. However, because this trend is not supported by the Quadra results, because of the limited amount of data, some of which is possibly contaminated (run D38B), and because the stability effects are not fully understood, the neutral Stanton number is not

formulated as a function of wind speed. It is an interesting observation that, on average, CTN for Z/L<0, 0.00108, is very nearly equal to CDN for 4.0< U10 <10 m/s, 0.00114, implying Zo≅ Zot≅ 0.0058 cm. It is possible that Zot remains constant above 10 m/s with CTN increasing due to Zo. If this is true, CTN could be obtained from an experimentally determined Zot and a Zo given from a CDN formulation, using equation 2.12.

Method Comparison

The bulk estimates of the sensible heat flux shown by the solid lines of figures 36 and 39, are calculated from the stability dependent CTN given by 6.4. As outlined in section 2.3, the neutral Stanton number is converted to a CT at the measurement height, wind speed and stability. The error in bulk estimates found from <wt> = CT UZ ΔT, equation 2.9, is about 2% from UZ, perhaps 10% from CTN and only 5% from Z/L, because the bulk stability estimate is always available. In addition considerable error is introduced through ΔT, which may sometimes be in error by 0.5°C. Even with a large ΔT of 5°C, the error is 10%, making the bulk sensible heat flux calculations more uncertain than those of the momentum flux. With a large possible error and problems with the data, it is difficult to compare the bulk and dissipation estimates in the time series. The Reynolds flux calculations (squares) lend credibility to the dissipation estimates (pluses), because of the generally excellent agreement between the two methods. Figure 39 shows the sensible heat flux time series from run D38B and (like the momentum flux of figure 34) the bulk, eddy correlation and the

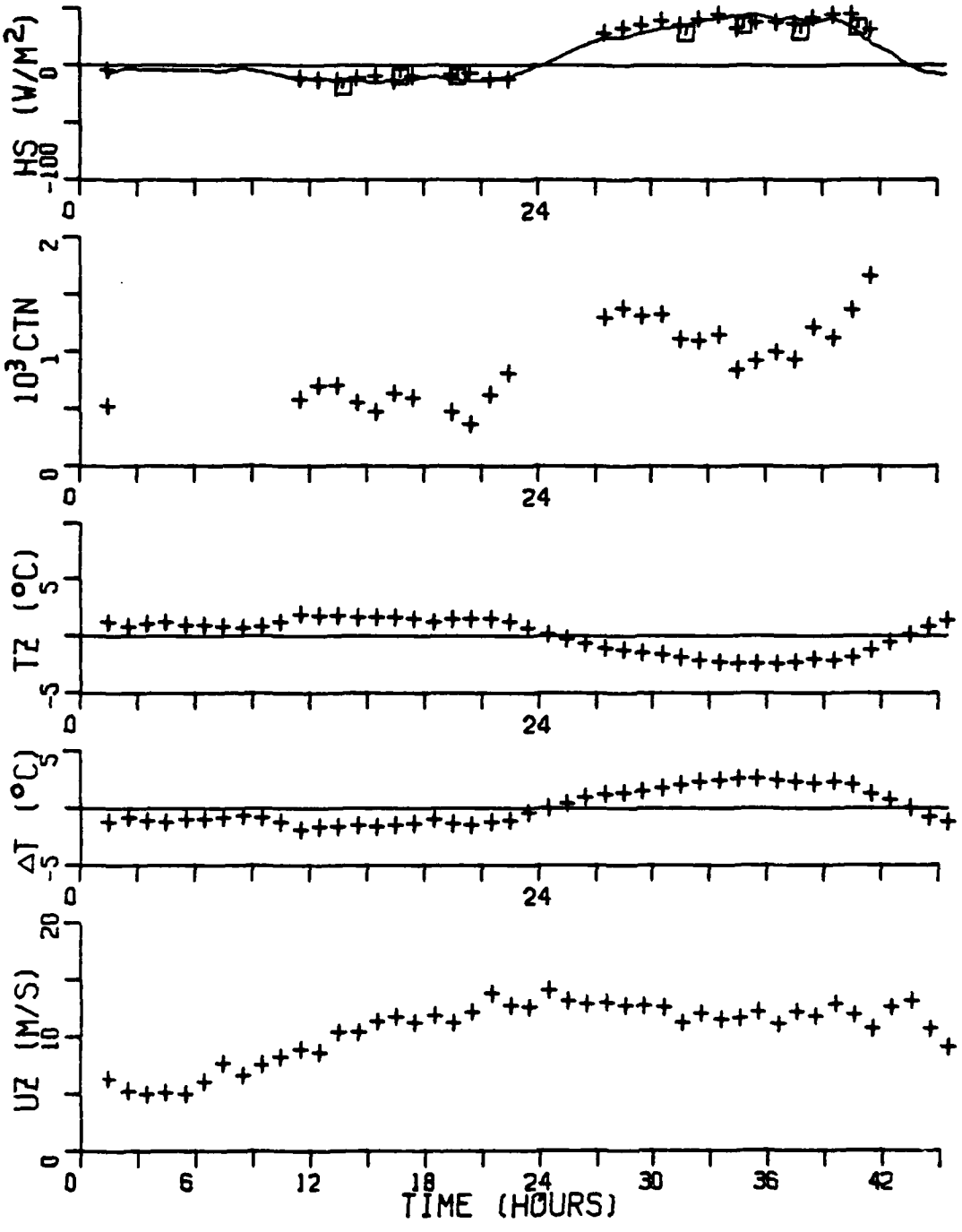

FIGURE 39 Sensible heat flux time series from run D38B (figure 34). Time is from 16:00 GMT March 12, 1977 and symbols are the same as in figure 36.

dissipation estimates of the sensible heat flux continue to agree for a considerable length of time. On the whole the sensible heat flux parameterization is compatible with the results of Friehe and Schmitt, 1976, and Smith, 1979, so a combination of all available data should give a CTN formulation capable of providing reasonable averages (over a few days or more) of sensible heat flux values, depending on the accuracy of ΔT. However, as with the momentum flux, there may be short lived situations, as possibly seen in D33C, where a parameterization, valid for long term averages, does not strictly apply. It is also possible that erronous ΔT values are causing the difference between the bulk and dissipation calculations between hours 2 and 10 of D33C, figure 36 and, as has been discussed, between hours 12 and 24.

CHAPTER 7 SUMMARY AND CONCLUSIONS

The experimental program described in this thesis successfully measured the momentum and sensible heat fluxes over the sea at winds between 4 and 26 m/s. As hoped, a great many hours of momentum flux data were suitable for analysis, but much less sensible heat flux and no moisture flux data were found to be reliable. Success depended chiefly on the performance of the sensors and on the establishment of the dissipation method as a viable means of measuring the fluxes of momentum and sensible heat.

The velocity sensor worked very well, but there were some problems with the temperature measurements and no humidity sensor was found to be suitable for remote operation in a salt-air environment. The Gill twin propeller-vane anemometer operated for periods of more than a month in adverse conditions without servicing. It provided the fluctuating horizontal and vertical velocities to the Reynolds flux system and responded to the lower frequencies of the downstream velocity spectrum's -5/3 region sufficiently for the molecular dissipation to be inferred, although the propeller responses first had to be determined. The distance constant was found to depend on the type and weight of propeller, the wind speed and the angle of attack. The humidity sensitivity of salt contaminated microbeads was recognized by the lack of low frequency variance in the temperature spectrum, but only sometimes were other characteristics, such as the absence of a -5/3 region, observed.

This behavior remains a major problem with the remote operation of this type of sensor. The response of the microbeads seemed to be limited by its protective enclosure and was described by a distance constant of about 0.90m, which is adequate for both the Reynolds flux and dissipation methods.

Reynolds flux measurements from the Bedford tower were shown to be realistic by comparisons with spectra, cospectra and turbulence statistics from previous studies. In addition, the drag coefficients and Stanton numbers were generally comparable to the results of Smith, 1979, however there is probably a bias to small drag coefficients at low wind speeds as a result of the Reynolds flux sampling. Universal shapes for the velocity spectra and cospectra in both the stable and unstable cases, were found from averages over the 196 momentum flux runs. With only 60 temperature runs available, there was considerable uncertainty in the normalized temperature spectrum and w,t cospectrum. The integration of all cospectra began at n=0.004, then the unstable and stable $\phi_{uw}(f)$ and the unstable and stable $\phi_{wt}(f)$ integrals were multiplied by 1.06, 1.005, 1.10 and 1.04, respectively, in order to account for the lower frequencies. This method was found to preserve covariance, on average, and to reduce the scatter in eddy correlation measurements caused by the uncertain low frequency contributions to the fluxes.

Reliable Reynolds flux estimates were needed for comparison with simultaneous dissipation calculations and the dissipation method was shown to give essentially the same results, on average. The agreement between the two methods was found to be best when the magnitude of the fluxes was large. In all but the most stable stratification (Z/L>0.05), u*DISS1, the neutral dissipation method, which does not require an explicit stability parameter, was found to be in quite good agreement (to within about 20%) with eddy correlation values of u*. The agreement between the two techniques improved, particularly the sensible heat flux calculations, when the stability modification of the logarithmic profiles and the buoyant production were incorporated into the dissipation method (u*DISS2 and <wt>DISS2). These corrections involved the stability parameter, for which a bulk estimate Z/L(ΔT) was shown to be a reasonable approximation, on average. A linear regression gave

$$u^*DISS = 0.96\ u^*FLUX + 0.025\ m/s\ ,$$

where the positive offset results from a tendency for <uw>DISS to be greater than <uw>FLUX by more than 30%, in the most stable runs (Z/L>0.10). In near neutral conditions (-0.45 <Z/L< 0.05) at all wind speeds the momentum flux calculations agreed to within 4%, on average. The agreement between the sensible heat flux calculations was very good, with a regression giving

$$\langle wt\rangle DISS = 1.04\ \langle wt\rangle FLUX.$$

The Bedford tower experiment established that reliable dissipation estimates of both the momentum and sensible heat fluxes and the bulk estimates of Z/L could be obtained from the CCGS Quadra. A favourable comparison of ship and tower dissipation drag coefficients showed the Bedford tower to be essentially an open ocean site, which allowed the combined 1591 hours of momentum flux and 260 hours of sensible heat flux measurements to be considered as a single open ocean data set.

The dissipation data showed the neutral drag coefficient to depend on wind speed, as approximated by

$$10^3 CDN = 1.14 \qquad 4 < U10 \leq 10 \text{ m/s}$$

$$10^3 CDN = 0.49 + 0.065\, U10 \qquad 10 < U10 < 26 \text{ m/s}.$$

Below 10 m/s the variability of CDN with wind speed, fetch, and stability was minimal, < 5% on average. Time series of calculated CDN's displayed about a 10% random fluctuation. Bulk estimates of the momentum flux were obtained from the above formulation by: first, shifting the measured wind speed to 10m with an iterative technique involving CDN; second, calculating CDN; third, shifting CDN to CD (the drag coefficient at the measurement height, Z, wind speed, UZ, and stability $Z/L(\Delta T)$); fourth, applying the bulk aerodynamic formula $-\langle uw \rangle = CD\, UZ^2$. It was shown that the neglect of Z/L would produce a minor error in the calculated U10 and CDN, but that the CD found in step 3 could be affected by as much as 20%. However this error was reduced to 5% by using the bulk stability estimate. Errors in the CDN formulation, UZ and Z/L could add up to 15% in the bulk

estimates, which were seen to give a good measure of the momentum flux averaged over a few days or more and a good hourly average when the wind was steady. Over periods of up to a day, the bulk and dissipation calculations were seen to consistently differ by as much as 30%. These discrepancies were found to be associated with varying winds, with the dissipation estimate being smaller on the rising wind and larger on the falling wind or after a change in wind direction. The conclusion drawn was that the surface roughness and hence drag coefficient depend on surface parameters which are a product of both past and present winds.

A constant neutral 10m drag coefficient was found to be an adequate description of almost all recent measurements over deep water, throughout the wind speed range, 4 to 10 m/s. The value of the constant varied from about 1.1×10^{-3} to 1.3×10^{-3}. This behavior has been found by the eddy correlation, dissipation and profile methods, but measurements from onshore or shallow water sites often displayed a distinctly different wind speed dependency. A reasonable compromise over the open ocean would be to use $10^3 CDN = 1.2$ in the bulk aerodynamic method for winds up to 11 m/s. At U10 = 11 m/s, the high wind speed regression of this study, $10^3 CDN = 0.49 + 0.065\ U10 \cong 1.2$. Since this regression fits the only other large set of open sea high wind speed data (Smith, 1979), it should give satisfactory CDN's at the higher wind speeds (to at least 26 m/s).

It was necessary to parameterize the sensible heat flux differently in stable and unstable stratification. The majority of the data were in the ranges $-40 < U10\ \Delta T < 60$ °Cm/s, $-0.3 < Z/L < 0.1$ and $6 < U10 < 18$ m/s, for which either

$$10^3\langle wt\rangle = 1.00\ U10\ \Delta T + 2.9\ ^\circ Cm/s \qquad \text{stable}$$

$$10^3\langle wt\rangle = 0.75\ U10\ \Delta T + 2.0\ ^\circ Cm/s \qquad \text{unstable}$$

or

$$10^3 CTN = 1.08 \qquad \text{unstable}$$

$$10^3 CTN = 0.68\ , \qquad \text{stable}$$

described the results. More measurements of CTN were needed in order to confirm or deny a wind speed dependency, which was suggested by some of the data. Bulk estimates of the sensible heat flux were obtained with $\langle wt\rangle = CT\ UZ\ \Delta T$, where CT was found from Z/L, CDN, CD and the stability dependent CTN. The errors were comparable to those of the bulk momentum flux estimates, except for the uncertainty in ΔT, which could have added considerable error depending on its magnitude. It was noted that all available data are reasonably consistent, making a good parameterization of the sensible heat flux feasible.

REFERENCES

Antonia, R. A., A. J. Chambers, S. Rajagopalan, K. R. Sreenivasan and C. A. Friehe, 1978: Measurement of turbulent fluxes in Bass Strait. J. Phys. Oc., 8: 28-37.

Banke, E. G. and S. D. Smith, 1973: Wind stress on arctic sea ice. J. Geophys. Res., 78: 7871-7883.

Baynton, H. W., 1976: Errors in wind run estimates from rotational anemometers. Bull. Am. Met. Soc., 57: 1127-1130.

Brocks, K. and L. Krügermeyer, 1970: The hydrodynamic roughness of the sea surface. Rep. No. 14, Institute For Radiometeorologie And Meteorologie, Hamburg University. Also in Gordon (ed.), Studies In Oceanography; Garden and Breach, New York, 1972: 75-92.

Burling, R. W. and R. W. Stewart, 1967: Ocean-Atmosphere Interaction (microprocesses). In Encyclopedia Of Oceanography; R. Fairbridge, ed., Rheinholdt, New York, 571-576.

Busch, N. E., 1977: Fluxes in the surface boundary layer over the sea. In Modelling And Prediction Of The Upper Layers Of The Oceans; E. B. Krauss, ed., Pergamon Press, Oxford, 72-91.

Charnock, H., 1955: Wind stress on a water surface. Q. J. R. Meteorol. Soc., 81: 639-692.

Deacon, E. L., 1959: The measurement of turbulent transfer in the lower atmosphere. Advances In Geophysics, 6: 211-228.

Deacon, E. L., 1973: Geostrophic drag coefficients. Boundary-Layer Meteorol., 5: 321-340.

De Leonibus, P. S., 1971: Momentum flux and ocean spectra observations from an ocean tower. J. Geophys. Res., 76: 6506-6527.

Denman, K. L. and M. Miyake, 1973: The behavior of the mean wind, the drag coefficient, and the wave field in the open ocean. J. Geophys. Res., 78: 1917-1931.

Dyer, A. J., 1974: A review of Flux-Profile relationships. Boundary-Layer Meteorol., 7: 363-372.

Dyer, A. J. and B. B. Hicks, 1970: Flux-Profile relationships in the constant flux layer. Q. J. R. Meteorol. Soc., 96: 715-721.

Fissel, D. B., S. Pond and M. Miyake, 1977: Computation of surface fluxes from climatological and synoptic data. Mon. Weather. Rev., 105: 26-36.

Francey, R. J. and J. R. Garratt, 1978: Eddy flux measurements over the open ocean and related transfer coefficients. Boundary-Layer Meteorol., 14: 153-166.

Friehe, C. A. and K. F. Schmitt, 1976: Parameterization of air-sea interface fluxes of sensible heat and moisture by bulk aerodynamic formulae. J. Phys. Oc., 6: 801-809.

Garratt, J. R., 1972: Studies of turbulence in the surface layer over water (Lough Neagh) PART II. Production and dissipation of velocity and temperature fluctuations. Q. J. R. Meteorol. Soc., 98: 642-657.

Garratt, J. R., 1977: Review of drag coefficients over oceans and continents. Mon. Weather. Rev., 105: 915-929.

Gill, G. C., 1975: Development and use of the Gill UVW anemometer. Boundary-Layer Meterol., 8: 475-495.

Hasse, L., 1970: On the determination of vertical transports of momentum and heat in the atmospheric boundary layer at sea. Tech. Rep. 188 Dept. Of Oceanography, Oregon State University.

Hertzman, O., M. Miyake and S. Pond, 1974: Ten years of meteorological data at ocean weather station PAPA. Manuscript Rep. No. 29, Institute Of Oceanography, University Of British Columbia: 46pp.

Hicks, B. B., 1972 A: Some evaluations of drag and bulk transfer coefficients over bodies of different sizes. Boundary-Layer Meteorol., 3: 201-213.

Hicks, B. B., 1972 B: Propeller anemometers as sensors of atmospheric turbulence. Boundary-Layer Meteorol., 3: 214-228.

Hoeber, H., 1969: Wind-, Temperatur- und Feuchteprofile in der wassernahen Luftschicht uber dem aquatiorialen Atlantik. Meteor Forschungsergebnisse, B, 4: 1-26.

Kaimal, J. C., J. C. Wyngaard, Y. Izumi and O. R. Coté, 1972: Spectral characteristics of surface-layer turbulence. Q. J. R. Meteorol. Soc., 98: 563-589.

Khalsa, S. J. S. and J. A. Businger, 1978: The drag coefficient as determined by the dissipation method and its relation to intermittent convection in the surface layer. Boundary-Layer Meteorol., 12: 273-297.

Kitaigorodskii, S. A., O. A. Kuznetsov, and G. N. Panin, 1973: Coefficients of drag, sensible heat and evaporation in the atmosphere over the surface of a sea. Izv., Atmospheric And Oceanic Physics, 9, No. 11: 1135-1141.

Kitaigorodskii, S. A. and M. M. Zaslavskii, 1974: A dynamical analysis of the drag coefficient at the sea surface. Boundary-Layer Meteorol., 6: 53-61.

Krauss, E. B., 1972: Atmosphere-Ocean Interaction. Oxford University Press, London, 275pp.

Lumley, J. L. and H. A. Panofsky, 1964: The Structure Of Atmospheric Turbulence. Interscience, New York, 239pp.

McBean, G. A., 1971: The variation of the statistics of wind temperature and humidity fluctuations with stability. Boundary-Layer Meteorol., 1: 438-457.

McBean, G. A. and M. Miyake, 1972: Turbulent transfer mechanisms in the atmospheric surface layer. Q. J. R. Meteorol. Soc., 98: 383-393.

McBean, G. A. and J. A. Elliott, 1975: The vertical transports of kinetic energy by turbulence and pressure in the boundary layer. J. Atmos. Sci., 32: 753-766.

Mitsuta, Y, and T. Fujitani, 1974: Direct measurements of turbulent fluxes on a cruising ship. Boundary-Layer Meteorol., 6: 203-217.

Miyake, M., M. Donelan, G. McBean, C. Paulson, F. Badgley and E. Leavitt, 1970 A: Comparison of turbulent fluxes over water determined by profile and eddy correlation techniques. Q. J. R. Meteorol. Soc., 96: 132-137.

Miyake, M., M. Donelan and Y. Mitsuta, 1970 B: Airborne measurements of turbulent fluxes. J. Geophys. Res., 75: 4506-4518.

Monin, A. S. and A. M. Yaglom, 1965; 1967: Statistical Fluid Dynamics Vols. I and II. Nauka, Moscow, 639pp; 720pp. (English Translation J. L. Lumley, ed., MIT Press).

Paquin, J. E. and S. Pond, 1971: The determination of the Kolmogoroff constants for velocity temperature and moisture from second and third order structure functions. J. Fluid Mech., 50: 257-269.

Paulson, C. A., 1970: Representation of wind speed and temperature profiles in the unstable atmospheric surface layer. J. Appl. Meteorol., 9: 857-861.

Paulson, C. A., E. Leavitt and R. G. Fleagle, 1972: Air-Sea transfer of momentum, heat and water determined from profile measurements during BOMEX. J. Phys. Oc., 2: 487-497.

Phelps, G. T., 1971: The fluxes of latent and sensible heat in the marine boundary layer. Ph.D. Thesis, Department Of Oceanography, Oregon State University: 117pp.

Phelps, G. T. and S. Pond, 1971: Spectra of the temperature and humidity fluctuations and of the fluxes of moisture and sensible heat in the marine boundary layer. J. Atmos. Sci., 28: 918-928.

Pond, S., 1968: Some effects of buoy motion on measurements of wind speed and stress. J. Geophys. Res., 73: 507-512.

Pond, S., G. T. Phelps, J. E. Paquin, G. A. McBean and R. W. Stewart, 1971: Measurements of the turbulent fluxes of momentum, moisture and sensible heat over the ocean. J. Atmos. Sci., 28: 901-917.

Pond, S. and W. G. Large, 1978: A system for remote measurements of air-sea fluxes of momentum, heat and moisture during moderate to strong winds. Manuscript Rep. No. 32, Institute Of Oceanography, University Of British Columbia: 55pp.

Pond, S., W. G. Large, M. Miyake and R. W. Burling, 1979: A Gill twin propeller-vane anemometer for flux measurements during moderate and strong winds. Boundary-Layer Meteorol., 16: 351-364.

Schmitt, K. F., C. A. Friehe and C. H. Gibson, 1978: Humidity sensitivity of atmospheric temperature sensors by salt contamination. J. Phys. Oc., 8: 151-161.

Sheppard, P. A., D. T. Tribble and J. R. Garratt, 1972: Studies of turbulence in the surface layer over water (Lough Neagh) Part I. Q. J. R. Meteorol. Soc., 98: 627-641.

Smith, S. D., 1979: Surface wind stress and heat flux measured over the Atlantic Ocean in gale force winds. Submitted to J. Phys. Oc.

Smith, S. D. and E. G. Banke, 1975: Variation of the sea surface drag coefficient with wind speed. Q. J. R. Meteorol. Soc., 101: 665-673.

Smith, S. D., R. J. Anderson, E. G. Banke, E. P. Jones, S. Pond and W. G. Large, 1976: A comparison of the air-sea interaction flux measurement systems of the Bedford Institute of Oceanography and the Institute of Oceanography, University of British Columbia. Bedford Institute Of Oceanography Report Series, BI-R-76-17: 41pp.

Stewart, R. W., 1974: The air sea momentum exchange. Boundary-Layer Meteorol., 6: 151-167.

Wieler, H. S. and R. W. Burling, 1967: Direct measurements of stress and spectra of turbulence in the boundary layer over the sea. J. Atmos. Sci., 24: 653-664.

Wiegel, R. L., 1964: Oceanographical Engineering, Prentice-Hall, Inc. Englewood Cliffs, N. J.: 511pp.

Wucknitz, J., 1976: Determination of turbulent fluxes of momentum and sensible heat from fluctuation measurements and the structure of the wind field over waves above the tropical atlantic during ATEX. Meteor B, No. 11: 25-50.

Wyngaard, J. C. and O. R. Coté, 1971: The budgets of turbulent kinetic energy and temperature variance in the atmospheric surface layer. J. Atmos. Sci., 28: 190-201.

APPENDIX THE INTERCOMPARISON RESULTS

RUN	TIME GMT	DATE 1976	UZ (M/S) °True	TZ °C	TSFC	Z/L	u* (m/s) FLUX	u* (m/s) DISS	10<wt> °Cm/s FLUX	10<wt> °Cm/s DISS
T1	17:00	17/ 9	6.4 232	16.8	17.5	-.12	0.197	0.193		
T2	18:00	17/ 9	6.4 240	16.6	17.5	-.13	0.173	0.171	0.038	0.043
T3	19:00	17/ 9	6.1 243	16.6	17.5	-.16	0.158	0.166	0.042	0.036
T4	20:00	17/ 9	6.3 236	16.3	17.5	-.17	0.197	0.167	0.051	0.031
T5	21:00	17/ 9	6.3 235	16.3	17.5	-.18	0.195	0.177	0.042	0.030
T6	3:00	18/ 9	6.8 238	17.1	17.5	-.09	0.176	0.224		
T7	4:00	18/ 9	7.7 232	17.2	17.5	-.05	0.229	0.244		
T8	5:00	18/ 9	7.3 243	16.9	17.5	-.08	0.225	0.240		
T9	0:00	19/ 9	5.8 233	17.1	16.7	0.00	0.185	0.215		
T10	1:00	19/ 9	6.1 233	17.2	16.7	0.01	0.179	0.211		
T11	2:00	19/ 9	6.2 228	17.1	16.7	-.01	0.192	0.207		
T12	3:00	19/ 9	6.8 236	17.0	16.7	-.01	0.187	0.217		
T13	14:00	19/ 9	6.8 167	16.7	16.3	-.01	0.227	0.250		
T14	18:00	19/ 9	6.0 199	17.4	16.0	0.09	0.164	0.170	-.022	-.034
T15	19:00	19/ 9	6.7 214	17.3	16.0	0.07	0.190	0.192	-.022	-.028
T16	20:00	19/ 9	8.4 209	16.9	16.0	0.02	0.207	0.235	-.003	-.017
T17	21:00	19/ 9	9.5 213	16.9	16.1	0.02	0.296	0.291	-.011	-.015
T18	22:00	19/ 9	10.4 212	17.0	16.2	0.01	0.349	0.326	-.014	-.019
T19	23:00	19/ 9	9.0 217	16.9	16.6	-.01	0.324	0.286	0.010	-.030
T20	0:00	20/ 9	8.5 226	16.8	16.8	-.03	0.287	0.270	0.021	-.043
T21	1:00	20/ 9	9.2 230	16.6	16.8	-.04	0.326	0.285	0.058	0.062
T22	2:00	20/ 9	8.6 234	16.3	16.9	-.06	0.266	0.272	0.063	0.081
T23	3:00	20/ 9	7.3 231	16.2	16.8	-.09	0.242	0.234	0.056	0.075
T24	4:00	20/ 9	6.8 236	16.2	16.8	-.10	0.220	0.229	0.040	0.063
T25	5:00	20/ 9	6.6 238	16.2	16.8	-.10	0.200	0.247	0.024	0.060
T26	6:00	20/ 9	7.0 233	16.2	16.7	-.08	0.220	0.238	0.032	0.058
T27	7:00	20/ 9	7.4 238	15.7	16.4	-.08	0.240	0.229	0.054	0.058
T28	8:00	20/ 9	7.6 250	15.3	16.3	-.11	0.221	0.228	0.048	0.058
T29	9:00	20/ 9	7.7 244	14.8	16.3	-.14	0.202	0.213	0.054	0.057
T30	14:00	20/ 9	7.3 220	16.7	16.3	0.00	0.219	0.204		
T31	15:00	20/ 9	6.9 220	16.8	16.4	-.00	0.187	0.191		
T32	16:00	20/ 9	8.0 221	16.3	16.4	-.03	0.244	0.239		
T33	17:00	20/ 9	7.5 220	16.8	16.6	-.02	0.240	0.235		
T34	18:00	20/ 9	5.9 220	17.3	16.7	0.01	0.168	0.180		
T35	5:00	21/ 9	7.2 201	17.1	16.8	-.01	0.246	0.267		
T36	6:00	21/ 9	6.8 204	17.3	16.9	-.00	0.222	0.242		
T37	7:00	21/ 9	7.5 198	17.4	16.9	0.01	0.242	0.264		
T38	8:00	21/ 9	8.7 197	17.5	17.0	0.00	0.267	0.290		
T39	9:00	21/ 9	8.3 193	17.6	17.1	0.00	0.258	0.270		
T40	10:00	21/ 9	8.2 190	17.9	17.2	0.01	0.290	0.267		
T41	11:00	21/ 9	8.4 182	18.0	17.2	0.02	0.259	0.273		
T42	12:00	21/ 9	9.1 178	18.3	17.2	0.04	0.238	0.253		
T43	13:00	21/ 9	8.6 182	18.4	17.2	0.04	0.263	0.277		
T44	14:00	21/ 9	8.6 180	18.4	17.3	0.03	0.278	0.285		
T45	15:00	21/ 9	9.0 183	18.6	17.4	0.04	0.295	0.302		
T46	16:00	21/ 9	9.5 183	19.0	17.4	0.05	0.302	0.317		
T47	19:02	23/ 9	9.9 231	16.4	16.9	-.04	0.362	0.298		
T48	20:00	23/ 9	10.1 230	16.6	16.9	-.03	0.335	0.318		
T49	23:00	23/ 9	11.7 224	16.1	17.0	-.04	0.359	0.359		

RUN	TIME GMT	DATE 1976	UZ	°TRUE	TZ	TSFC	Z/L	u* (m/s) FLUX	u* (m/s) DISS	10<wt> FLUX	10<wt> DISS
T50	2:00	24/ 9	11.9	228	15.5	17.0	-.06	0.396	0.367		
T51	5:00	24/ 9	10.2	229	15.6	16.5	-.06	0.356	0.326		
T52	11:00	24/ 9	9.6	215	16.1	16.3	-.03	0.321	0.298		
T53	13:16	24/ 9	9.8	211	16.4	16.4	-.02	0.340	0.302		
T54	14:32	24/ 9	10.3	208	16.7	16.6	-.01	0.303	0.311		
T55	20:12	24/ 9	7.2	210	16.2	15.9	-.01	0.231	0.247		
T56	11:00	27/ 9	11.4	162	14.7	16.0	-.06	0.394	0.349		
T57	12:11	27/ 9	12.1	162	15.0	15.9	-.04	0.458	0.365		
T58	13:38	27/ 9	13.5	166	15.8	15.8	-.01	0.442	0.438		
T59	15:42	27/ 9	11.9	167	16.8	15.2	0.03	0.448	0.368		
T60	16:36	27/ 9	11.1	194	16.6	14.5	0.05	0.338	0.360	-.146	-.160
T61	20:14	27/ 9	15.2	210	16.7	14.2	0.04	0.585	0.529	-.302	-.257
T62	23:00	27/ 9	10.7	228	15.8	14.1	0.04	0.331	0.352	-.121	-.144
T63	11:00	28/ 9	9.8	11	10.9	14.7	-.19	0.300	0.308	0.236	0.250
T64	12:48	28/ 9	8.5	10	10.4	15.1	-.29	0.253	0.264	0.233	0.260
T65	23:00	28/ 9	12.0	311	10.8	14.0	-.12	0.379	0.413	0.284	0.352
T66	5:00	29/ 9	8.9	333	8.5	14.7	-.35	0.339	0.298	0.388	0.413
T67	17:00	29/ 9	10.0	230	12.4	16.0	-.16	0.341	0.321	0.324	0.294
T68	18:06	29/ 9	11.0	232	12.8	15.5	-.11	0.370	0.352		
T69	19:48	29/ 9	10.2	226	13.3	14.3	-.06	0.356	0.321		
T70	23:00	29/ 9	11.8	222	13.9	13.7	-.01	0.392	0.410		
T71	2:00	30/ 9	13.6	236	14.1	13.2	0.01	0.420	0.437		
T72	5:00	30/ 9	10.1	243	13.4	12.8	0.01	0.352	0.329		
T73	11:30	30/ 9	8.3	239	12.4	13.1	-.07	0.270	0.256	0.059	0.075
T74	2:23	10/10	13.9	194	18.8	16.2	0.04	0.523	0.496	-.276	-.246
T75	5:23	10/10	17.1	191	19.4	16.3	0.04	0.638	0.670	-.368	-.374
T76	8:23	10/10	12.7	224	16.5	16.2	-.00	0.476	0.470	-.055	-.064
T77	11:23	10/10	15.8	223	17.1	16.2	0.01	0.660	0.580	-.043	-.067
T78	12:53	10/10	17.5	232	16.6	16.1	0.00	0.714	0.682		
T79	14:01	10/10	17.8	234	15.6	16.0	-.01	0.762	0.676		
T80	17:23	10/10	19.2	238	13.8	15.1	-.02	0.786	0.755		
T81	20:23	10/10	16.6	254	12.2	14.2	-.04	0.641	0.624		
T82	22:23	10/10	14.0	268	11.5	13.6	-.05	0.523	0.504		
T83	23:23	10/10	13.6	271	11.1	13.3	-.06	0.442	0.495		
T84	2:23	11/10	12.3	265	10.1	12.4	-.07	0.396	0.417		
T85	5:23	11/10	10.5	269	9.2	12.5	-.14	0.401	0.373		
T86	16:01	14/10	7.7	177	13.3	7.7	0.30	0.173	0.203	-.027	-.052
T87	17:17	14/10	10.2	174	13.6	8.3	0.18	0.318	0.297	-.112	-.105
T88	18:35	14/10	11.4	179	13.2	10.2	0.08	0.355	0.376	-.162	-.158
T89	20:17	14/10	6.3	242	12.1	10.7	0.09	0.224	0.237		
T90	8:23	15/10	16.1	259	7.6	10.5	-.05	0.625			
T91	11:23	15/10	15.7	263	7.9	10.1	-.04	0.692			
T92	12:29	15/10	14.4	263	7.7	9.7	-.05	0.515			
T93	14:23	15/10	14.6	259	8.2	9.3	-.03	0.559			
T94	17:23	15/10	13.7	259	10.5	9.0	0.02	0.546	0.491		
T95	19:00	15/10	13.2	260	11.4	8.8	0.04	0.535	0.496	-.186	-.187
T96	2:10	27/11	12.4	199	7.9	5.7	0.04	0.496	0.441	-.181	-.168
T97	2:10	28/11	11.3	215	8.1	5.4	0.07	0.377	0.416	-.173	-.229
T98	0:00	3/12	11.7	123	5.4	4.6	0.02	0.393	0.411	-.052	-.059

AD-A081 392 BRITISH COLUMBIA UNIV VANCOUVER INST OF OCEANOGRAPHY F/G 4/2
THE TURBULENT FLUXES OF MOMENTUM AND SENSIBLE HEAT OVER THE OPE--ETC(U)
AUG 79 W G LARGE N00014-76-C-0446
UNCLASSIFIED NL

3 OF 3
AD A081392

END
DATE FILMED
4-80
DTIC

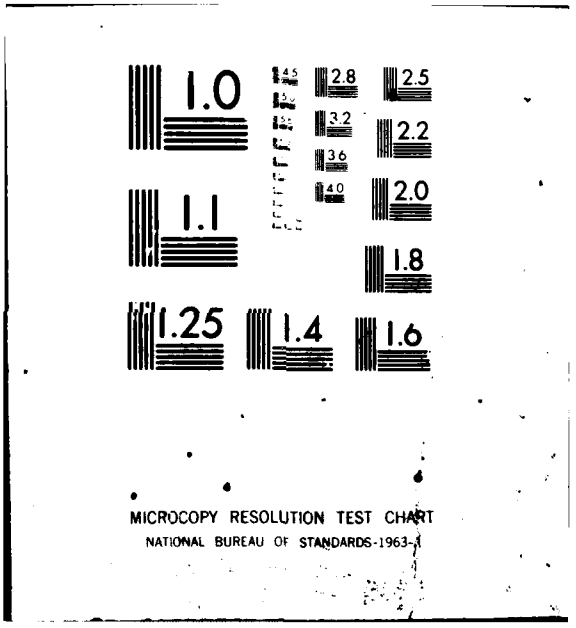
1.0
2.8
2.5
3.2
2.2
3.6
4.0
2.0
1.1
1.8
1.25
1.4
1.6
MICROCOPY RESOLUTION TEST CHART
NATIONAL BUREAU OF STANDARDS-1963-A

RUN	TIME GMT	DATE 1976	UZ	°TRUE	TZ	TSFC	Z/L	u* (m/s) FLUX	u* (m/s) DISS	10<wt> FLUX	10<wt> DISS
T99	6:00	3/12	12.4	216	6.9	4.6	0.05	0.424	0.447	-.180	-.185
T100	9:00	3/12	17.9	250	3.1	4.6	-.02	0.826	0.752		
T101	12:00	3/12	18.6	264	-2.5	4.6	-.09	0.733	0.737		
T102	15:00	3/12	18.5	274	-9.7	4.6	-.19	0.746	0.724		
T103	18:00	3/12	16.9	278	-11.	4.6	-.26	0.672	0.690		
T104	21:00	3/12	15.0	270	-12.	4.5	-.33	0.552	0.588		
T105	0:00	4/12	16.8	267	-11.	4.5	-.25	0.735	0.690		
T106	3:00	4/12	19.3	269	-9.6	4.5	-.17	0.817	0.806		
T107	6:00	4/12	15.9	266	-10.	4.4	-.27	0.633	0.599		
T108	9:00	4/12	16.0	261	-8.9	4.3	-.22	0.551	0.559		
T109	12:00	4/12	14.4	264	-7.8	4.3	-.26	0.500	0.495		
T110	15:00	4/12	10.7	261	-5.8	4.2	-.34	0.352	0.414		
T111	15:00	7/12	11.7	169	2.5	3.5	-.04	0.418	0.380	0.179	0.200
T112	18:00	7/12	14.6	139	4.1	3.5	0.01	0.478	0.519		
T113	21:00	7/12	17.1	143	5.8	3.6	0.03	0.660	0.651	-.131	-.125
T114	0:00	8/12	18.6	153	7.6	3.5	0.04	0.746	0.736	-.385	-.352
T115	3:00	8/12	18.9	159	7.8	3.6	0.04	0.728	0.729	-.435	-.516
T116	6:00	8/12	13.3	170	7.9	3.6	0.08	0.518	0.506	-.372	-.452
T117	18:00	9/12	14.6	300	-11.	3.6	-.31	0.601	0.598		
T118	21:00	9/12	18.3	302	-14.	3.5	-.27	0.640	0.739		
T119	0:00	10/12	17.1	302	-17.	3.4	-.33	0.675	0.695		
T120	3:00	10/12	15.6	292	-17.	3.4	-.38	0.656	0.607		
T121	6:00	10/12	16.9	289	-15.	3.3	-.31	0.487	0.592		
T122	9:00	10/12	13.5	278	-14.	3.3	-.45	0.463	0.485		
T123	2:00	11/12	10.5	211	5.2	3.3	0.06	0.362	0.348	-.069	-.089
T124	8:00	11/12	12.4	220	5.9	3.4	0.06	0.483	0.462	-.159	-.152
T125	11:00	11/12	15.3	230	6.3	3.5	0.04	0.661	0.578	-.228	-.176
T126	14:00	11/12	16.0	231	6.5	3.5	0.04	0.606	0.613	-.251	-.186
T127	17:00	11/12	17.2	291	1.8	3.5	-.03	0.645	0.673		
T128	20:00	11/12	16.0	290	-1.0	3.5	-.08	0.565	0.591		
T129	23:00	11/12	11.9	308	-2.6	3.5	-.21	0.378	0.433		
T130	14:00	12/12	12.6	201	1.6	3.4	-.06	0.446	0.405	0.265	0.296
T131	5:00	14/12	14.2	317	-14.	3.2	-.35	0.531	0.541		
T132	8:00	14/12	14.6	312	-16.	3.2	-.43	0.534	0.543		
T133	23:00	14/12	13.2	218	-7.0	3.0	-.27	0.493	0.456		
T134	2:00	15/12	18.2	220	2.2	3.0	-.01	0.769	0.735		
T135	5:00	15/12	17.5	219	3.9	2.9	-0.01	0.693	0.681	-.023	-.047
T136	8:00	15/12	15.9	213	4.8	2.9	0.03	0.663	0.602	-.132	-.082
T137	11:00	15/12 1977	15.6	231	5.4	2.9	0.04	0.613	0.592		
T138	0:48	13/ 3	10.6	233	1.9	0.0	0.06	0.221	0.264	-.097	-.146
T139	9:48	17/ 3	10.4	236	1.8	0.2	0.05	0.363	0.355	-.142	-.104
T140	12:48	17/ 3	11.2	240	1.6	0.3	0.03	0.395	0.387	-.071	-.097
T141	15:48	17/ 3	11.0	234	1.5	0.2	0.04	0.356	0.359	-.079	-.061
T142	18:48	17/ 3	12.6	259	1.0	0.3	0.01	0.456	0.456		
T143	21:48	17/ 3	12.8	270	-0.3	0.3	-.02	0.440	0.464		
T144	0:48	18/ 3	12.6	278	-1.3	0.2	-.04	0.442	0.457		
T145	3:48	18/ 3	10.5	280	-1.9	0.2	-.09	0.360	0.387	0.214	0.253
T146	6:48	18/ 3	11.3	271	-2.4	0.2	-.09	0.389	0.371	0.268	0.237
T147	9:48	18/ 3	11.7	270	-2.2	0.2	-.07	0.380	0.410	0.227	0.279

RUN	TIME GMT	DATE 1977	UZ	°TRUE	TZ	TSFC	Z/L	u* (m/s) FLUX	u* (m/s) DISS	10<wt> FLUX	10<wt> DISS
T148	12:48	18/ 3	11.5	282	-1.7	0.2	-.06	0.405	0.421		
T149	15:48	18/ 3	12.7	254	0.4	0.3	-.00	0.398	0.444		
T150	6:48	19/ 3	17.3	61	-1.0	0.3	-.02	0.694	0.685		
T151	9:48	19/ 3	12.8	16	-1.7	0.2	-.05	0.458	0.488		
T152	12:48	19/ 3	16.4	347	-2.8	0.2	-.05	0.646	0.645		
T153	15:48	19/ 3	17.6	325	-2.9	0.3	-.05	0.685	0.708		
T154	18:48	19/ 3	14.1	323	-2.8	0.3	-.08	0.469	0.530		
T155	0:48	20/ 3	10.7	296	-1.9	0.2	-.08	0.347	0.405		
T156	21:48	24/ 3	12.3	358	-0.7	0.1	-.03	0.369	0.425		
T157	0:48	25/ 3	12.2	356	-1.1	-0.1	-.03	0.359	0.415		
T158	3:48	25/ 3	11.3	357	-0.9	-0.2	-.03	0.321	0.369		
T159	9:48	25/ 3	10.7	353	-0.5	-0.2	-.02	0.321	0.360		
T160	12:48	25/ 3	10.3	3	0.3	-0.2	0.01	0.290	0.329		
T161	15:48	25/ 3	10.6	359	1.5	-0.2	0.05	0.310	0.342		
T162	18:48	25/ 3	10.5	358	2.2	0.0	0.07	0.276	0.341		
T163	21:48	25/ 3	10.4	356	0.9	0.0	0.03	0.312	0.368		
T164	3:48	26/ 3	10.7	353	0.1	0.0	-.00	0.303	0.352		
T165	6:48	26/ 3	10.5	350	0.1	0.0	0.00	0.259	0.333		
T166	9:48	26/ 3	10.3	353	0.5	0.0	0.01	0.267	0.333		
T167	12:48	26/ 3	11.4	352	1.3	0.0	0.04	0.328	0.369		
T168	15:48	26/ 3	10.6	351	0.9	0.0	0.02	0.323	0.365		
T169	18:48	26/ 3	12.2	17	1.4	0.0	0.03	0.388	0.424		
T170	21:48	26/ 3	12.3	14	1.0	0.0	0.02	0.395	0.421		
T171	3:48	27/ 3	10.8	10	1.4	0.0	0.04	0.341	0.371		
T172	12:48	27/ 3	11.3	4	1.6	0.0	0.04	0.315	0.370		
T173	15:48	27/ 3	10.4	17	2.4	0.0	0.07	0.313	0.350		
T174	18:48	27/ 3	10.9	3	3.5	0.0	0.10	0.266	0.335		
T175	21:48	27/ 3	8.0	1	2.7	0.0	0.13	0.235	0.287		
T176	21:48	29/ 3	8.6	172	2.2	0.0	0.10	0.232	0.298		
T177	18:48	31/ 3	11.5	168	3.0	0.0	0.08	0.367	0.413		
T178	21:48	31/ 3	7.8	204	3.1	0.0	0.16	0.200	0.242		
T179	12:48	3/ 4	12.6	147	0.6	0.0	0.01	0.451	0.428		
T180	15:48	3/ 4	14.2	125	1.2	0.0	0.02	0.562	0.531		
T181	18:48	3/ 4	11.4	170	3.1	0.0	0.09	0.407	0.445		
T182	3:48	4/ 4	19.1	288	1.8	0.0	0.02	0.626	0.762		
T183	6:48	4/ 4	18.0	300	-0.3	0.0	-.01	0.684	0.723		
T184	9:48	4/ 4	16.2	313	-1.4	0.0	-.03	0.610	0.628		
T185	12:48	4/ 4	15.2	311	-0.7	0.0	-.01	0.511	0.566		
T186	15:48	4/ 4	13.5	315	0.4	0.0	0.01	0.462	0.519		
T187	18:48	4/ 4	10.8	321	1.7	0.0	0.05	0.311	0.388		
T188	21:48	4/ 4	10.9	311	1.8	0.0	0.05	0.316	0.374		
T189	3:48	6/ 4	15.1	189	6.0	0.0	0.09	0.566	0.573		
T190	6:48	6/ 4	13.0	209	4.7	0.0	0.11	0.482	0.471		
T191	9:48	6/ 4	10.7	223	1.3	0.0	0.04	0.346	0.399		
T192	12:48	6/ 4	12.4	224	1.3	0.0	0.03	0.466	0.460		
T193	15:48	6/ 4	12.4	220	1.2	0.0	0.02	0.460	0.448		
T194	18:48	6/ 4	14.5	223	1.9	0.0	0.03	0.545	0.540		
T195	21:48	6/ 4	13.2	223	1.5	0.0	0.03	0.461	0.494		
T196	0:48	7/ 4	11.6	217	0.9	0.0	0.02	0.406	0.427		